A STUDY OF $\bar{p}$d INTERACTIONS FROM 1.09 TO 1.43 GeV/c

Dissertation for the Degree of Ph. D

MICHIGAN STATE UNIVERSITY

PAUL DANIEL ZEMANY, Jr.

1975

ABSTRACT

A STUDY OF $\bar{p}d$ INTERACTIONS
FROM 1.09 TO 1.43 GeV/c

By

Paul Daniel Zemany, Jr.

The reaction and topological cross sections for $\bar{p}n$ interaction producing 3 or 5 charged particles are measured. This is done using data from the Brookhaven National Laboratory 31-inch deuterium filled bubble chamber.

The s-channel behavior of intermediate states of the reaction $\bar{p}n \rightarrow 2\pi^+3\pi^-$, in particular the $\rho°\rho°\pi^-$ state, are examined for possible structure at a center of mass energy of 2190 MeV. With a 90% confidence, no enhancement is found at a level of 0.7 mb if the width is assumed to be ±50 MeV. In addition, the complications involved in using a deuterium target as a source of neutrons are investigated using $\bar{p}n$ annihilations. The results indicate discrepancies with the assumption that deuterons can be used as a source of quasi-free neutrons. In this work, double scattering effect accounts for approximately 30% of the apparent $\bar{p}n$ annihilation events. An examination of the properties of protons emerging from the $\bar{p}d$ annihilations

indicates that the data can be properly described if and only if effects of double scattering are considered.

A STUDY OF $\bar{p}d$ INTERACTIONS

FROM 1.09 TO 1.43 GeV/c

By

Paul Daniel Zemany, Jr.

A DISSERTATION

Submitted to
Michigan State University
in partial fulfillment of the requirements
for the degree of

DOCTOR OF PHILOSOPHY

Department of Physics

1975

ACKNOWLEDGMENTS

I would like to express my thanks to Dr. Z. Ming Ma, my major professor, for many comments and suggestions involving this work. Also the advice of Professor G. A. Smith is greatly appreciated. Many thanks go to the MSU scanning and measuring staff and the Brookhaven National Laboratory bubble chamber staff. Finally, I would like to thank my wife, Hye Son, for encouragement and assistance during the preparation of this dissertation.

TABLE OF CONTENTS

CHAPTER Page

LIST OF TABLES

Table Page

LIST OF FIGURES

Figure		Page
5.3	Invariant Mass Distributions of π^+p_s and π^-p_s Systems	71
5.4	Cosine Distribution of Protons	73
5.5	Invariant Mass Distributions of π^+p and π^-p Systems	78
5.6	Cross Sections for $\pi^+p(A)$ and $\pi^-p(B)$ . . .	80
5.7	Four Prong Double Scattering Fits	97
5.8	Six Prong Double Scattering Fits	99
5.9	Invariant Mass Distributions of π^+p_s and π^-p_s Systems	105
5.10	Cosine between the Beam Direction and the π^+p_s Momentum Direction	107
E.1	Spectator Proton ϕ Distribution	143

CHAPTER I

INTRODUCTION

The study of $\bar{p}d$ interaction can be used to obtain information about the $\bar{p}n$ system. In the first approximation, one can regard the deuteron as two separate particles. Therefore, information about $\bar{p}n$ reactions can be obtained in a direct manner. This approximation is, in fact, not valid when more detailed examinations of the deuteron are made. First of all, the proton and the neutron in the deuteron are not stationary and are known to have an expected Fermi momentum of about 45 MeV/c. Therefore, the total available energy in the collision center of mass varies according to the initial momentum of the target neutron. In addition, the presence of a spectator proton may affect the dynamics of the collision process. The proton may screen the neutron from the incident antiproton, thus reducing the probability for a $\bar{p}n$ interaction. Furthermore, the presence of two nucleons at close range may cause the antiproton to double scatter in traversing the deuteron. This may happen in two ways: First, the antiproton may interact with one of the nucleons before it does with the other. Second, particles produced by the first collision may interact with the spectator nucleon. These double scattering processes will be shown to account for an excess of high momentum protons observed in the reaction $\bar{p}d \rightarrow p_s$ + mesons. Since there has been no complete description of double scattering in absorptive type reactions, one of the objectives of this dissertation is to develop a comprehensive model for double scattering that is applicable to $\bar{p}d$ annihilation reactions. Such a model is of great importance for studies involving a deuteron target because the presence of a spectator nucleon is often used to identify the type of reaction. As it will be shown in Chapter V, double scattering modifies the expected characteristics of a spectator nucleon. Therefore, it is important to understand the nature of such a modification. For example, one must take account of the fact that double scattering causes an excess of high momentum spectators. Therefore, to measure reaction cross sections based on a sample of events with a spectator momentum cut becomes considerably more complicated than just a simple correction using a deuteron wave function. Also, double scattering can modify the characteristics of the initial or final states of the reaction. These modifications are important in considering s-channel resonances, resonance production and reaction cross sections. The double scattering model developed here will be shown to be in excellent agreement with the data.

Some of the considerations discussed above were not applied by Abrams _et al._[1] in determining the total nucleon antinucleon cross sections for pure isospin one and isospin zero states. Using an impulse approximation, Abrams _et al._ reported the existence of two isospin one and one isospin zero enhancements between 1 and 3 GeV/c incident antiproton momentum.

The observation of a narrow bump near 2190 MeV was reported by Kalbfleisch _et al._[2] in the reaction $\bar{p}p \rightarrow \rho^\circ\rho^\circ\pi^\circ$. These authors suggested that it might provide a partial explanation for one of the I=1 enhancements (called π_1^* (2190)) observed in the total cross section measurement. However, Donald _et al._[3] and Handler _et al._[4] failed to confirm this effect in similar experiments. Since the $\bar{p}n$ system is a pure I=1 state, the effect should be twice as prevalent as that in a $\bar{p}p$ system. In this work, the reaction $\bar{p}n \rightarrow 2\pi^+3\pi^-$ is investigated for a possible s-channel enhancement near 2190 MeV.

As a by-product of this work, the $\bar{p}n$ reaction and topological cross sections involving 3 and 5 charged secondaries are measured and presented here.

CHAPTER II

EVENT AND FIT SELECTIONS

2.1 Introduction

The major fraction of the sample used in this work came from 150,000 triad exposure taken at the Brookhaven National Laboratory 31-inch deuterium filled bubble chamber. The incident antiproton momenta were 1.09, 1.19, 1.31, and 1.43 GeV/c. The film was divided into 72 sets with three views per set. Twenty-four of these sets were taken at 1.31 GeV/c and the remaining sets were evenly divided among the other momentum values.

Only a certain subset of the interactions visible on the film was used in this study. This subset consisted of any event in which the antiproton appears to interact with the neutron and result in 3 or 5 charged secondaries. First, a set of events satisfying the scanning criteria was measured. Then, the relevant events were obtained by a kinematic analysis of these events.

2.2 Selection of the Events to be Measured

The desired sample consists of events in which the antiproton appears to interact with the neutron and produce

3 or 5 visible charged particles. Depending on its momentum, the spectator proton may or may not produce a visible track in the bubble chamber. Therefore, events of interest will have 3, 4, 5 or 6 outgoing tracks. These events will be referred to as 3, 4, 5 or 6 prong events. In the even prong events, one of the positive tracks is assumed to be the spectator proton.

Using the above considerations, a set of rules was set up to determine if an event is to be measured. These rules were devised to select all the desired events with as little contaminations as possible. The events satisfying any of the following criteria were measured:

A) Any three or five prong event.

B) Any four or six prong event with a stopping proton. (A stopping proton is defined by a heavily ionizing track with three or less gaps. It must not resemble the characteristic manner, of $\pi\mu e$ decay.)

C) Any four or six prong event if the ionization density of one of the positive tracks is equal to or greater than that of the beam in all three views. This track must not decay in the manner of $\pi\mu e$. (See Figure 2.1 for the definition of a positive track.)

In addition, only the events due to a beam track interacting

Figure 2.1

Typical Bubble Chamber Photograph

The fiducial volume is defined between the two lines. The antiprotons enter the chamber at the bottom of the Figure. Three events are shown:

A) Four Prong Event with a Stopping Proton. The stopping proton is at the 8 o'clock position. A track produced by a π^+ is at the 4 o'clock position. Two remaining tracks were produced by π^-.

B) Four Prong Event with a Fast Proton. The fast proton is the positive track at the 2 o'clock position. This track has a greater ionization than the other tracks in the event.

C) Five Prong Event. The positive track at the 9 o'clock position is not a proton, despite its high ionization, because it is observed to decay. (Note the light track which is produced as a result of the decay.)

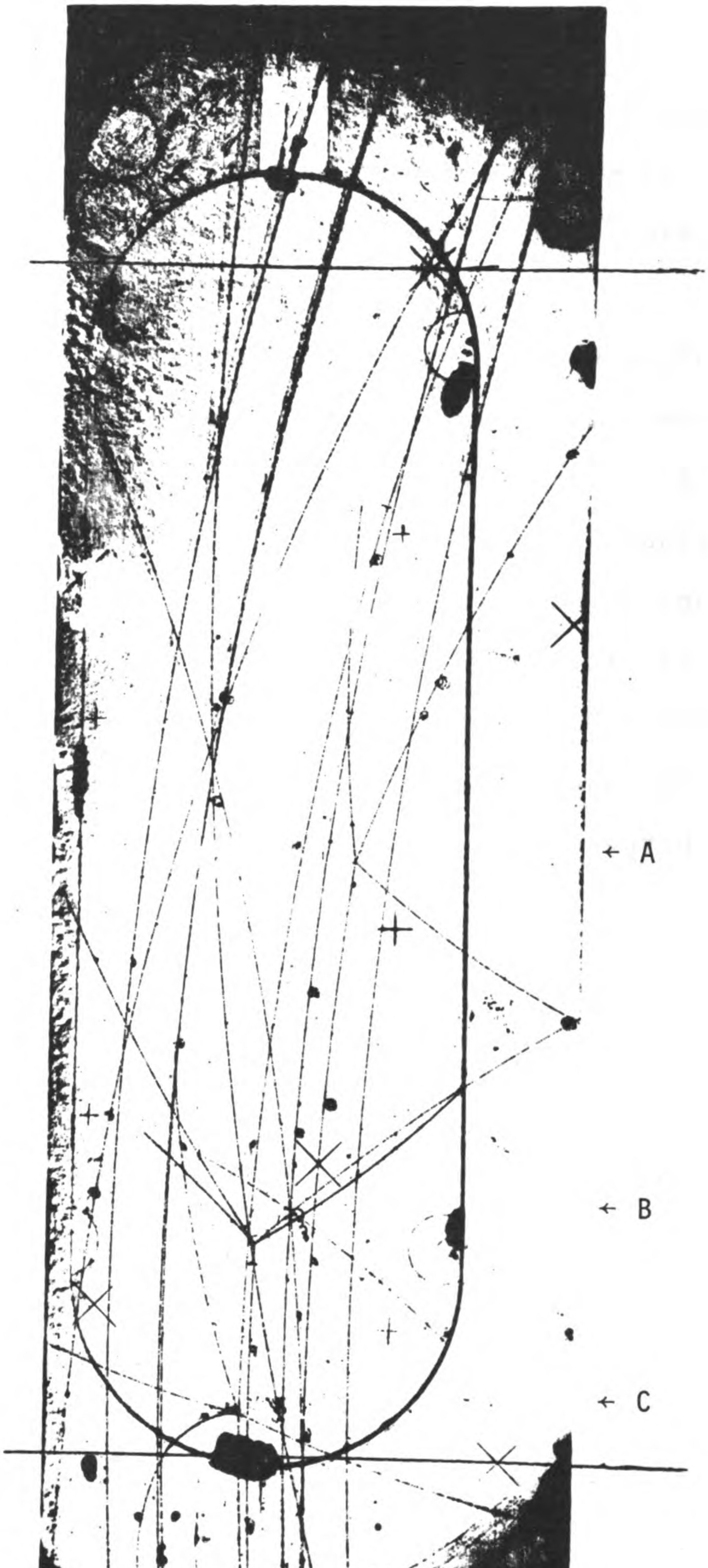
A
B
C

within the fiducial volume of the chamber (see Figure 2.1) were measured. Events with the vertex obscured by other tracks were not measured but were recorded for correction purposes.

Category A contains events in which the proton is moving too slow to produce a visible track. The momentum of these protons is usually less than 100 MeV/c. A proton having a momentum greater than 100 MeV/c will usually produce a visible track in the chamber. Category B contains events with a visible stopping proton. Most of the remaining desired events are contained in category C. These events usually have protons with a momentum greater than about 200 MeV/c. Table 2.1 summarizes the measured sample of events.

Table 2.1

Total Events Measured

Momentum GeV/c	3 Prong	4 Prong	5 Prong	6 Prong
1.09	5418	7495	2519	2341
1.19	7943	10164	3670	3398
1.31	14457	1853	7053	6578
1.43	9898	12868	4566	4528

2.3 Processing the Measured Sample

The events selected in Section 2.2 were then measured using an image plane digitizer (IPD). This machine projects the film onto a surface. The x and y coordinates of several points on the image of each track were recorded on a magnetic tape for three stereo views. Then, the data on the tape were processed through the PANAL[9] - TVGP[10] - SQUAW[11] chain of programs. The PANAL program converts the data from the IPD machine to a form suitable for TVGP. TVGP uses the PANAL output to reconstruct the tracks in a three dimensional space from the optical properties of the chamber and the known value of the magnetic field in the chamber. The particles that produced outgoing tracks were assumed to have a mass of a π, k, or p. The reconstructed track information for a given event was then used by SQUAW to perform kinematic fits. The reaction hypotheses are listed in Table 2.2 A summary of the number of fitted events on the final tape written by SQUAW is presented in Table 2.3.

Table 2.2

Reaction Hypotheses

3 or 4 Prong Events

Reaction	Number of Constraints	Mark Number
$\bar{p}d \rightarrow p_s p p \pi^-$	4	3
$\bar{p}d \rightarrow p_s \pi^+ 2\pi^-$	4	8
$\bar{p}d \rightarrow p_s k^+ k^- \pi^-$	4	30
$\bar{p}d \rightarrow p_s \pi^- 2\pi^- \pi^\circ$	1	9
$\bar{p}d \rightarrow p_s \pi^+ 2\pi^- + mm$	0	10
$\bar{p}d \rightarrow p_s k^+ k^- \pi^- + mm$	0	31
$\bar{p}d \rightarrow p_s p \bar{p} \pi^- + mm$	0	5
$\bar{p}d \rightarrow n_s 2\pi^+ 2\pi^-$	1	16
$\bar{p}d \rightarrow n_s 2\pi^+ 2\pi^- + mm$	0	17

5 or 6 Prong Events

Reaction		
$\bar{p}d \rightarrow p_s 2\pi^+ 3\pi^-$	4	8
$\bar{p}d \rightarrow p_s k^+ k^- \pi^+ 2\pi^-$	4	30
$\bar{p}d \rightarrow p_s 2\pi^+ 3\pi^- \pi^\circ$	1	9
$\bar{p}d \rightarrow p_s 2\pi^+ 3\pi^- + mm$	0	10
$\bar{p}d \rightarrow p_s k^+ k^- \pi^+ 2\pi^- + mm$	0	31
$\bar{p}d \rightarrow n_s 3\pi^+ 3\pi^-$	1	16
$\bar{p}d \rightarrow n_s 3\pi^+ 3\pi^- + mm$	0	17

Table 2.3

Events on the Final Tape

Momentum GeV/c	3 Prong	4 Prong	5 Prong	6 Prong
1.09	5063	6937	2285	2060
1.19	7567	9411	3347	2945
1.31	13634	17274	6379	5791
1.43	9427	12062	4164	3970

2.4 Fit Selection

The SQUAW program often gives acceptable fits to several kinematic hypotheses for each event. Therefore, a procedure to select the correct fit was devised. This procedure was to compare the projected ionization density of the outgoing tracks predicted by mass interpretation of a given fit to the projected ionization of the data. It was often necessary to examine the event in all three views in order to determine the mass of the particle that produced the track. The chosen fit was required to be consistent with the results of the ionization scan. The comparison indicated that fits involving the four constraint reactions $\bar{p}d \rightarrow p_s\bar{p}p\pi^-$, $\bar{p}d \rightarrow p_s\pi^+2\pi^-$, and $\bar{p}d \rightarrow p_s2\pi^+3\pi^-$ could be reliably selected using kinematic criteria. This was done by requiring the missing mass squared (the square of the magnitude of the missing four momentum) to be within two standard deviations of zero. If the event had a multiple fit involving these reactions, the fit with the highest confidence level was chosen.

For the remainder of the events, the fit ambiguities could not be resolved on an event by event basis by using the missing mass squared and confidence level. A large fraction of these events were contained in category C (see Section 2.2). Therefore, an ionization scan was performed on all events in category C, which contains about 40,000 events, to settle the ambiguities involving the mass interpretations of tracks. In addition, events with either $\bar{p}d \rightarrow p_s k^+ k^- \pi^-$ or $\bar{p}d \rightarrow p_s k^+ k^- 2\pi^- \pi^+$ fits were checked in the ionization scan. These fits were assigned to an event only if the ionization density predicted by the fit agrees with the observed ionization density.

In addition to producing charged particles, annihilation reactions may also produce neutral particles. The fit hypotheses involving neutral particles are zero constraint or one constraint fits (see Table 2.2). Non-strange neutral particles are often not observable in a bubble chamber. Therefore, the total four momentum of the neutral particles cannot be directly measured. However, it can be inferred using conservation of four momentum for a given reaction. If only one neutral particle is produced, the square of the "missing" four momentum, which is called the missing mass squared, is equal to the mass squared of the particle. In the case of two or more neutral particles, the missing mass squared is equal to the center of mass energy squared of the neutral particle system. If no neutral particles are produced, the missing mass squared is zero. Since the resolution of the measuring system is folded into the missing mass squared distribution, the peaks due to the one constraint or four constraint type reactions acquire a characteristic width.

The missing mass squared distribution can be used to determine the number of events involving single π° production. This is done by examining the missing mass squared distribution for events having track ionization consistent with a fit hypothesis of the type $\bar{p}d \rightarrow p_s$ + charged pions + neutral particles. Since the events producing only charged particles have already been assigned fits, these are not included in the distributions. The resulting missing mass squared distributions are shown in Figure 2.2. In each plot, a prominent peak at the π° mass squared is seen. The sum of the shaded area and unshaded area represent the total missing mass squared distribution for single π° events and multi-neutral events. The events in the unshaded area, which represent candidates for single π° production, were obtained by requiring the missing mass squared of events with a fit hypothesis involving a single π° to be within two standard deviation of the mass squared

Figure 2.2

Missing Mass Squared Distributions

Zero constraint fits - shaded area
One constraint fits - unshaded area

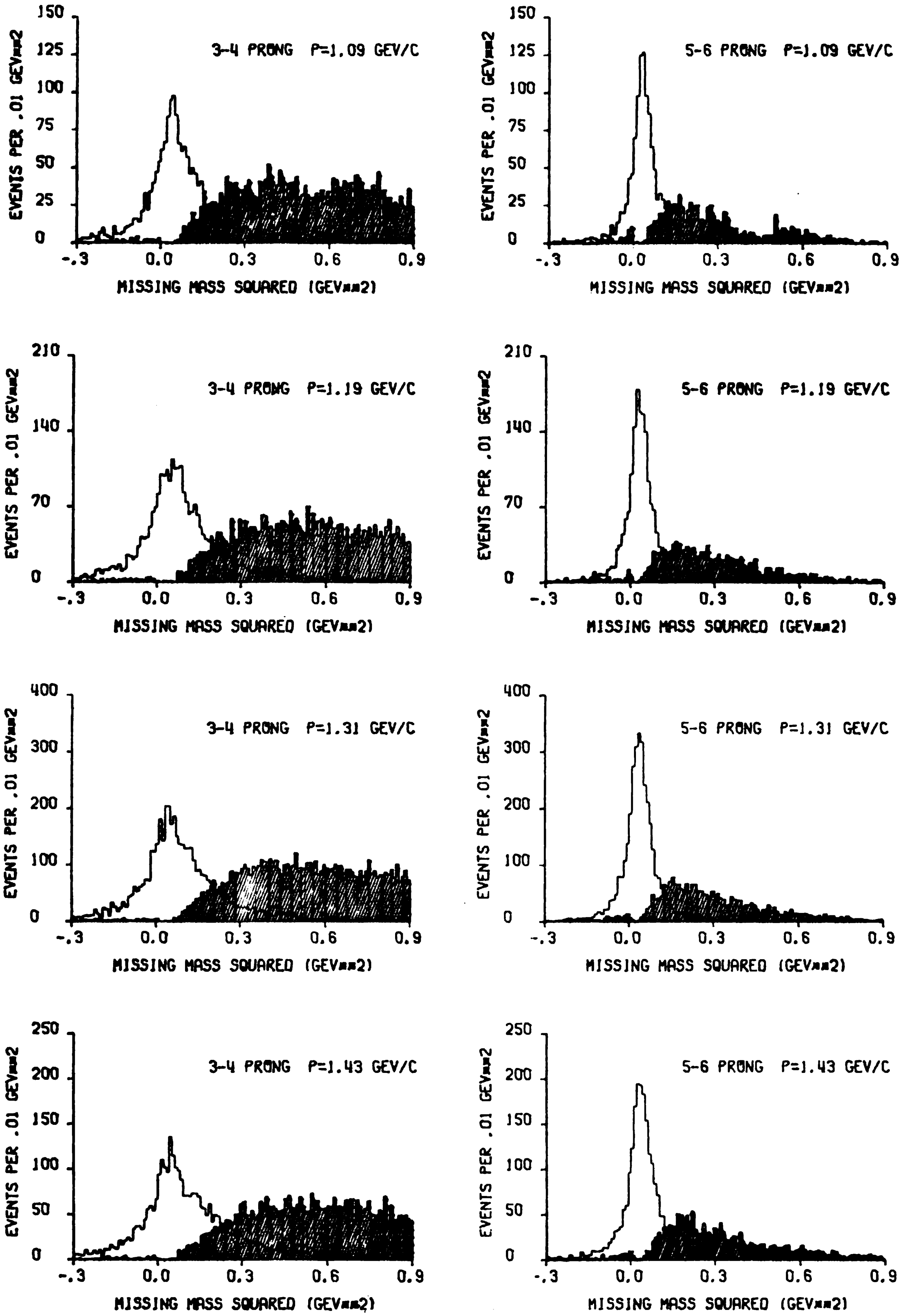
3-4 PRONG P=1.09 GEV/C
5-6 PRONG P=1.09 GEV/C
3-4 PRONG P=1.19 GEV/C
5-6 PRONG P=1.19 GEV/C
3-4 PRONG P=1.31 GEV/C
5-6 PRONG P=1.31 GEV/C
3-4 PRONG P=1.43 GEV/C
5-6 PRONG P=1.43 GEV/C
EVENTS PER .01 GEV**2
MISSING MASS SQUARED (GEV**2)
-.3
0.0
0.3
0.6
0.9
0
25
50
75
100
125
150
70
140
210
200
300
400
250

of a π°. The shaded area represents events producing two or more neutral particles.

The π° peaks, particularly the three and four prong topologies, appear to be asymmetric with respect to the known π° mass squared value. Therefore, the number of events for single π° production channels must be corrected. The correct number of events is found by splitting the π° peak at the π° mass squared. Unlike the high mass side of the π° peak, the low mass side is not contaminated by multi-neutral type events. Therefore, the number of single π° production events is found by doubling the number of events in the low mass side of the π° peak.

CHAPTER III

ANTIPROTON NEUTRON TOPOLOGICAL AND REACTION CROSS SECTIONS

3.1 Introduction

The cross section, σ, is related to the probability that an incident particle will interact with a particle in the target. If the beam intensity is initially I_o, then the cross section can be defined by:

$$I = I_o \, e^{-n\sigma x} \qquad (3.1)$$

Here, I is the intensity of the beam after it has traveled a distance x into the target and n is the number of target particles per unit volume.

In $\bar{p}d$ interaction, several different final states result when the antiproton interacts with the deuteron. Therefore, the total cross section is a sum of partial cross sections representing each final state. This chapter presents the cross sections due to antiproton neutron interactions resulting in final states with 3 or 5 charged particles and zero or more neutral particles. The $\bar{p}n$ reactions are assumed to be characterized by the presence of a spectator proton. The fact that the proton may screen the neutron from the antiproton is taken into consideration.

3.2 Cross Section Equivalent for an Event

The cross section equivalent for an event, R, can be used to determine the cross section for a given topology if the number of events corresponding to the given reaction or topology is known. The value of R can be found from the total $\bar{p}d$ cross section, σ_t, by defining a reaction volume and counting the number of beam particles, N_b, entering the reaction volume. These numbers can be used to determine the total number of interactions in the reaction volume by:

$$N_t = N_b\,(1 - e^{-\ell/\ell_o}). \tag{3.2}$$

Here, ℓ is the effective length of the reaction volume and ℓ_o is given by:

$$\ell_o = 2/(\sigma_t \rho A_o). \tag{3.3}$$

The quantities A_o and ρ are the Avagodro number and the density of liquid deuterium respectively. The reaction volume was defined by:

$$-10.0 \leq x \leq 10.0 \text{ cm}, \tag{3.4a}$$

and $$-24.0 \leq y \leq 17.6 \text{ cm}, \tag{3.4b}$$

where x and y are coordinates measured from the center of the bubble chamber. Values for σ_t were taken from reference 1 and the effective length of the reaction volume was calculated by Mountz.[12] A detailed discussion of N_b is presented in Appendix B. Then, R can be found by:

$$R = \sigma_t/N_t. \tag{3.5}$$

However, in a bubble chamber, not all the interactions are visible. The invisible or missing interactions are due to low t elastic scattering. In Appendix E, the amount of missing cross section, σ_m, is estimated. To account for the effects of this missing cross section, σ_t was replaced by the observable part of the cross section σ_t-σ_m. The value of R, however, is not very sensitive to this change. The change in R due to this correction is less than 1%. Table 3.1 summarizes the numbers used in the calculation of R.

Table 3.1

Cross Section Equivalent for an Event

Momentum	Number of Beams	ℓ(cm)	σ_t(mb)	σ_t-σ_m(mb)	R(μb/event)
1.09	168924	41.96	200.31	200.31	3.880
1.19	258789	41.94	195.56	166.66	2.523
1.31	498757	41.68	191.50	162.60	1.312
1.43	331612	41.79	184.56	155.66	1.957

3.3 Scanning, Measuring, and Systematic Losses

To calculate the cross section from R, the true number of events involving the desired reaction must be known. The final sample does not contain all the $\bar{p}n$ events because of scanning, measuring, and systematic losses. These losses must be determined before the cross sections can be obtained.

To determine the scanning efficiency, ε_s, a sample of film was rescanned and the resulting event sample was compared to the original event sample. Since the loss of events is assumed to be random, the scanning efficiency can be calculated using the number of events in common between the two scans and the number of events contained in one scan but not the other. The resulting values of ε_s are listed below. Scanning efficiencies in category C have no significant difference, within statistical uncertainty, for different beam momenta. Therefore, scanning efficiencies for the combined four or combined six prong samples are used. Appendix B gives the details of the calculation.

Measured events that do not appear on the final data tape are due to measuring losses. These losses are taken into account by the measuring efficiency, ε_m, which is calculated in Appendix C. The resulting measuring efficiencies are presented in Table 3.3.

Table 3.2

Scanning Efficiencies

Categories A & B Events		Category C Events	
p(GeV/c)	ε_s	Event Type	ε_s
1.09	.901±.007	4 Prong	.836±.004
1.19	.871±.006	6 Prong	.857±.007
1.31	.872±.006		
1.43	.883±.005		

Table 3.3

Measuring Efficiencies

p(GeV/c)	3 Prong	4 Prong	5 Prong	6 Prong
1.09	.938±.0034	.930±.0030	.911±.0050	.884±.0067
1.19	.957±.0024	.930±.0026	.916±.0047	.871±.0058
1.31	.947±.0019	.938±.0018	.908±.0035	.884±.0040
1.43	.956±.0021	.941±.0021	.916±.0042	.881±.0049

In addition to the scanning and measuring inefficiencies, events with apparent proton ionization higher than that of the beam track were rejected by scanners due to criterion C (see Section 2.2). This was due to a judgment error of the scanner and caused a loss of some events having high momentum protons. Since these events were not lost at random, this effect cannot be accounted for by the scanning efficiency. The losses due to this effect are calculated in Appendix E. The true number of events can be found from the number of measured events, N_o, and the number of unmeasured events, N_{loss} by:

$$N_e = (N_o + N_{loss})/(\varepsilon_s \times \varepsilon_m). \qquad (3.6)$$

The values of N_o and N_{loss} are presented in Appendices A and E.

3.4 Screening Corrections

To obtain the $\bar{p}n$ reaction cross sections, a correction must be made to account for the screening of the neutron by the proton. The screening correction factor is defined by:

$$S \equiv \frac{\sigma_{\bar{p}n} + \sigma_{\bar{p}p}}{\sigma_{\bar{p}d}} \qquad (3.7)$$

The values of S, calculated from cross sections in reference 1, are shown below.

Table 3.4

Screening Correction

Momentum (GeV/c)	Screening Correction S
1.09	1.10
1.19	1.10
1.31	1.10
1.43	1.11

The $\bar{p}n$ reaction cross sections are corrected for the screening effect by assuming that screening applies equally to all the reactions.

3.5 Topological and Reaction Cross Sections

By using the numbers discussed in Sections 3.2-3.4, the measured cross sections are given by:

$$\sigma = R(N_o + N_{loss})/(\varepsilon_m \times \varepsilon_s) \qquad (3.8)$$

The reaction cross sections for $\bar{p}n$ interaction are corrected for screening by multiplying by S. The results are summarized in Tables 3.5 and 3.6 and Figures 3.1-3.5. The higher momentum data of Eastman *et al.*[13] are shown for comparisons.

Table 3.5

$\bar{p}d \to p_s + \ldots$ Topological Cross Sections

Momentum (GeV/c)	3 Prong	4 Prong	5 Prong	6 Prong
1.09	17.73±.50	17.09±.65	8.41±.28	5.95±.29
1.19	17.65±.41	15.91±.54	8.34±.25	5.82±.23
1.31	16.99±.47	15.23±.46	8.26±.23	5.97±.23
1.43	16.93±.44	15.82±.51	7.94±.23	5.60±.23

Table 3.6

$\bar{p}n$ Reaction Cross Sections

3-4 Prong Events

Momentum GeV/c	$\bar{p}p\pi^-$	$\pi^+2\pi^-$	$\pi^+2\pi^-\pi^\circ$	$K^+K^-\pi^-$	Multi-neutral	Total
1.09	.26±.05	2.16±.17	11.38±.53	.24±.05	24.32±.88	38.36±1.45
1.19	.68±.07	1.80±.13	10.91±.45	.25±.06	23.28±.74	36.92±1.11
1.31	1.40±.08	1.61±.09	9.36±.33	.22±.04	22.86±.65	35.44± .98
1.43	2.59±.14	1.43±.10	8.93±.35	.26±.05	23.14±.70	36.35±1.04

5-6 Prong Events

Momentum GeV/c	$2\pi^+3\pi^-$	$2\pi^+3\pi^-\pi^\circ$	$K^+K^-\pi^+2\pi^-$	Multi-neutral	Total
1.09	4.08±.26	6.82±.37	.09±.03	4.82±.28	15.81±.62
1.19	4.01±.22	6.43±.29	.16±.03	4.99±.24	15.59±.50
1.31	3.68±.17	6.70±.24	.16±.03	5.12±.21	15.66±.45
1.43	3.40±.17	6.27±.27	.16±.03	5.19±.24	15.02±.48

Figure 3.1

Topological Cross Sections

x 3 prong $\bar{p}d \rightarrow p_s + \ldots$ topological cross section

■ 4 prong $\bar{p}d \rightarrow p_s + \ldots$ topological cross section

\- 5 prong $\bar{p}d \rightarrow p_s + \ldots$ topological cross section

□ 6 prong $\bar{p}d \rightarrow p_s + \ldots$ topological cross section

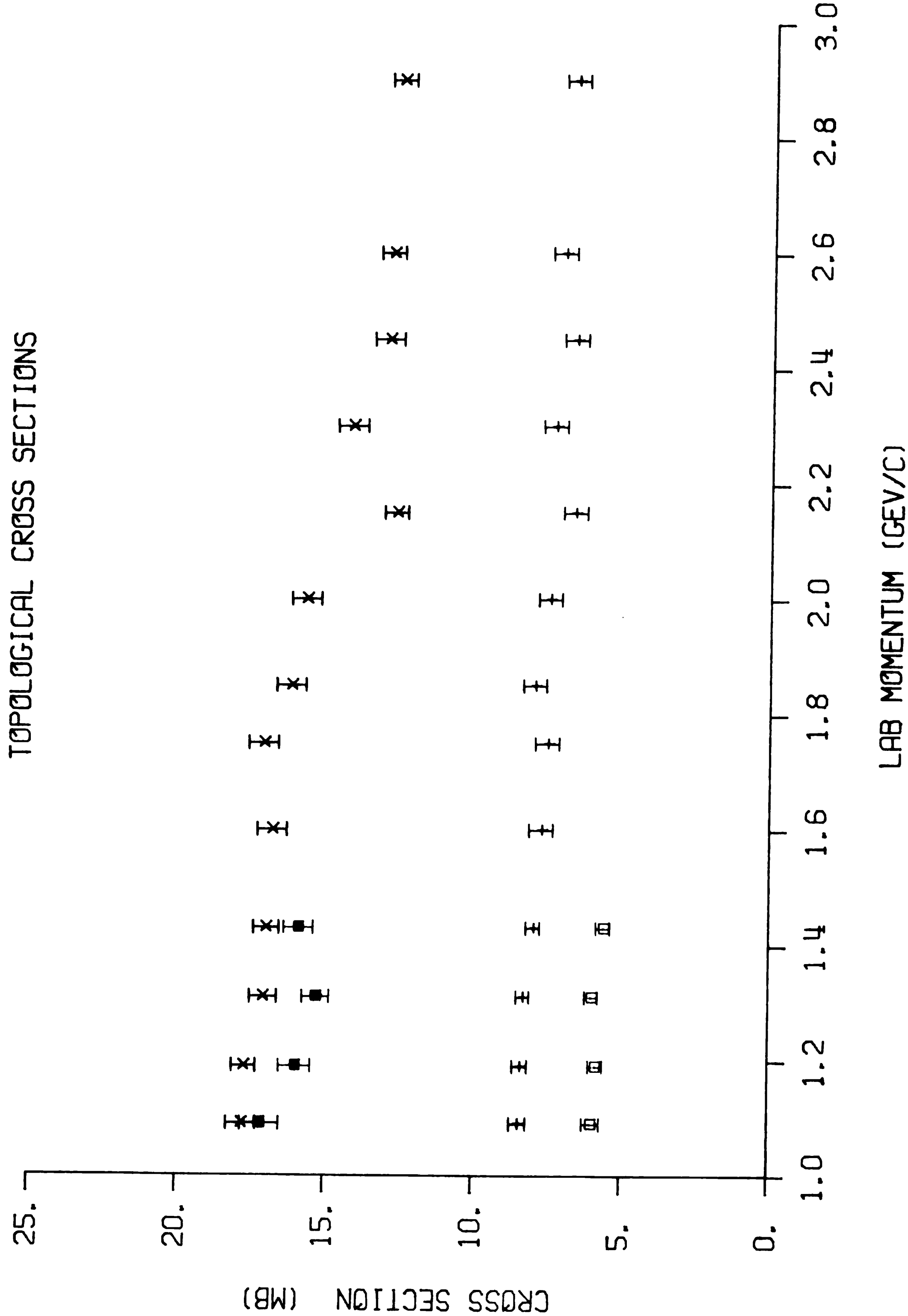
TOPOLOGICAL CROSS SECTIONS
CROSS SECTION (MB)
LAB MOMENTUM (GEV/C)
0.
5.
10.
15.
20.
25.
1.0
1.2
1.4
1.6
1.8
2.0
2.2
2.4
2.6
2.8
3.0

Figure 3.2

$\bar{p}n \rightarrow \bar{p}p\pi^-$ cross section

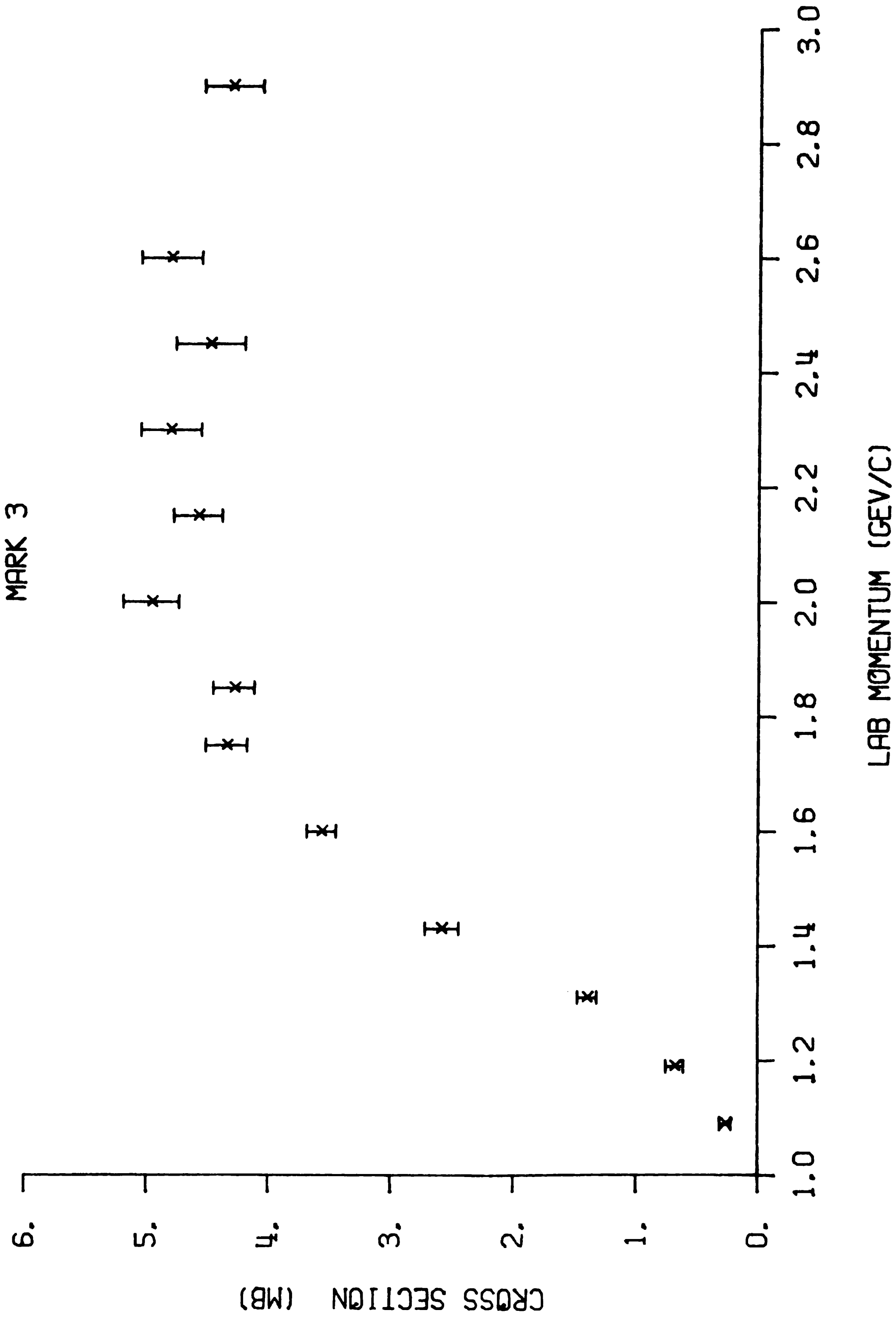
MARK 3
LAB MOMENTUM (GEV/C)
CROSS SECTION (MB)
1.0
1.2
1.4
1.6
1.8
2.0
2.2
2.4
2.6
2.8
3.0
0.
1.
2.
3.
4.
5.
6.

Figure 3.3

Cross sections for $\bar{p}n \rightarrow 2\pi^-\pi^+$
and $\bar{p}n \rightarrow 3\pi^-2\pi^+$

- $\bar{p}n \rightarrow 2\pi^-\pi^+$

x $\bar{p}n \rightarrow 3\pi^-2\pi^+$

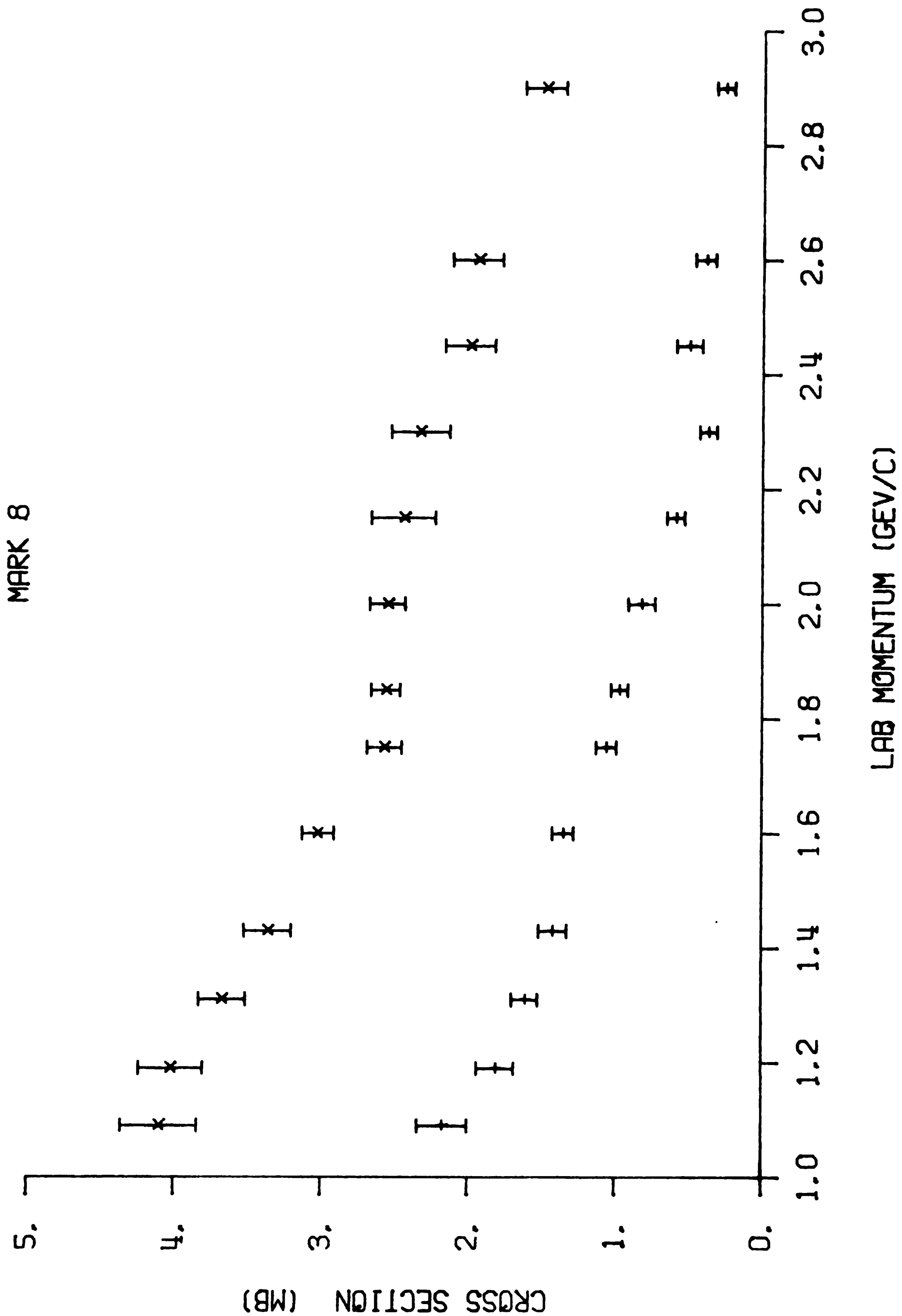
MARK 8
LAB MOMENTUM (GEV/C)
CROSS SECTION (MB)
1.0 1.2 1.4 1.6 1.8 2.0 2.2 2.4 2.6 2.8 3.0
0. 1. 2. 3. 4. 5.

Figure 3.4

$\bar{p}n \rightarrow 2\pi^-\pi^+\pi^o$ cross section

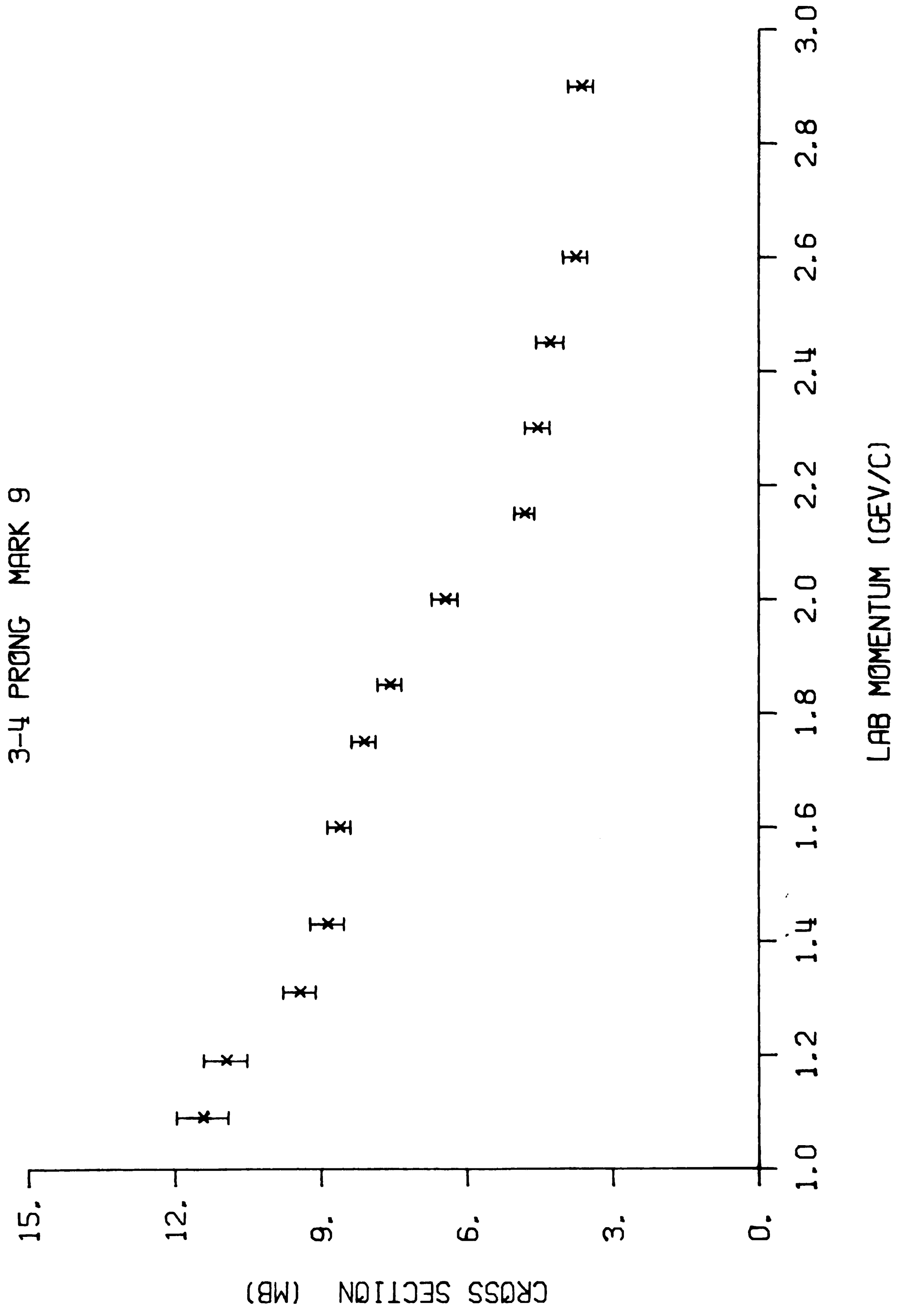
3-4 PRONG MARK 9
CROSS SECTION (MB)
LAB MOMENTUM (GEV/C)
0.
3.
6.
9.
12.
15.
1.0
1.2
1.4
1.6
1.8
2.0
2.2
2.4
2.6
2.8
3.0

Figure 3.5

$\bar{p}n \rightarrow 3\pi^-2\pi^+\pi^\circ$ cross section

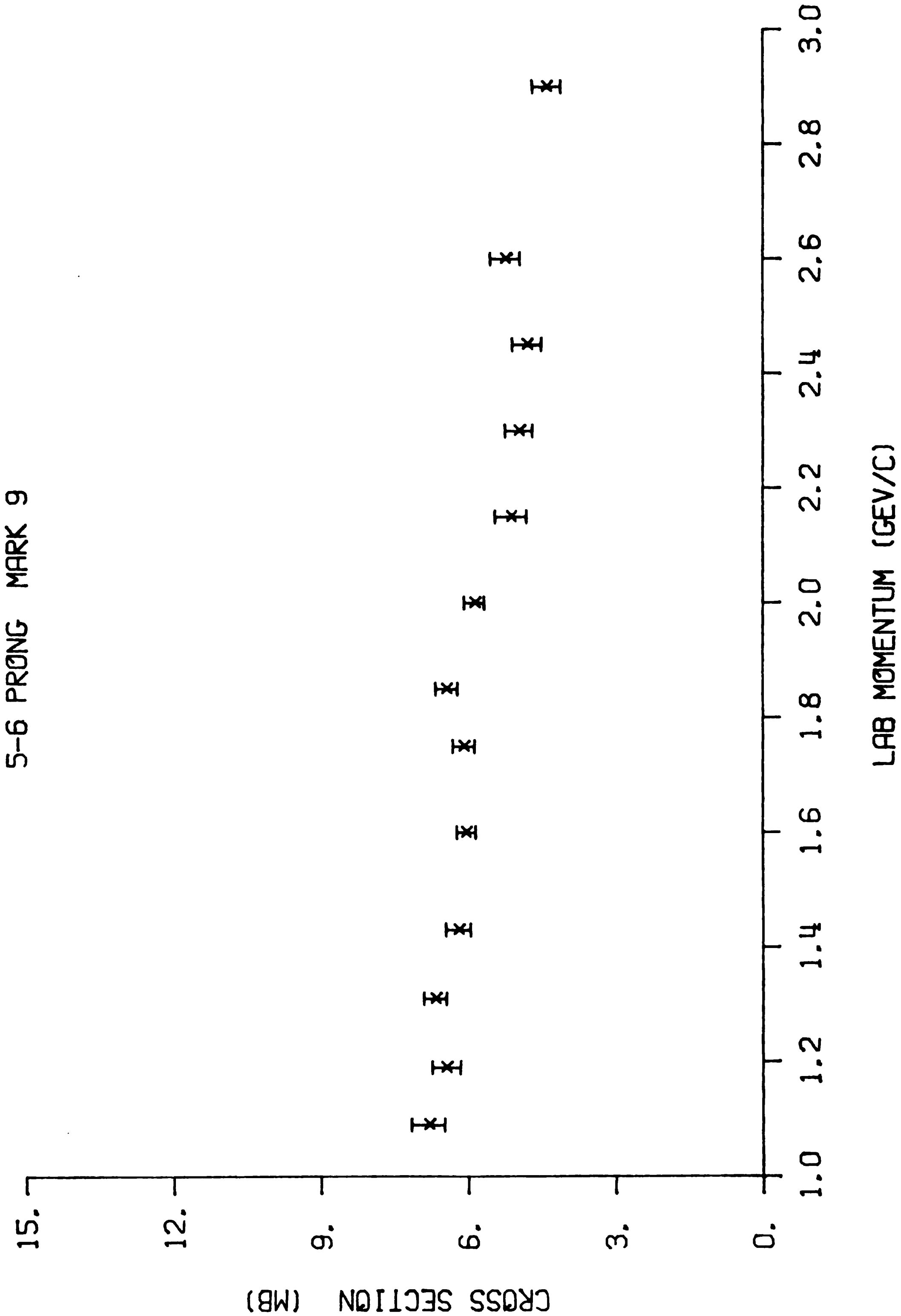
5-6 PRØNG MARK 9
LAB MØMENTUM (GEV/C)
CRØSS SECTIØN (MB)
0.
3.
6.
9.
12.
15.
1.0
1.2
1.4
1.6
1.8
2.0
2.2
2.4
2.6
2.8
3.0

CHAPTER IV

DOUBLE RHO PRODUCTION IN $\bar{p}n \rightarrow 3\pi^- 2\pi^+$

4.1 Introduction

In a high statistics counter experiment by Abrams *et al.*,[1] an enhancement near the center of mass energy of 2190 ± 10 MeV was observed in the total $\bar{p}d$ and $\bar{p}p$ cross sections. By assuming an impulse approximation for interactions on the deuteron and that the enhancement has a Breit-Wigner line shape, these authors deduced that this structure is an I=1 state with a width of 85 MeV. The reported height of this enhancement was 5.5 mb. Since this enhancement may be due to a resonance, a threshold effect or both, there have been several attempts to uncover its source.[2-8, 15] In studying the reaction $\bar{p}p \rightarrow 2\pi^+ 2\pi^- \pi^\circ$, Kalbfleisch *et al.*[2, 15] reported observation of a s-channel structure in the reaction $\bar{p}p \rightarrow \rho^\circ \rho^\circ \pi^\circ$. These authors suggested that this structure, having a mass of 2190 MeV and a width between 20 and 80 MeV, may be partially responsible for the 2190 MeV enhancement in the total $\bar{p}p$ cross section. However, Donald *et al.*[3] and Handler *et al.*[4] failed to confirm the Kalbfleisch result in similar experiments.

Since the $\bar{p}n$ system is a pure I=1 state and the $\bar{p}p$ system is an equal admixture of I=1 and I=0 states, an I=1 s-channel resonance should be twice as prevalent in the $\bar{p}n$ system. In particular, the reaction $\bar{p}n \rightarrow 3\pi^-2\pi^+$ should have an enhancement twice as large as the 0.5 ± .1 mb enhancement reported by Kalbfleisch in $\bar{p}p \rightarrow 2\pi^-2\pi^+\pi^\circ$ if the amplitude for producing the $\rho\rho$ system in an I=0 state is dominant. Kalbfleisch[15] suggested that the $\rho\rho$ sub-system is I=0 because their cross sections for $\rho^\circ\rho^\pm\pi^\mp$ show no bump while the $\rho^+\rho^-\pi^\circ$ cross section shows a "probable" bump. It is of interest to see if this enhancement is present in the reaction $\bar{p}n \rightarrow 3\pi^-2\pi^+$. Therefore, the intermediate states of the reaction $\bar{p}n \rightarrow 3\pi^-2\pi^+$, in particular the $\rho^\circ\rho^\circ\pi^-$ state, have been examined for possible s-channel structure.

4.2 The Reaction $\bar{p}n \rightarrow 3\pi^-2\pi^+$

The reaction $\bar{p}n \rightarrow 3\pi^-2\pi^+$ has been examined at thirteen different beam momenta values: 1.09, 1.19, 1.31, 1.43, 1.60, 1.75, 1.85, 2.00, 2.15, 2.30, 2.45, 2.60 and 2.90 GeV/c. The data were collected in three different bubble chamber experiments. The four lowest momentum values were from data described in Chapter II. The higher momentum values were taken in two different experimental runs in the Argonne National Laboratory 30-inch deuterium filled bubble chamber. The details of these data are described elsewhere.[13]

To be included in this analysis, an event must have a fit to the reaction $\bar{p}d \rightarrow p_s 3\pi^- 2\pi^+$ satisfying the criteria described in Section 2.4. In addition, the spectator proton momentum was required to be less than 190 MeV/c. The purpose of this cut is to remove events in which both nucleons participate in the scattering processes. The momentum distribution of protons from the reaction $\bar{p}d \rightarrow p_s 3\pi^- 2\pi^+$ shows evidence for this double scattering process (see Figure 4.1). The solid curves represent predictions of the deuteron wave function. As can be seen in the figure, there is a definite excess above 200 MeV/c. This excess is attributable to the double scattering effect and will be discussed in detail in Chapter V. All the data satisfying the above conditions are used to examine s-channel structure of the intermediate states of $\bar{p}n \rightarrow 3\pi^- 2\pi^+$ for possible resonances.

4.3 The Intermediate States in $\bar{p}n \rightarrow 3\pi^- 2\pi^+$

There are several possible intermediate states in the reaction $\bar{p}n \rightarrow 3\pi^- 2\pi^+$ involving the production of 2π, 3π, or 4π resonances. Table 4.1a lists the masses and widths of the well-known resonances and bumps which might be involved. To decide which of these resonances are produced in this reaction, the invariant mass distributions for each possible

Table 4.1a

Mass and Width of Pion Resonances and Bumps

Resonance	Mass (MeV)	Width (MeV)	Decay Mode
ρ°	745	135	2π
f	1269	156	2π
A_2	1310	100	$\rho\pi \rightarrow 3\pi$
A_3	1640	Broad	$f\pi \rightarrow 3\pi$
A_1	1070	Broad	$\rho\pi \rightarrow 3\pi$
g	1680	160	4π

Table 4.1b

Charge and Number of Combinations

System	Charge	Number of combinations/event
2π	-2	3
2π	0	6
2π	+2	1
3π	-3	1
3π	-1	6
3π	+1	3
4π	-2	2
4π	0	3

Figure 4.1

Momentum Distributions of Protons from the Reaction $\bar{p}d \rightarrow p_s\ 3\pi^-2\pi^+$

A) Events from the data with beam momenta of 1.09, 1.19, 1.31, and 1.43 GeV/c.

B) Events from the data with beam momenta of 1.60, 1.75, 1.85, and 2.00 GeV/c.

Also shown is the expectation distribution of the internal Fermi momentum of the deuteron. This distribution has been normalized to the data below 190 MeV/c.

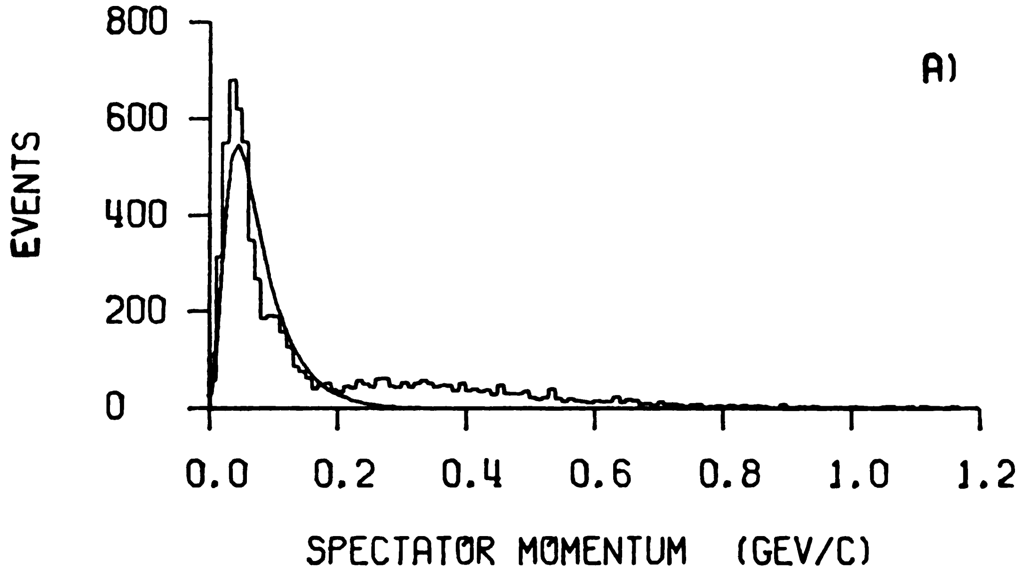
800
600
400
200
0
EVENTS
A)
0.0
0.2
0.4
0.6
0.8
1.0
1.2
SPECTATOR MOMENTUM (GEV/C)

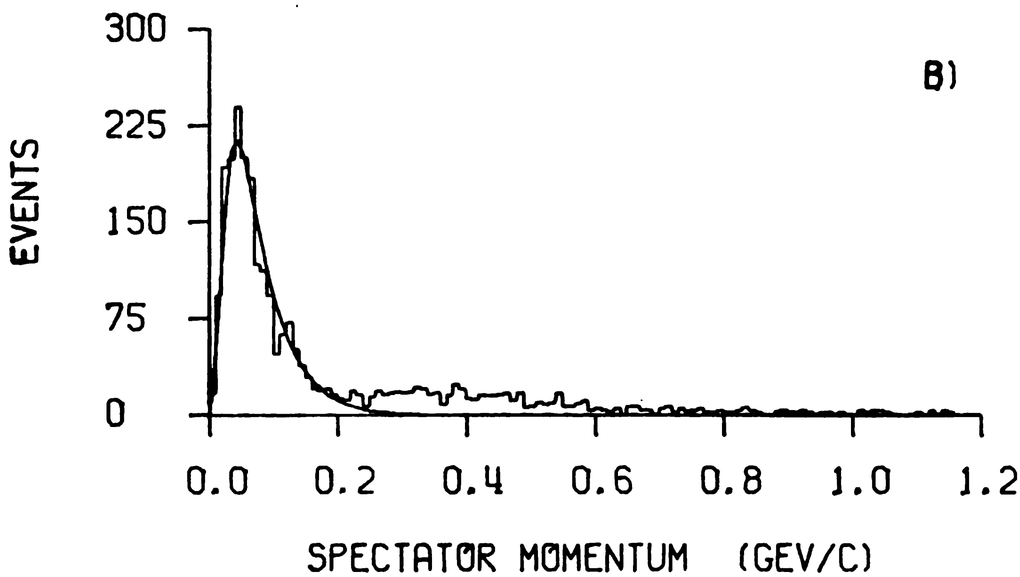
300
225
150
75
0
EVENTS
B)
0.0
0.2
0.4
0.6
0.8
1.0
1.2
SPECTATOR MOMENTUM (GEV/C)

2π, 3π, and 4π charge states were examined. These distributions, which are shown in Figure 4.2, contain events from the four lowest incident beam momentum settings. Table 4.1b shows the possible charge states and the corresponding number of pion combinations. Inspection of the invariant mass distributions show that the ρ° is the only resonance that is obviously present. Similarly, the higher momentum data also involve only ρ° production.[54] Therefore, for the purpose of this work, it will be assumed that the $\bar{p}n$ annihilation into five charged pions can only proceed by the following reactions:

$$\bar{p}n \rightarrow 3\pi^- 2\pi^+ \tag{4.1a}$$

$$\bar{p}n \rightarrow \rho^\circ 2\pi^- \pi^+ \tag{4.1b}$$

$$\bar{p}n \rightarrow \rho^\circ \rho^\circ \pi^- \tag{4.1c}$$

These reactions will be referred to as nonresonant, single rho, and double rho production respectively.

To determine the fractional amounts of each type of production, distinguishing characteristics must be found. There are six possible $\pi^+\pi^-$ pairs in the $3\pi^-2\pi^+$ final state which could be a ρ° candidate. For single rho or double rho production, only one or two of these pairs are in the ρ° signal. The remaining $\pi^+\pi^-$ pairs comprise the background distribution. Both the shape of the background distribution and the fractional amount of $\pi^+\pi^-$ pairs in the ρ° signal

Figure 4.2

Invariant Mass Distribution of Pion Systems
(1666 Events)

(A) $\pi^+\pi^-$ Invariant Mass

(B) $\pi^-\pi^-$ Invariant Mass

(C) $\pi^+\pi^+$ Invariant Mass

(D) $\pi^-\pi^+\pi^+$ Invariant Mass

(E) $\pi^-\pi^-\pi^+$ Invariant Mass

(F) $\pi^-\pi^-\pi^-$ Invariant Mass

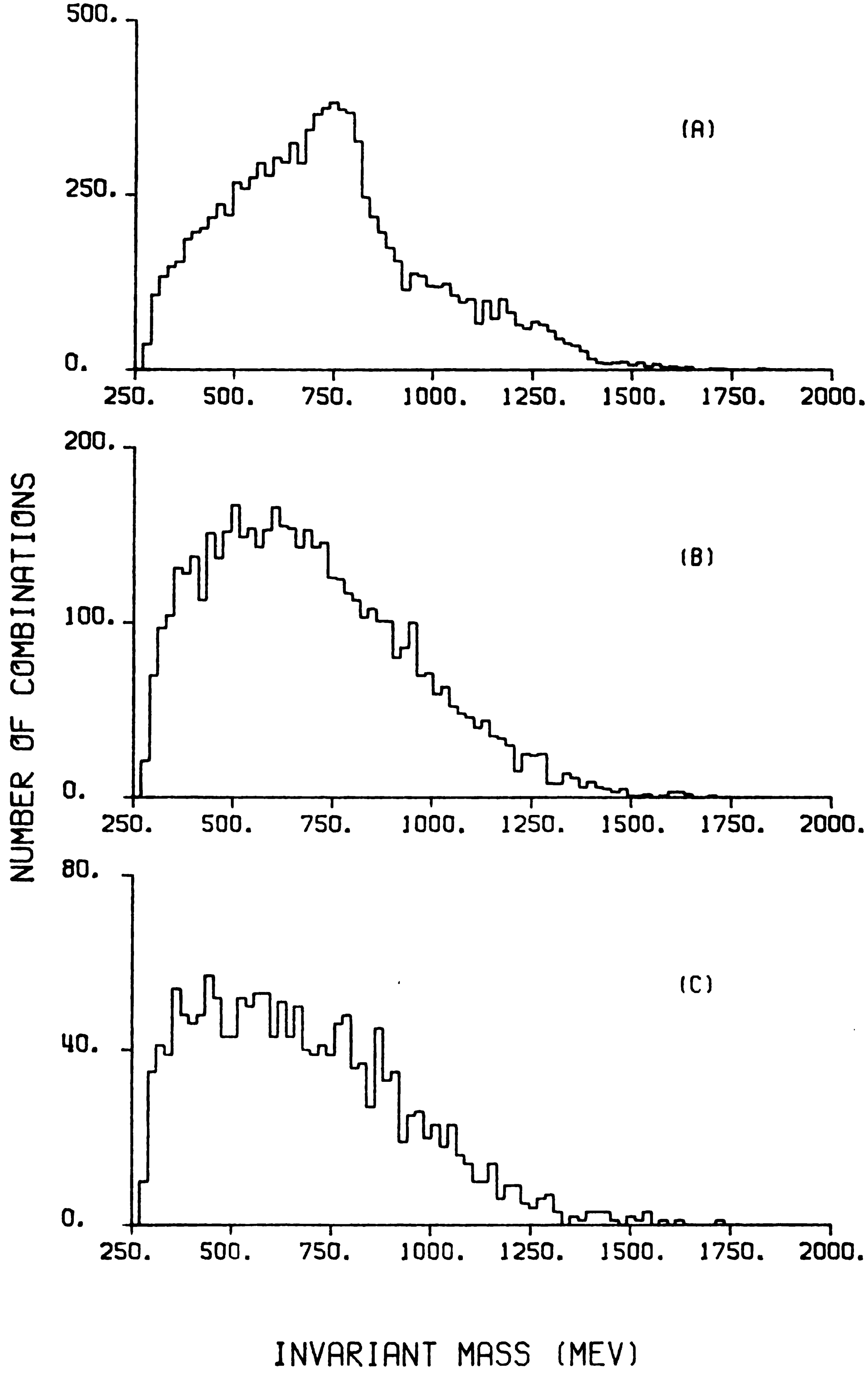
500.
250.
0.
250. 500. 750. 1000. 1250. 1500. 1750. 2000.
(A)
200.
100.
0.
250. 500. 750. 1000. 1250. 1500. 1750. 2000.
(B)
80.
40.
0.
250. 500. 750. 1000. 1250. 1500. 1750. 2000.
(C)
NUMBER OF COMBINATIONS
INVARIANT MASS (MEV)

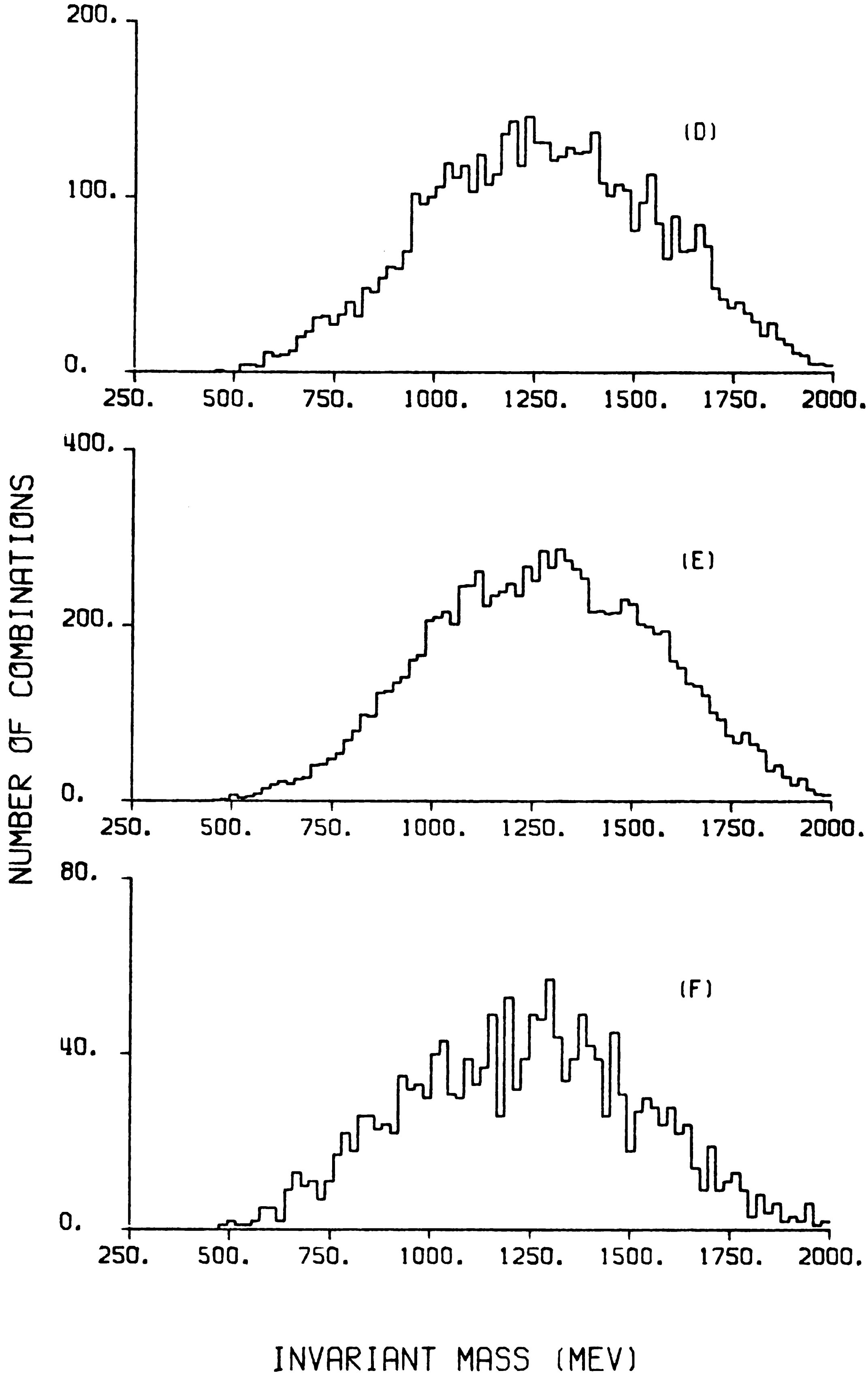

200.
100.
0.
(D)
250.
500.
750.
1000.
1250.
1500.
1750.
2000.
400.
200.
0.
(E)
80.
40.
0.
(F)
NUMBER OF COMBINATIONS
INVARIANT MASS (MEV)

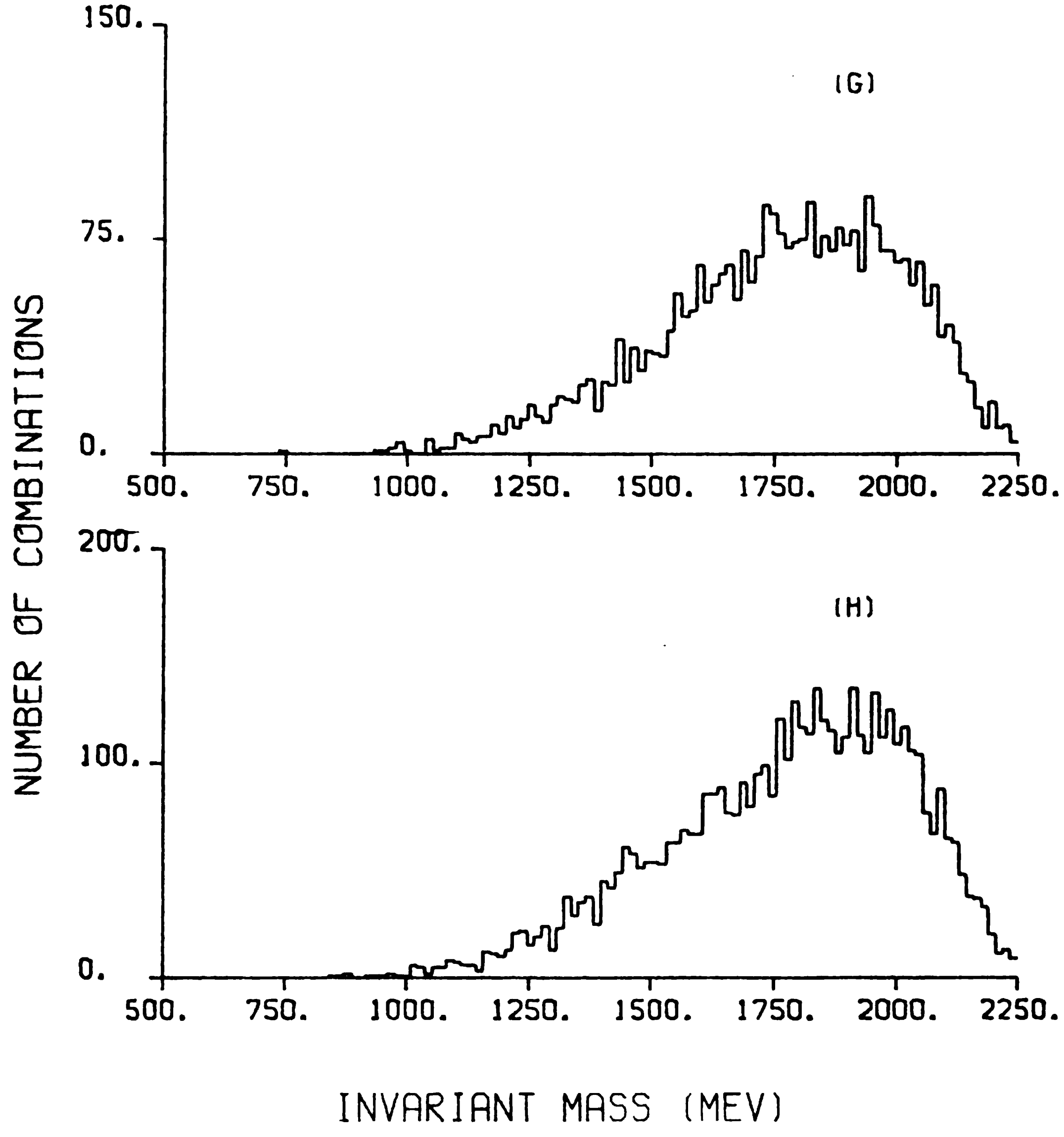
150.
75.
0.
(G)
500.
750.
1000.
1250.
1500.
1750.
2000.
2250.
200.
100.
0.
(H)
500.
750.
1000.
1250.
1500.
1750.
2000.
2250.
NUMBER OF COMBINATIONS
INVARIANT MASS (MEV)

depend on amounts of each type of production. The features of each type of production were simulated using the Monte Carlo event generating program SAGE.[16] In each case, a simple statistical model type mechanism is assumed. The results show that the $\pi^+\pi^-$ invariant mass distributions involving nonresonant production, single rho background and double rho background are similar in shape. This is shown in Figure 4.3. The main difference between single rho and double rho production appears to be in the fractional amounts of $\pi^+\pi^-$ pairs in the $\rho°$ signal. For single rho production 1/6 of the $\pi^+\pi^-$ pairs are contained in the $\rho°$ signal. The corresponding number for double rho production is 1/3.

Because of the similarities in the invariant mass distributions, it is possible for a combination of nonresonant production and double rho production to look like single rho production. Therefore, an anticorrelation between the amount of $\rho°\rho°\pi^-$ and $\rho°2\pi^-\pi^+$ is expected in fitting the $\pi^+\pi^-$ mass distributions to the data.

4.4 Analysis Procedures

The $\pi^+\pi^-$ invariant mass distribution of the data is assumed to be the sum of the Monte Carlo generated $\pi^+\pi^-$ invariant mass distributions for nonresonant, $\rho°2\pi^-\pi^+$ and $\rho°\rho°\pi^-$ channels. Fitting was done using the following expression:

Figure 4.3

Nonresonant and Double Rho Background
$\pi^{+}\pi^{-}$ Invariant Mass Distributions

The dashed curve is the nonresonant invariant mass distribution. The solid curve is the double rho background invariant mass distribution.

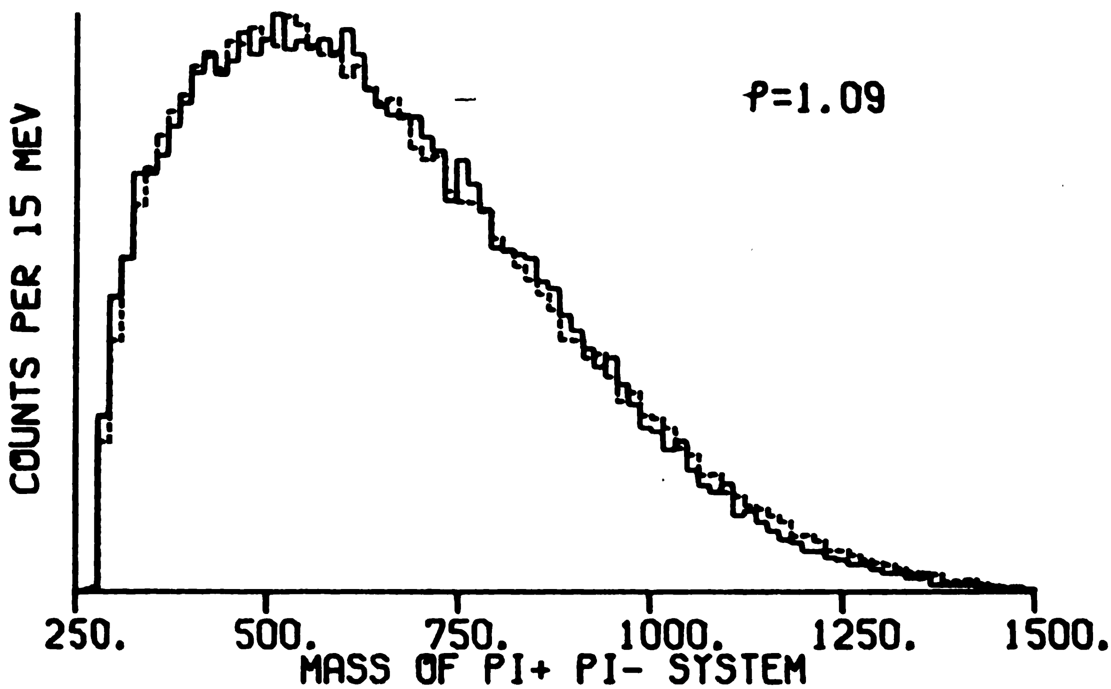
ρ=1.09
COUNTS PER 15 MEV
250.
500.
750.
1000.
1250.
1500.
MASS OF PI+ PI- SYSTEM

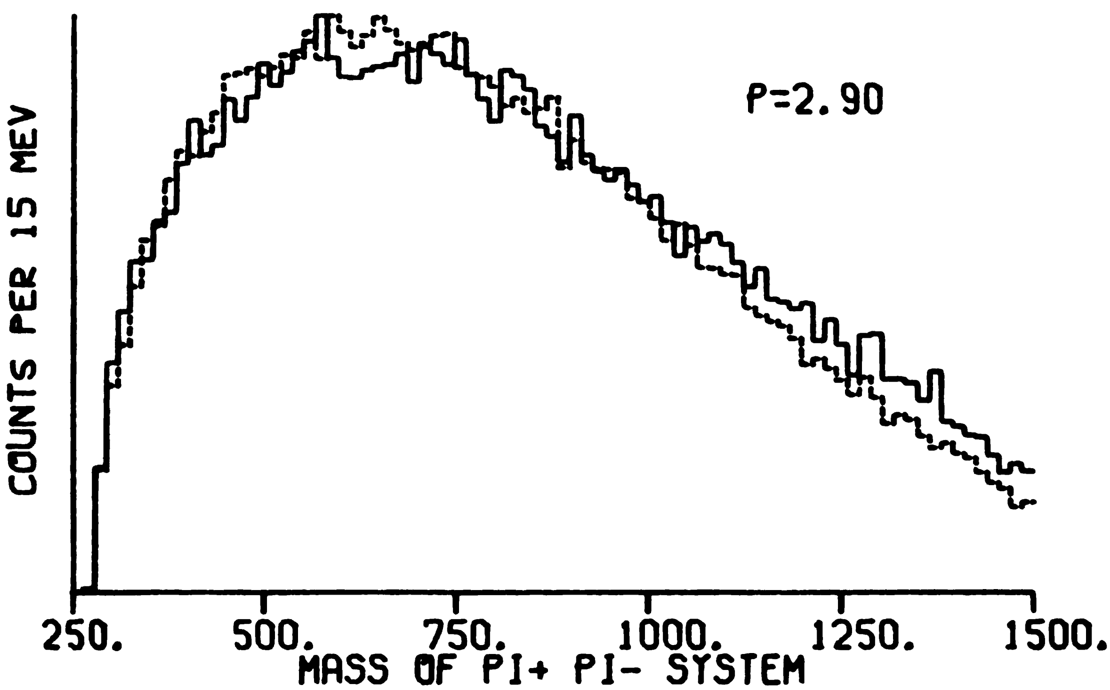
ρ=2.90
COUNTS PER 15 MEV
250.
500.
750.
1000.
1250.
1500.
MASS OF PI+ PI- SYSTEM

$$M = (1 - A - B)\, M_n + AM_s + BM_d \qquad (4.2)$$

Here, M_n, M_s, and M_d are the $\pi^+\pi^-$ invariant mass distributions of the nonresonant, $\rho^\circ 2\pi^-\pi^+$, and $\rho^\circ\rho^\circ\pi^-$ Monte Carlo events respectively. The sums of each of these Monte Carlo distributions are normalized to the sum of the data sample. The quantities A and B are fit parameters corresponding to the fractional amounts of $\rho^\circ 2\pi^-\pi^+$ and $\rho^\circ\rho^\circ\pi^-$ production.

The center of mass energy (ECM) for each beam momentum setting is not well defined. This is caused by the resolution in beam momentum, energy loss of the beam as it passes through the chamber, and the Fermi momentum of the nucleons in the deuteron. A spread of ±17 MeV in the center of mass energy is caused by the Fermi momentum of the target. The energy resolution of the beam and energy loss in the chamber each cause a ±2 MeV spread in ECM. In addition, experimental measurement errors cause a ±10 MeV resolution error in ECM. Combining these errors in quadrature gives a ECM resolution of ±20 MeV. Since this spread could inhibit the observation of s-channel structure, least squares fits were made to determine parameters in Equation 4.2 for each beam momentum setting as well as for data grouped in 40 MeV center of mass energy (ECM) bands. The fitted results for each ECM band were used in the next section to calculate the probability of having an enhancement in $\rho^\circ\rho^\circ\pi^-$ production. The numbers of events corresponding to each momentum setting or ECM band are shown in Table 4.2.

Figure 4.4 and 4.5 show the results of these fits. The contours, which correspond to one standard deviation, show that there is a strong anticorrelation between A.and B. Since the only distinguishing feature between $\rho^\circ 2\pi^-\pi^+$ and $\rho^\circ\rho^\circ\pi^-$ production appears to be in the strength of the ρ signal, it is possible for a combination of $\rho^\circ\rho^\circ\pi^-$ and nonresonant 5π production to appear to be $\rho^\circ 2\pi^-\pi^+$ production. Therefore, the only meaningful information that can be obtained from the invariant mass distribution is the fractional amount of $\pi^+\pi^-$ pairs in the ρ signal. To find this fraction, the following expression was used to fit the data:

$$M = (1-f)\, M_n + fM_r \tag{4.3}$$

Here, M_n is the 5π phase space distribution and M_r is given by M_n times a Breit-Wigner function having the mass and width of the ρ°. The sums of M_n and M_r are each normalized to the data. Therefore, f gives the fraction of $\pi^+\pi^-$ pairs in the data resulting from the decay of a ρ°. The resulting values of f are presented in Table 4.3 and Figure 4.6.

4.5 Interpretation of the Fit Results

As seen in Figure 4.6, the fractional amount of signal shows no obvious s-channel structure. In particular, assuming that the amounts of $\rho^\circ 2\pi^-\pi^+$ and $\rho^\circ\rho^\circ\pi^-$ production

Table 4.2

Events Used in Fit

P(GeV/c)	Events	ECM Band (GeV)	Events
1.09	680	2.09 - 2.13	633
1.19	997	2.13 - 2.17	1171
1.31	1852	2.17 - 2.21	1494
1.43	1123	2.21 - 2.25	920
1.60	679	2.27 - 2.31	381
1.75	381	2.32 - 2.36	352
1.85	383	2.36 - 2.40	336
2.00	380	2.41 - 2.45	241
2.15	277	2.46 - 2.50	135
2.30	252	2.52 - 2.56	222
2.45	248	2.57 - 2.61	180
2.60	266	2.62 - 2.66	191
2.90	217	2.72 - 2.76	90

Figure 4.4

Fractional Amounts of $\rho^\circ 2\pi^-\pi^+$ and $\rho^\circ\rho^\circ\pi^-$ Production at Each Beam Momentum

The contours correspond to one standard deviation.

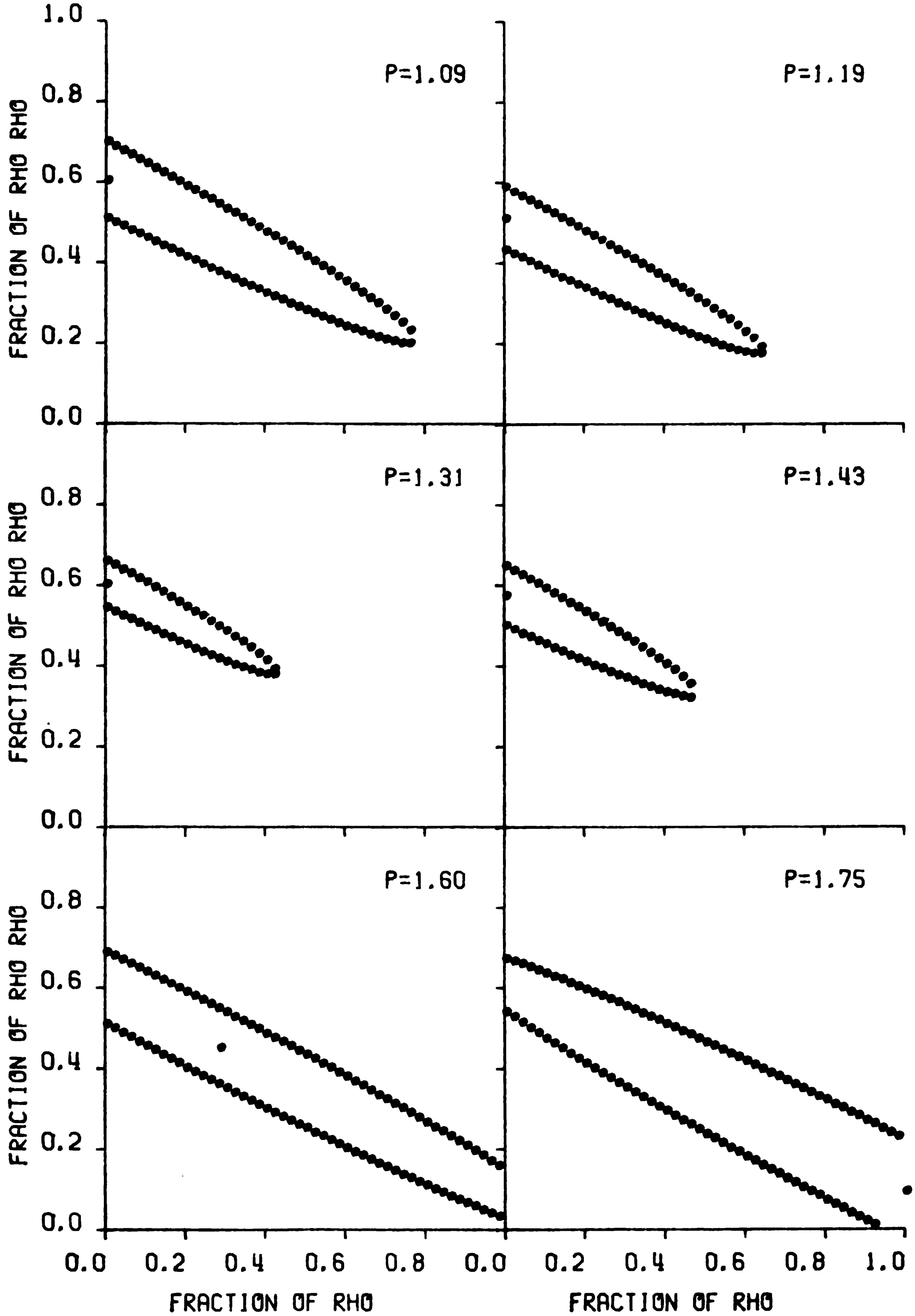
P=1.09
P=1.19
P=1.31
P=1.43
P=1.60
P=1.75
FRACTION OF RHO RHO
FRACTION OF RHO
1.0
0.8
0.6
0.4
0.2
0.0

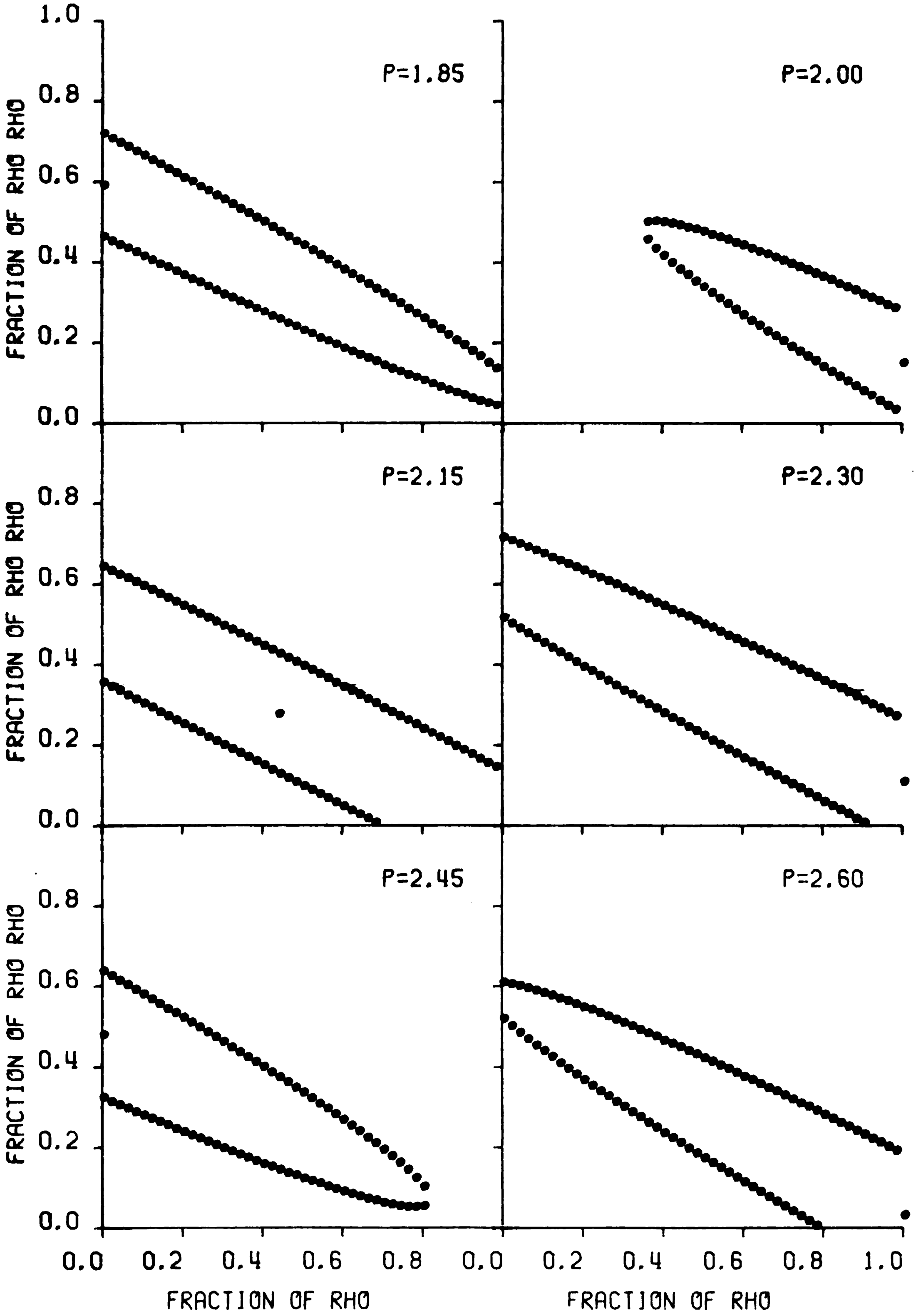
P=1.85
P=2.00
P=2.15
P=2.30
P=2.45
P=2.60
1.0
0.8
0.6
0.4
0.2
0.0
FRACTION OF RHO RHO
0.0
0.2
0.4
0.6
0.8
1.0
FRACTION OF RHO

Figure 4.5

Fractional Amounts of $\rho^\circ 3\pi^-\pi^+$ and $\rho^\circ\rho^\circ\pi^-$ Production at Each ECM Band

The contours correspond to one standard deviation.

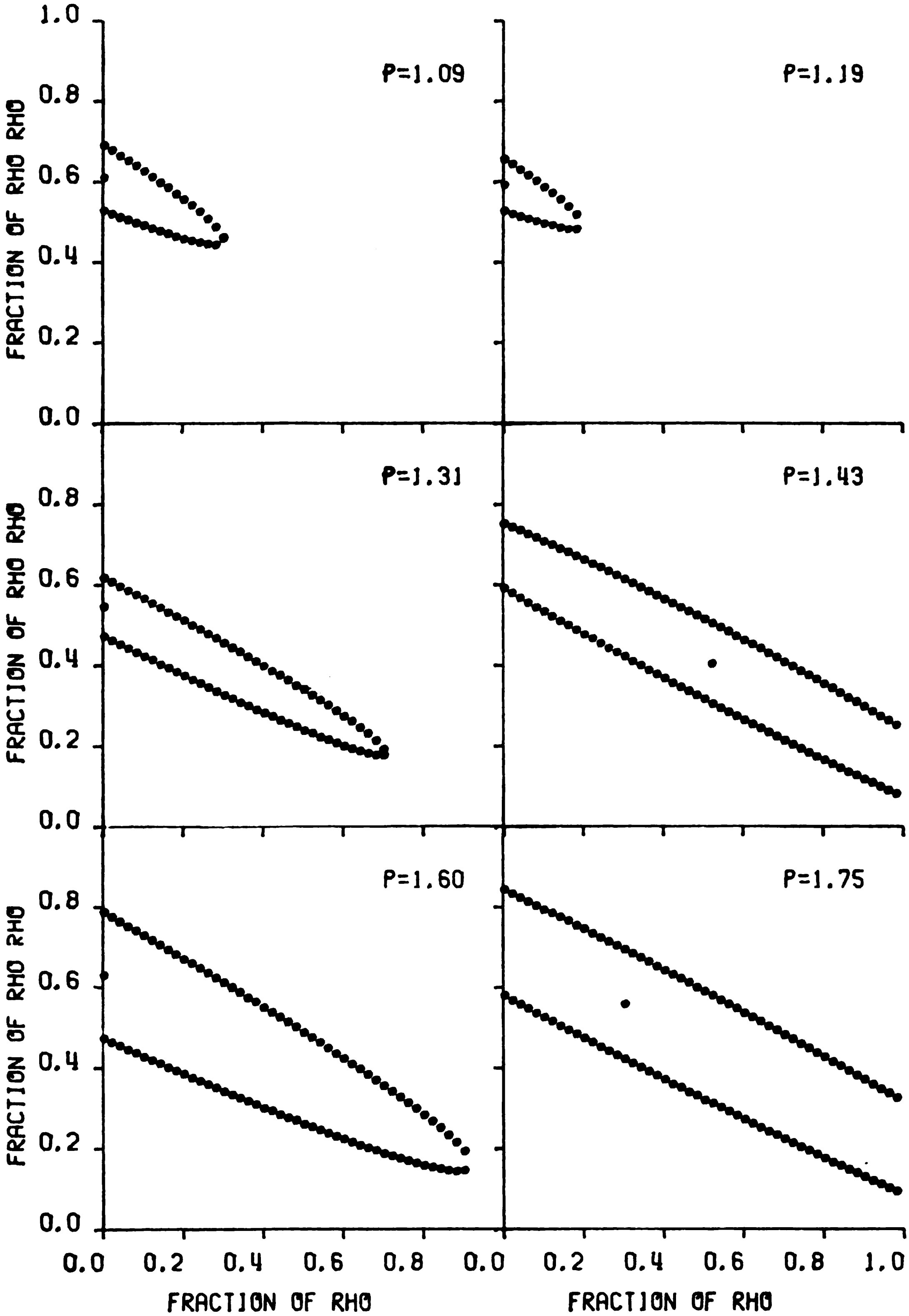
P=1.09
P=1.19
P=1.31
P=1.43
P=1.60
P=1.75
FRACTION OF RHO RHO
FRACTION OF RHO RHO
FRACTION OF RHO RHO
1.0
0.8
0.6
0.4
0.2
0.0
0.0
0.2
0.4
0.6
0.8
1.0
FRACTION OF RHO
FRACTION OF RHO

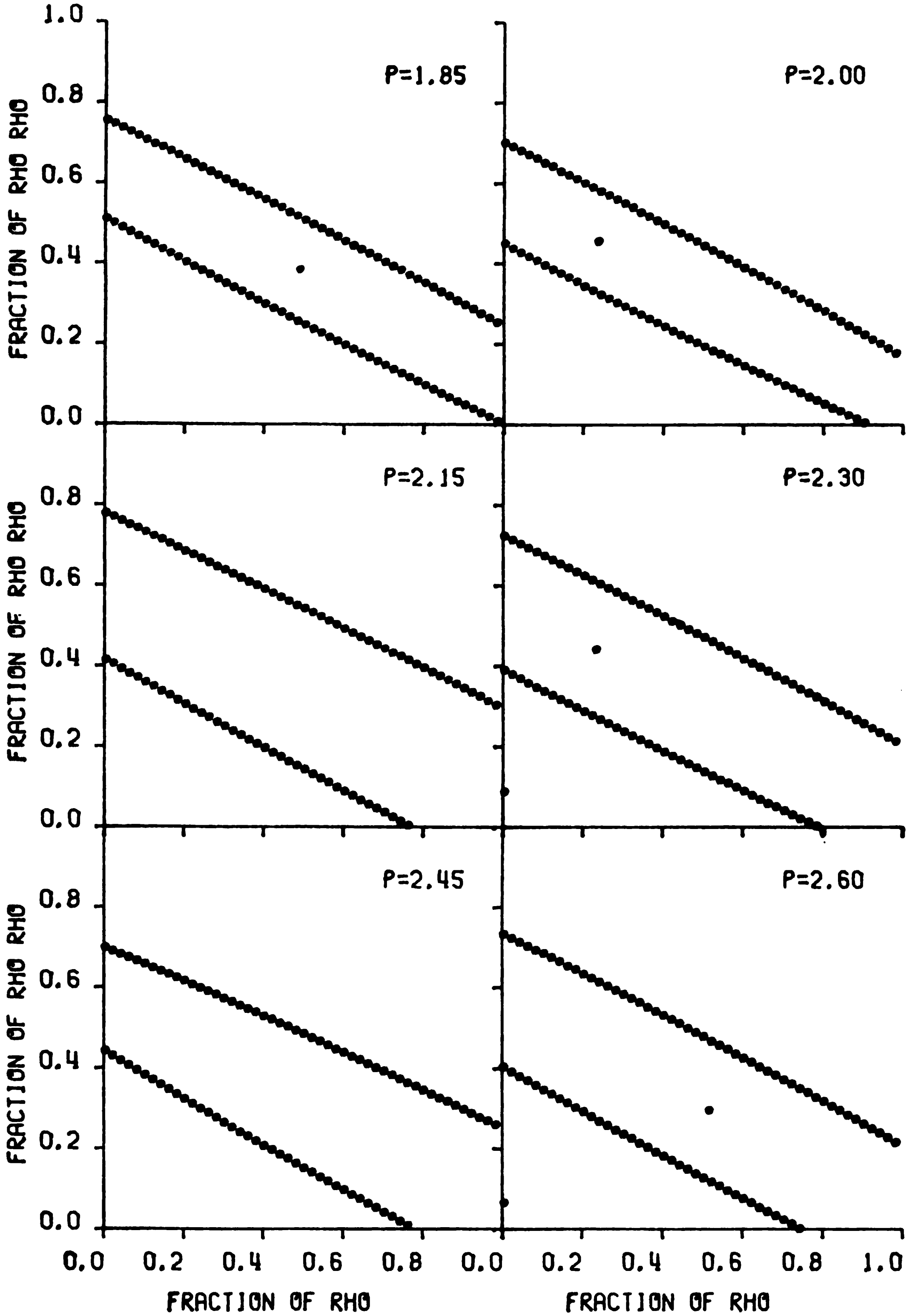

P=1.85
P=2.00
P=2.15
P=2.30
P=2.45
P=2.60
FRACTION OF RHO RHO
FRACTION OF RHO RHO
FRACTION OF RHO RHO
1.0
0.8
0.6
0.4
0.2
0.0
0.0
0.2
0.4
0.6
0.8
0.0
0.2
0.4
0.6
0.8
1.0
FRACTION OF RHO
FRACTION OF RHO

Table 4.3

Fractional Rho Signal

P(GeV/c)	Fraction	ECM Band (GeV)	Fraction
1.09	.201 ± .029	2.09 - 2.13	.202 ± .027
1.19	.169 ± .025	2.13 - 2.17	.197 ± .021
1.31	.200 ± .019	2.17 - 2.21	.181 ± .024
1.43	.191 ± .024	2.21 - 2.25	.221 ± .033
1.60	.198 ± .029	2.27 - 2.31	.209 ± .052
1.75	.197 ± .042	2.32 - 2.36	.235 ± .046
1.85	.197 ± .043	2.36 - 2.40	.209 ± .044
2.00	.217 ± .042	2.41 - 2.45	.190 ± .043
2.15	.165 ± .046	2.46 - 2.50	.195 ± .068
2.30	.203 ± .050	2.52 - 2.56	.185 ± .056
2.45	.161 ± .052	2.57 - 2.61	.188 ± .059
2.60	.182 ± .046	2.62 - 2.66	.187 ± .054
2.90	.178 ± .049	2.72 - 2.76	.193 ± .060

Figure 4.6

Fractional Amount of $\pi^+\pi^-$ Pairs in the ρ° Signal

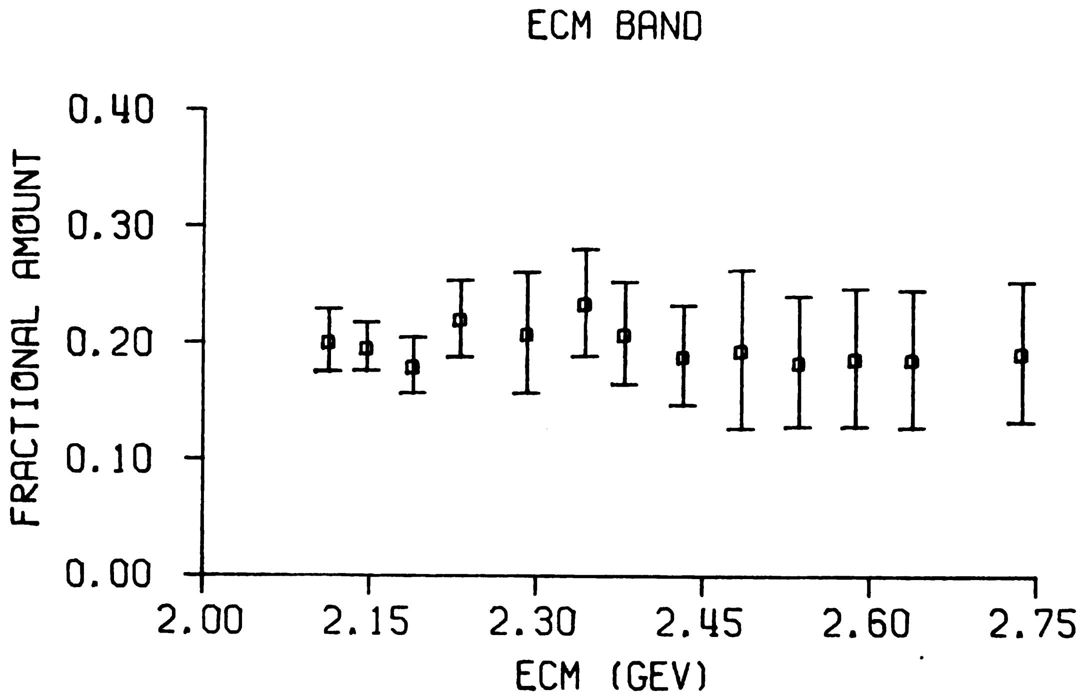
ECM BAND
FRACTIONAL AMOUNT
0.40
0.30
0.20
0.10
0.00
2.00
2.15
2.30
2.45
2.60
2.75
ECM (GEV)

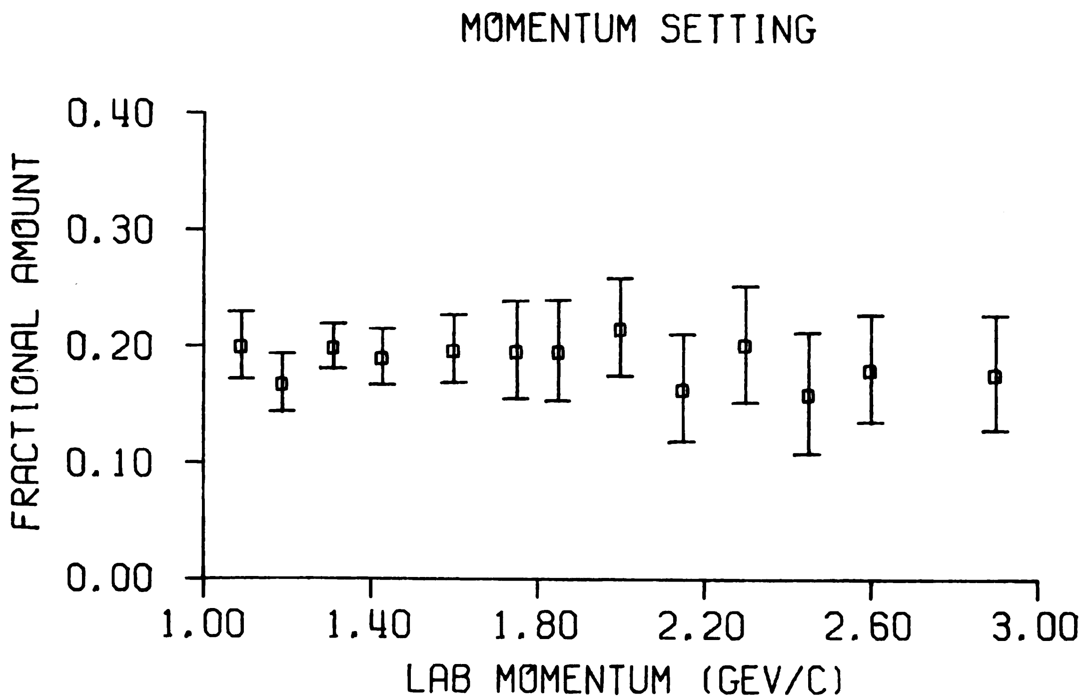
MOMENTUM SETTING
FRACTIONAL AMOUNT
0.40
0.30
0.20
0.10
0.00
1.00
1.40
1.80
2.20
2.60
3.00
LAB MOMENTUM (GEV/C)

do not change in such a way to keep the fractional ρ signal constant, no obvious s-channel structure is observed. Assuming that the behavior of the $\rho^\circ 2\pi^-\pi^+$ channel is smooth in this energy range, a 1 mb enhancement in $\rho^\circ\rho^\circ\pi^-$ at 1.31 GeV/c (ECM = 2190 MeV) corresponds to an enhancement of 0.09 in the fractional ρ signal. This follows from the fact that if the reaction $\bar{p}n \rightarrow 3\pi^-2\pi^-$ proceeded purely via the $\rho^\circ\rho^\circ\pi^-$ intermediate state, two out of six $\pi^+\pi^-$ combinations would have been in the ρ° signal therefore, f must be approximately 1/3.

To determine the probability of an enhancement of a given height, one must first assume a possible width. Then, the ECM resolution is folded in and the resulting distribution plus a background term is fitted to the data. The four values of fractional ρ° signal from 1.09 to 1.43 GeV/c were fitted using a flat background plus an ECM resolved Breit-Wigner function. Different widths and heights for the enhancement were assumed in the fits. The probability of having a 1 mb enhancement in $\rho^\circ\rho^\circ\pi^-$ production, which is expected from the Kalbfleisch result, depends on the width of the enhancement. Using the lower limit of ±20 MeV, given by Kalbfleisch, gives a probability of 0.03 (χ^2 = 6.7/2 degrees of freedom). For a ±80 MeV wide enhancement, the probability is 0.14 (χ^2 = 3.4/2 degrees of freedom).

CHAPTER V

DOUBLE SCATTERING EFFECTS IN THE DEUTERON

5.1 Introduction

Since there exist no sources of free neutrons, the deuteron is often used to provide a quasi-free neutron target. In the impulse approximation, one assumes that the deuteron break-up occurs spontaneously upon impact by the projectile particle. Each of the constituent nucleons carries away a momentum which can be predicted by the deuteron wave functions. The constituent nucleon that did not participate in the reaction with the beam particle is called a spectator. The momentum distribution of the spectators may be found from the deuteron wave function, $\phi(p)$, by $\phi^2(p)p^2$. Figure 5.1A shows such a distribution. The probability of finding a spectator proton with a given momentum value peaks sharply at 45 MeV/c and declines to zero at about 300 MeV/c. However, numerous investigations have shown that there is an excess, over the dueteron wave function prediction, of spectator protons with momentum greater than 200 MeV/c.[13, 17, 18] Dean[19] explains this

Figure 5.1

Spectator Momentum Distributions

(A) Reid soft core deuteron wave function

(B) Four prong data

(C) Six prong data

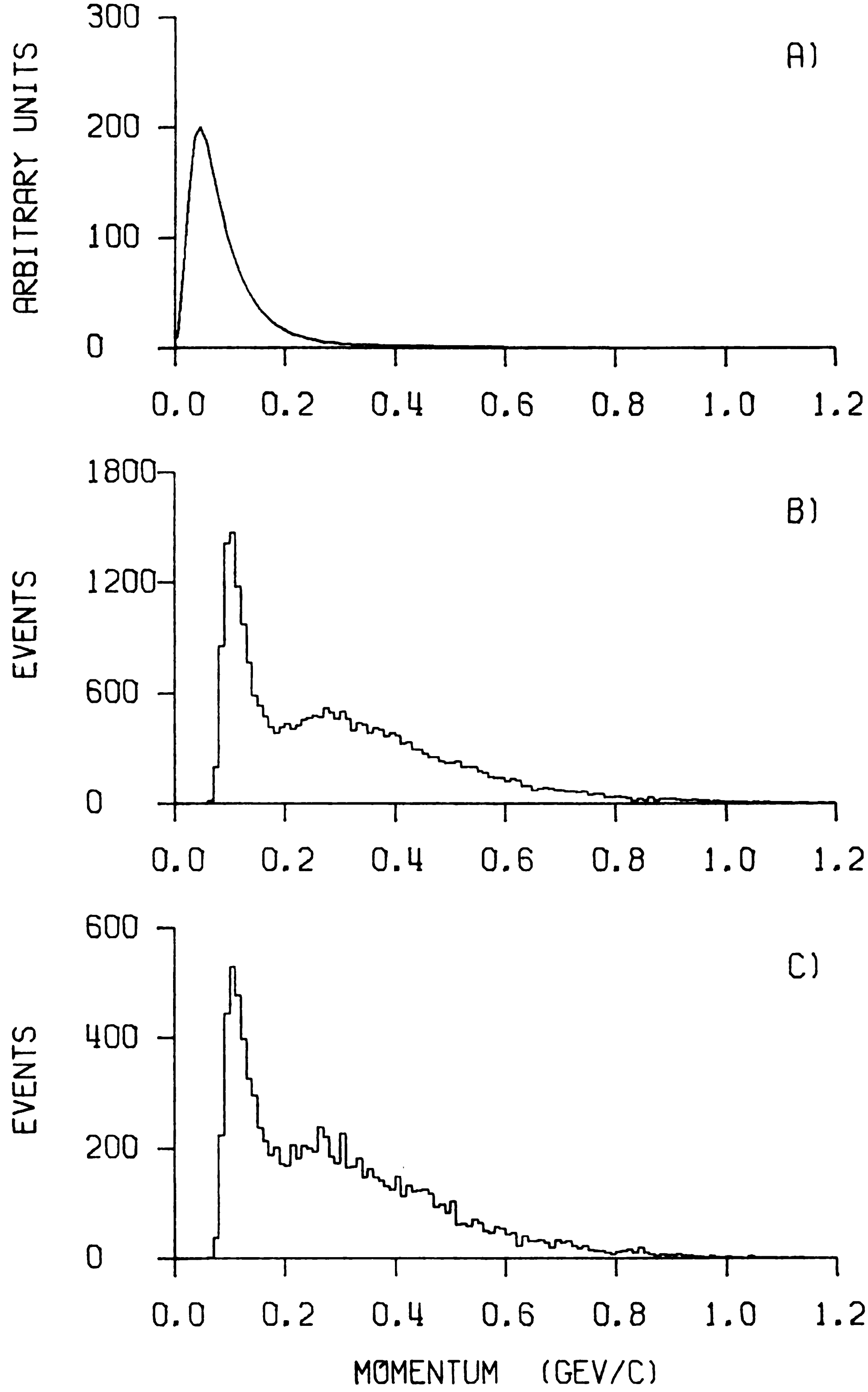

300
200
100
0
ARBITRARY UNITS
A)
0.0
0.2
0.4
0.6
0.8
1.0
1.2
1800
1200
600
0
EVENTS
B)
0.0
0.2
0.4
0.6
0.8
1.0
1.2
600
400
200
0
EVENTS
C)
0.0
0.2
0.4
0.6
0.8
1.0
1.2
MOMENTUM (GEV/C)

excess of high momentum spectator protons by calculating the multiple scattering correction using Glauber multiple diffraction theory.[20, 21] Glauber theory, which considers the involvement of both nucleons in the scattering, has been used by Ma et al.[22] to describe $\bar{p}d$ elastic scattering between 1.6 and 2.0 GeV/c.

In $\bar{p}n$ annihilation reactions using a deuteron target, a similar excess was also found. In this work, a definitive study of the double scattering processes in $\bar{p}n$-like annihilation reactions will be presented. Two types of double scattering mehcanisms will be discussed. One type, which is called final state interaction (FSI), results from scattering with the spectator nucleon by one of the particles from the $\bar{p}N$ annihilation. The other double scattering process results when the antiproton elastically scatters from the proton before it annihilates with the neutron. This is called initial state interaction (ISI).

Since $\bar{p}n$ annihilation reactions at the beam momenta used in this study, 1.09-1.43 GeV/c, produce mostly pions,(see Chapter III), the following reactions will be discussed:

$$\bar{p}d \rightarrow p_s 2\pi^- \pi^+ j\pi^\circ \qquad j \geq 0 \tag{5.1}$$

$$\bar{p}d \rightarrow p_s 3\pi^- 2\pi^+ j\pi^\circ \qquad j \geq 0 \tag{5.2}$$

The set of reactions given by Equation 5.1 appears in the data as three or four prong events. Five or six prong type events are described by Equation 5.2. These two sets of reactions will be considered separately. However, the individual reactions of each set will not be considered separately because it is observed in Chapter II that an event separation of the individual reactions is not possible for $j > 1$. In addition, all four beam momenta, 1.09, 1.19, 1.31, and 1.43 GeV/c, will be combined when comparing the data to the model.

5.2 Evidence for Double Scattering

The momentum distributions of protons emerging from apparent $\bar{p}n$ annihilations in a deuterium target are shown in Figure 5.1 B-C. Also shown is the deuteron wave function prediction of the internal Fermi momentum distribution of the deuteron. The prediction was made from the Reid soft core wave function.[23] If the idea that the deuteron break-up occurs spontaneously when the incident particle interacts with one of the nucleons is indeed correct, the momentum distribution of the spectator nucleon should follow the curve in Figure 5.1A. (This process will be referred to as single scattering.) To compare the momentum distributions of protons emerging from $\bar{p}n$ annihilations to the impulse approximation prediction, the fact that low momentum protons are not always observable in the bubble chamber must be considered. In Appendix E, it is shown that protons having a momentum between 70 and 130 MeV/c are systematically lost. Protons having a momentum less than 70 MeV are not able to produce observable tracks in the bubble chamber. By comparing the data to impulse approximation prediction above 130 MeV/c, one can see that there is a region of excess above 200 MeV/c. This excess appears to be in the form of a broad peak or bump centered at 300 MeV/c. Similarly, this excess is present when the data are compared with other deuteron wave functions.[24-28]

The probability of finding the deuteron with a neutron-proton separation of r is greatest for $r \simeq 2$ fm. This probability is given by $\phi^2(r)r^2$ where $\phi(r)$ is the deuteron radial wave function. Since the nucleon dimensions are of the order of one fermi, both nucleons may be involved in a scattering process. Two possible ways the proton could be involved are depicted in Figure 5.2. The first diagram (called final state interaction or FSI) describes a pion, from the $\bar{p}n$ annihilation, interacting with the proton. The second is called initial state interaction or ISI. Here, the antiproton scatters from the proton before $\bar{p}n$ annihilation takes place. To determine the presence of FSI and ISI, one must look for features characteristic of these processes.

Figure 5.2

Final State Interaction Process and
Initial State Interaction Process

(See text for detailed description.)

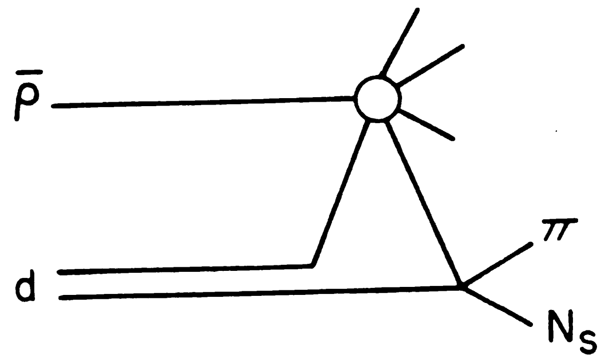

(FSI)

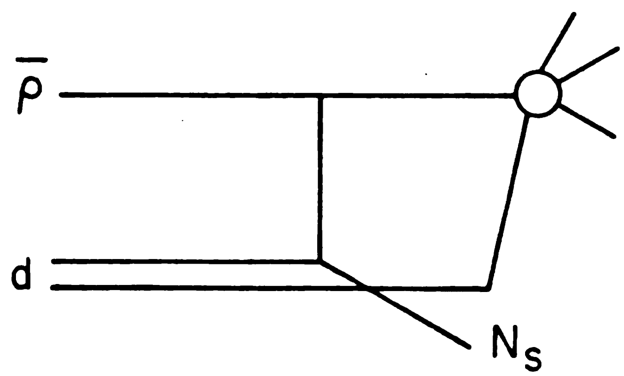

(ISI)

Since FSI results when a pion scatters from the spectator nucleon, production of the $\Delta(1236)$ resonance is expected. Figure 5.3 shows the $\pi^+ p_s$ and $\pi^- p_s$ invariant mass distributions. For comparison, the $\pi^- p_s$ distribution is normalized to the $\pi^+ p_s$ distributioh. Only events with spectator momenta above 190 MeV/c were used in the plot. By comparison, one observes a peak in the $\pi^+ p$ mass distribution characteristic of the $\Delta(1236)$ resonance. Both π^- and π^+ may scatter from the proton. However, since the $\pi^- p$ cross section is smaller than the $\pi^+ p$ cross section in the $\Delta(1236)$ mass range, the peak in the $\pi^- p$ mass distribution will not be as apparent as the $\pi^+ p$ peak. In addition, there is one more π^- than π^+ in an event, therefore assuming only one pion scatters from the proton, the peak in the $\pi^- p$ mass distribution will have more background than the peak in the $\pi^+ p$ mass distribution.

ISI results when the antiproton elastically scatters from one constituent nucleon before annihilation by the other. This elastic scattering imparts a transverse momentum to the spectator nucleon. Therefore, the distribution of the cosine of the angle between the beam and spectator nucleon should show a bump characteristic of elastic scattering. Figure 5.4 shows the cosine distribution for the spectator for three spectator momentum ranges. The first range $p_s < 190$ MeV/c appears to be smooth. A peak at

Figure 5.3

Invariant Mass Distributions of
π^+p_s (unshaded) and π^-p_s (shaded) Systems

(A) Four prong events

(B) Six prong events

The π^-p_s distribution has been normalized to the π^+p_s distribution. The momentum of the spectator proton is greater than 190 MeV/c.

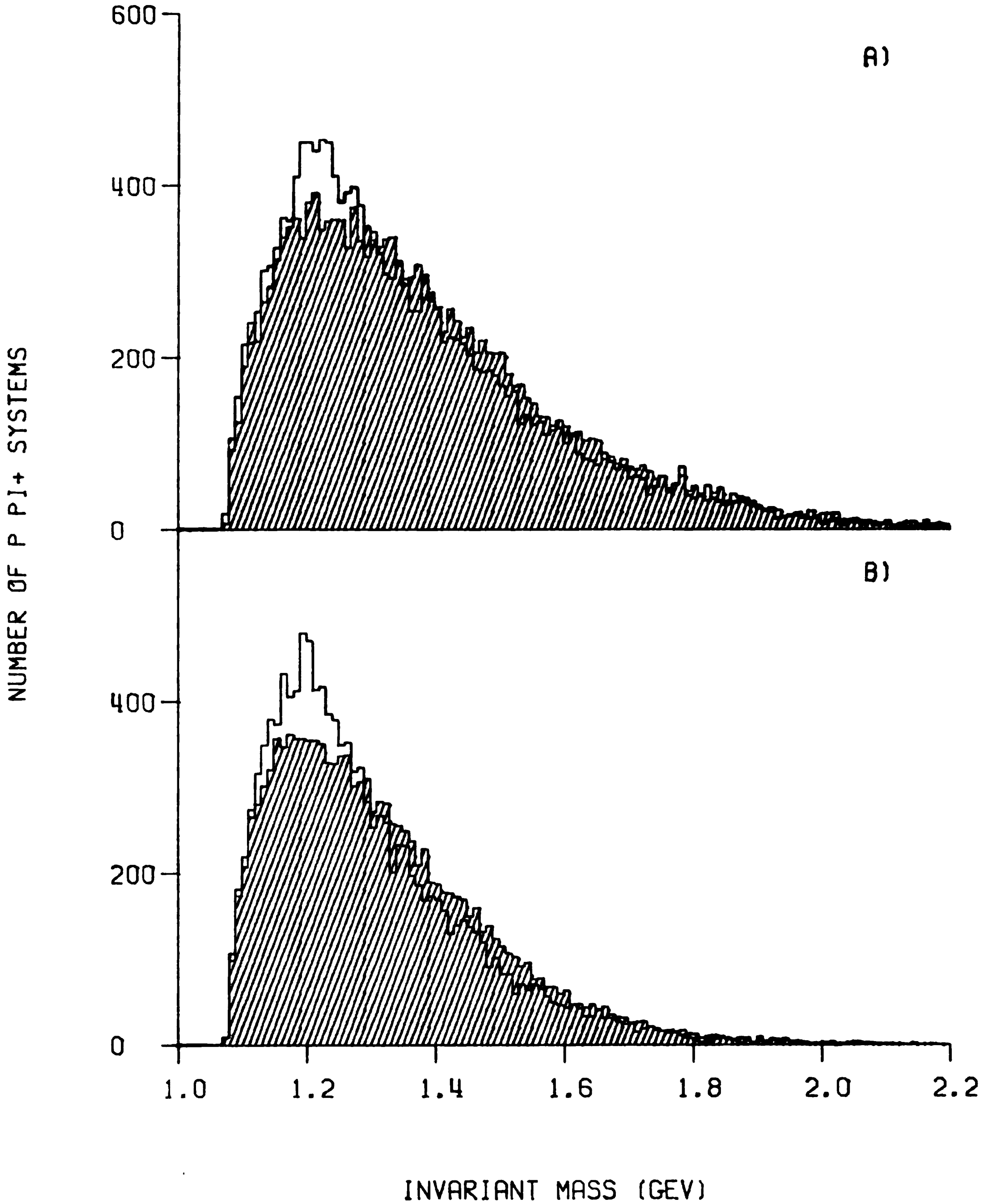
A)
B)
600
400
200
0
400
200
0
1.0
1.2
1.4
1.6
1.8
2.0
2.2
NUMBER OF P PI+ SYSTEMS
INVARIANT MASS (GEV)

Figure 5.4

Cosine Distribution of Protons

(A) $p \leq 190$ MeV/c

(B) $190 < p \leq 350$ MeV/c

(C) $p > 350$ MeV/c

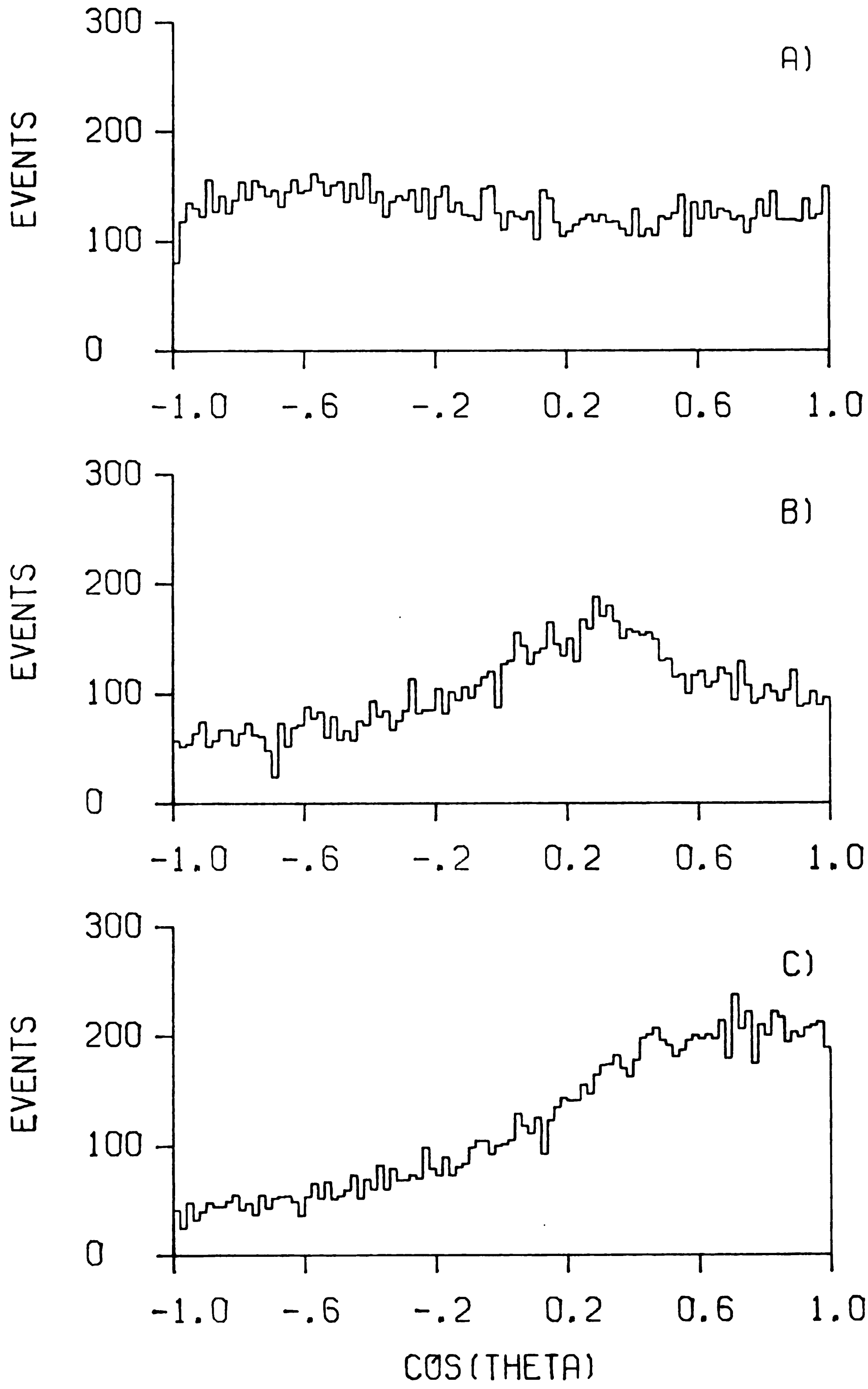

300
200
100
0
EVENTS
A)
-1.0
-.6
-.2
0.2
0.6
1.0
300
200
100
0
EVENTS
B)
-1.0
-.6
-.2
0.2
0.6
1.0
300
200
100
0
EVENTS
C)
-1.0
-.6
-.2
0.2
0.6
1.0
CØS(THETA)

cos (θ) between 0.2 and 0.4 is seen for spectator momenta in the range 190-350 MeV/c. This peak is also observed for spectator momentum greater than 350 MeV/c.

In summary, properties of protons emerging from apparent $\bar{p}n$-like annihilation cannot be described by a simple impulse model. The discrepancies can be seen in the spectator momentum distribution, the invariant mass of the π^+p and π^-p systems, and the cosine of the angle between the spectator proton and the beam. These distributions show features characteristic of double scattering.

5.3 Final State Interaction

The products of antiproton-neutron annihilation processes are mainly pions. An estimate of the extent of final state interaction can be made from the pion nucleon cross section, $\sigma_{\pi N}$, and the mean inverse square proton neutron separation in the deuteron $\langle 1/r^2 \rangle$. The probability that a pion from the annihilation will interact with the spectator nucleon can be estimated by:

$$P = \frac{\sigma_{\pi N}}{4\pi} \left\langle \frac{1}{r^2} \right\rangle \qquad (5.3)$$

Using values of ~.25 Fm^{-2} for $\langle 1/r^2 \rangle$ and ~60 mb for $\sigma_{\pi N}$ gives a value of ~.12 for P. Effects which are attributable to FSI have been observed in other data.[29, 30] However, a complete and detailed description of the FSI process has not been attempted. In this section, a model describing FSI in the reaction $\bar{p}d \to p_s$ + pions is developed.

The probability that a pion from the annihilation will interact with the spectator depends on the neutron-proton separation. This probability is greater for smaller values of n-p separation. Large values at internal Fermi momentum of the deuteron can be related to smaller values of the neutron-proton separation by the Fourier transform. Therefore, FSI will have a greater probability to occur if the internal Fermi momentum of the deutron is large. To incorporate this feature in the model, the following amplitude for FSI was assumed:

$$F(r) = Cf_{\pi N}\frac{\phi(r)}{r} \tag{5.4}$$

Here, $\phi(r)$ is the radial deuteron wave function and $f_{\pi N}$ is the πN scattering amplitude. C is a normalization constant. The factor $1/r$, which can be thought of as the amplitude for spherical waves of pions, takes account of the fact that FSI was a greater chance to occur if r is small. To obtain the momentum space representation of F(r), the Fourier transform was used.

$$f(p) = C'f_{\pi N} \int \frac{\phi(r)}{r} e^{-ip\cdot r} d^3r \tag{5.5}$$

$$= C'f_{\pi N}\, g(p) \tag{5.6}$$

In performing the integral over r, it was assumed that $f_{\pi N}$ could be taken outside the integration. This assumption is valid because $f_{\pi N}$ does not explicitly depend on the value of r. Then, the probability for FSI, expressed in momentum space, is given by:

$$P(p) = 4\ C'^2 \sigma_{\pi N}\ g^2(p) p^2 \qquad (5.7)$$

To calculate $\sigma_{\pi N}$, which depends on the pion nucleon invariant mass, elastic scattering was assumed to be dominant. The validity of this assumption is based on the fact that much of the invariant phase space of the pion nucleon system is in a region where pion production is unimportant. (See Figure 5.5) In this region, most of the cross section is due to elastic or charge exchange scattering. If the invariant mass of the pion nucleon system is less than 1400 MeV/c, less than 17% of the total π^+p or π^-p cross section is due to inelastic scattering. This is shown in Figure 5.6.[32, 33] One sees that inelastic scattering is important above 1500 MeV. However, Figure 5.5 shows that pion nucleon systems above 1500 MeV represent a small fraction of the total sample. This small fraction, along with the high cross section in the $\Delta(1236)$ mass region causes the elastic scattering processes to dominate. An estimate of the relative importance of inelastic processes compared to elastic processes can be made by considering

Figure 5.5

Invariant Mass Distributions of
π^+p and π^-p Systems

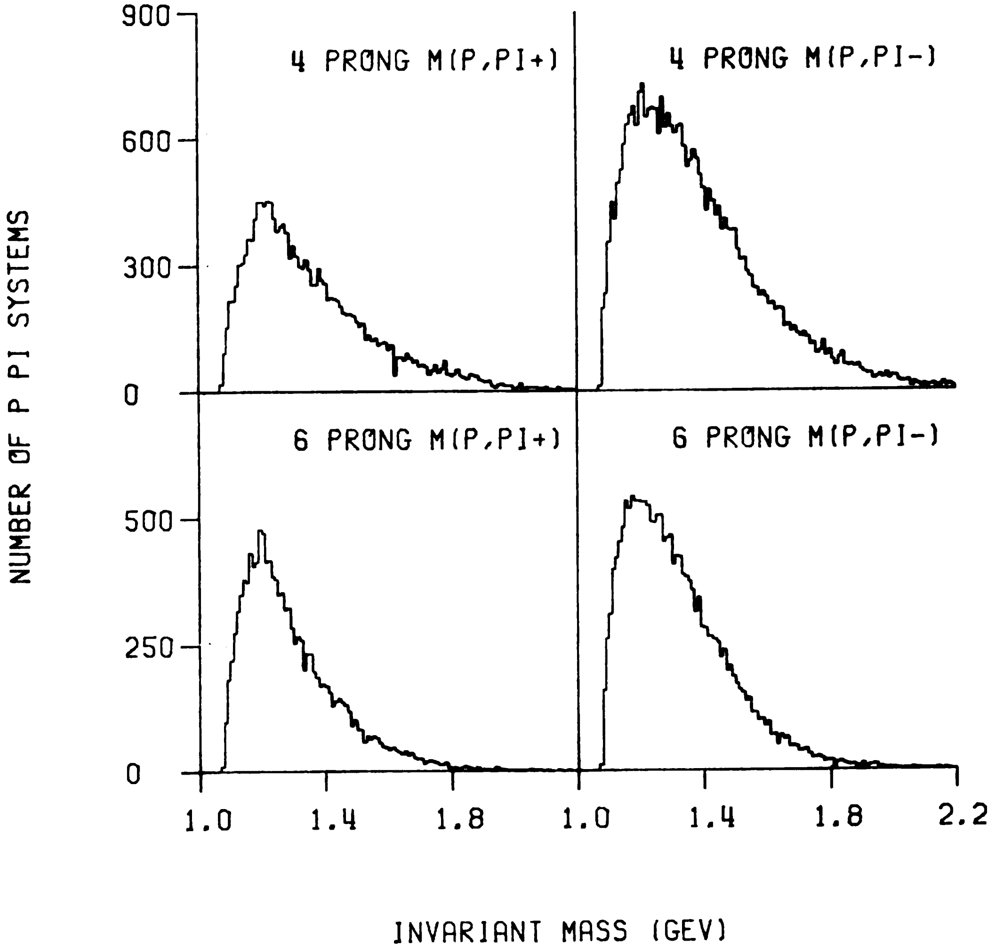

900
600
300
0
500
250
0
4 PRONG M(P,PI+)
4 PRONG M(P,PI-)
6 PRONG M(P,PI+)
6 PRONG M(P,PI-)
NUMBER OF P PI SYSTEMS
1.0
1.4
1.8
1.0
1.4
1.8
2.2
INVARIANT MASS (GEV)

Figure 5.6

Cross Sections for π^+p(A) and π^-p(B)

The total cross section is denoted by + and the elastic plus charge exchange cross section is denoted by □ . The difference between the two curves represents pion production processes.

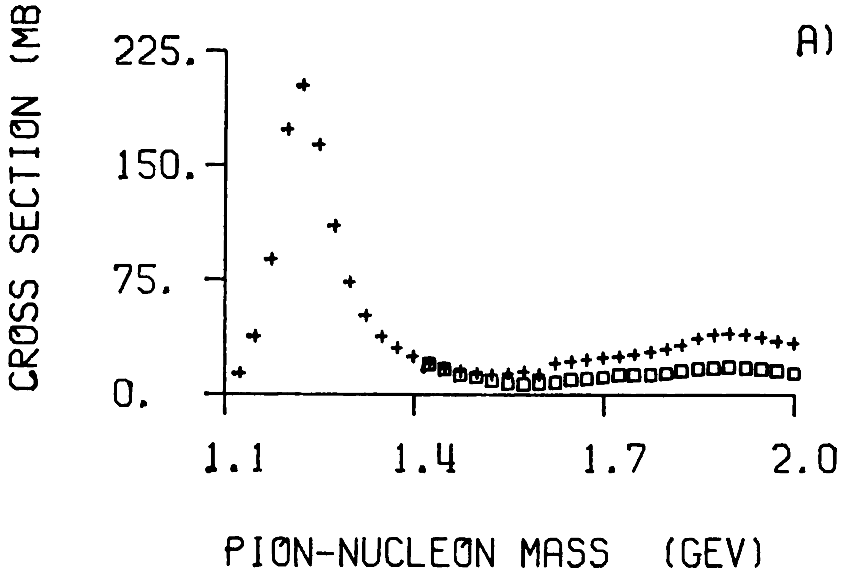
A)
CROSS SECTION (MB)
225.
150.
75.
0.
1.1
1.4
1.7
2.0
PION-NUCLEON MASS (GEV)

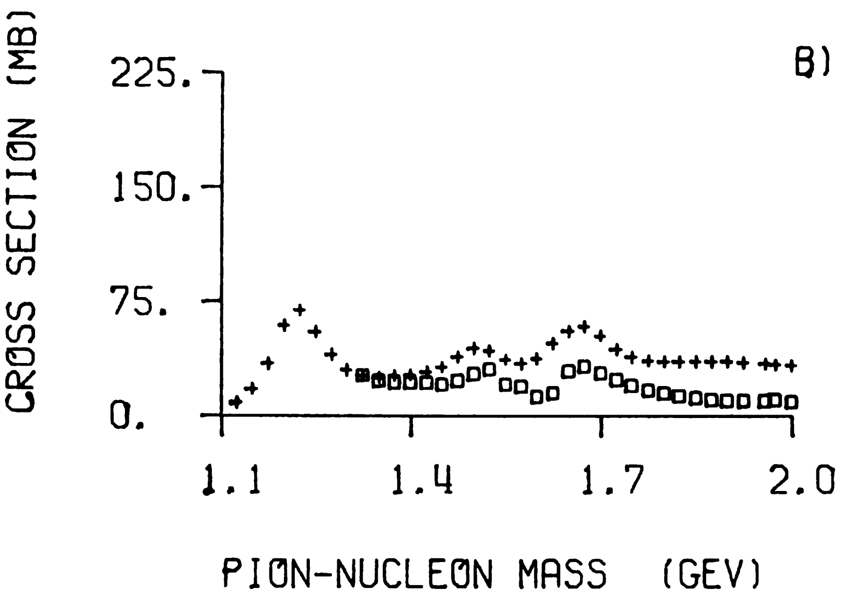
B)
CROSS SECTION (MB)
225.
150.
75.
0.
1.1
1.4
1.7
2.0
PION-NUCLEON MASS (GEV)

the following integrals:

$$I_{el} = \int \sigma_{el} \, (\pi N_s) \, \frac{d^3\vec{p}}{E} \; , \qquad (5.8a)$$

$$I_{in} = \int \sigma_{in} \, (\pi N_s) \, \frac{d^3\vec{p}}{E} \; . \qquad (5.8b)$$

Here $\sigma_{el}(\pi N_s)$ and $\sigma_{in}(\pi N_s)$ are the elastic and inelastic parts of the total pion nucleon cross section. The factor $\frac{d^3\vec{p}}{E}$ is the invariant phase space of the pion nucleon systems in the double scattering process,and was obtained by assuming that the Fermi momentum distribution of the constituent nucleon is given by $\phi^2(p)p^2$ and the momentum distribution of the pions is given by a statistical model for annihilation. The values of I_{el} and I_{in}, whose sum has been normalized to unity, are shown below:

Table 5.1

Relative Importance of Elastic and Inelastic πN FSI

	4 prong π^-p	4 prong π^+p	6 prong π^-p	6 prong π^+p
elastic or charge exchange	.85	.94	.91	.97
inelastic	.15	.06	.09	.03

The table shows that the fraction of π^+p inelastic FSI is smaller than the fraction of π^-p inelastic FSI. This is caused by the fact that the π^+p cross section is higher than the π^-p cross section in $\Delta(1236)$ mass region. This fact also causes the π^+ to be involved in FSI more often than the π^-. Since inelastic scattering plays a minor role in FSI, it will not be considered here. Only elastic and charge exchange scattering will be included.

Characteristics of elastic and charge exchange scattering are taken from phase shift analysis by Donnachie, Kirsopp and Lovelace.[34] These results were used to calculate both the total pion nucleon cross section, $\sigma_{\pi N}$, and the differential elastic scattering cross section $d\sigma_{\pi N}/d\Omega$. The total cross section is needed to calculate the probability for double scattering. If double scattering occurs, $d\sigma_{\pi N}/d\Omega$ was used to obtain the momentum transfer between the pion and the spectator nucleon.

Tables 5.2 and 5.3 list the $\bar{p}N$ reactions and the types of scattering involved in FSI. $\bar{p}N$ annihilations producing up to seven pions were considered. The cross sections for producing more than seven pions are small in our momentum range. A total of fourteen reactions were considered for three or four prong topologies and nine reactions were considered for five or six prong topologies. Each type of FSI was assigned a code depending on its effect on

Table 5.2

3-4 Prong Terms

Reaction	Type of Scattering	Code
$\bar{p}d \rightarrow p_s\pi^+2\pi^-j\pi^\circ$	$\pi^+p \rightarrow \pi^+p$	1
$j = 0,1,2,3,4$	$\pi^-p \rightarrow \pi^-p$	1
	$\pi^-p \rightarrow \pi^\circ n$	2
	$\pi^\circ p \rightarrow \pi^\circ p$	1
	$\pi^\circ p \rightarrow \pi^+n$	2
$\bar{p}d \rightarrow n_s2\pi^+2\pi^-j\pi^\circ$	$\pi^-n \rightarrow \pi^-n$	3
$j = 0,1,2,3$	$\pi^+n \rightarrow \pi^+n$	3
	$\pi^+n \rightarrow \pi^\circ p$	4
	$\pi^\circ n \rightarrow \pi^\circ n$	3
	$\pi^\circ n \rightarrow \pi^-p$	5
$\bar{p}d \rightarrow n_s\pi^+\pi^-j\pi^\circ$	$\pi^+n \rightarrow \pi^+n$	3
$j = 1,2,3,4,5$	$\pi^-n \rightarrow \pi^-n$	3
	$\pi^\circ n \rightarrow \pi^\circ n$	3
	$\pi^+n \rightarrow \pi^\circ p$	5
	$\pi^\circ n \rightarrow \pi^-p$	4

Code 1 $\bar{p}n$ annihilation counted as a $\bar{p}n$ type event.

Code 2 $\bar{p}n$ annihilation leaving $\bar{p}n$ topology.

Code 3 $\bar{p}p$ annihilation counted as a $\bar{p}p$ type event.

Code 4 $\bar{p}p$ annihilation leaving $\bar{p}p$ topology into $\bar{p}n$ 3-4 prong topology

Code 5 $\bar{p}p$ annihilation leaving $\bar{p}p$ topology into a $\bar{p}n$ topology which is not 3 or 4 prong.

Table 5.3

5-6 Prong Terms

Reaction	Type of Scattering	Code
$\bar{p}d \to p_s 2\pi^+ 3\pi^- j\pi^\circ$	$\pi^+ p \to \pi^+ p$	1
$j = 0,1,2$	$\pi^- p \to \pi^- p$	1
	$\pi^- p \to \pi^\circ n$	2
	$\pi^\circ p \to \pi^\circ p$	1
	$\pi^\circ p \to \pi^+ n$	2
$\bar{p}d \to n_s 3\pi^+ 3\pi^- j\pi^\circ$	$\pi^- n \to \pi^- n$	3
$j = 0,1$	$\pi^+ n \to \pi^+ n$	3
	$\pi^+ n \to \pi^\circ p$	4
	$\pi^\circ n \to \pi^\circ n$	3
	$\pi^\circ n \to \pi^- p$	5
$\bar{p}d \to n_s 2\pi^+ 2\pi^- j\pi^\circ$	$\pi^+ n \to \pi^+ n$	3
$j = 1,2,3$	$\pi^\circ n \to \pi^\circ n$	3
	$\pi^\circ n \to \pi^\circ n$	3
	$\pi^+ n \to \pi^\circ p$	5
	$\pi^\circ n \to \pi^- p$	4

Code 1 $\bar{p}n$ annihilation counted as a $\bar{p}n$ type event

Code 2 $\bar{p}n$ annihilation leaving $\bar{p}n$ topology

Code 3 $\bar{p}p$ annihilation counted as a $\bar{p}p$ type event

Code 4 $\bar{p}p$ annihilation leaving $\bar{p}p$ topology into $\bar{p}n$ 5-6 prong topology

Code 5 $\bar{p}p$ annihilation leaving $\bar{p}p$ topology into a $\bar{p}n$ topology which is not 5 or 6 prong.

the topology of the event. These codes are listed on Tables 5.2 and 5.3. The events with codes 1 or 4, which have a $\bar{p}n$ type topology, are present in the measured sample of the data. The code 1 events are $\bar{p}n$ annihilations in which a pion interacts with the spectator proton. The code 4 events are $\bar{p}p$ annihilations which have a $\bar{p}n$ type topology. These events have a proton because a pion from the $\bar{p}p$ annihilation scatters on the spectator neutron by a charge exchange process. Charge exchange scattering also causes some $\bar{p}n$ annihilations to have a topology characteristic of $\bar{p}p$ annihilations. These events, which have been assigned code 2, do not appear in the measured sample.

To describe the effects of FSI, $\bar{p}n$ and $\bar{p}p$ annihilation events were generated using the Monte Carlo event generating program SAGE.[16] The proton and neutron were assumed to have equal but opposite momentum values given by the momentum distribution $\phi^2(p)p^2$. The generated event was weighted by the flux factor to account for the Fermi motion of the target. The probability that one of the pions resulting from the annihilation will scatter from the remaining nucleon depends on the pion-nucleon invariant mass. The cross-section, $\sigma_{\pi N}$, and angular distribution of the pions, $d\sigma_{\pi N}/d\Omega$, in the double scattering process are given by Donnachie, Kirsopp and Lovelace.[11] Monte Carlo events were generated for each of the 23 reactions listed on

Tables 5.2 and 5.3. For each of these reactions, the fractional amount of different types of FSI was determined. These fractions, which are summarized in Tables 5.4-5.7, are determined for the following three categories of events:

1) $\bar{p}p$ FSI events having a $\bar{p}n$ topology due to charge exchange scattering
2) $\bar{p}n$ FSI events having a $\bar{p}p$ topology due to charge exchange scattering
3) $\bar{p}n$ FSI events having a $\bar{p}n$ topology

To compare the model to the data, only the Monte Carlo events in categories 1 or 3 were used. The category 2 events are not present in the measured sample. The Monte Carlo events were used to predict the spectator momentum distribution, the $\pi^+ p_s$ invariant mass distribution, and the cos (θ) distribution. These three distributions were generated for the three or four prong and five or six prong topologies by combining the Monte Carlo events of the appropriate reactions. To combine the Monte Carlo events, the number of events in the distribution from the ith reaction is given by:

$$N_i \propto \sum_j P_j(p)\sigma_i \qquad (5.9)$$

Here, σ_i is the cross section for the ith $\bar{p}N$ reaction. In addition, the cos (θ) and invariant mass distributions contain only the events with proton momentum greater than or equal to 190 MeV/c.

Table 5.4

FSI Model Predictions p = 1.09 GeV/c

Reaction	$\bar{p}n$ FSI	$\bar{p}n$ FSI Leaving $\bar{p}n$ Topology	$\bar{p}p$ FSI Entering $\bar{p}n$ Topology	Topology
$\bar{p}p \to 2\pi^{+}2\pi^{-}$	-	-	.041	4
$\bar{p}p \to 2\pi^{+}2\pi^{-}\pi^{\circ}$	-	-	.046	4
$\bar{p}p \to 2\ ^{+}2\ ^{-}2\ ^{\circ}$	-	-	.067	4
$\bar{p}p \to 2\pi^{+}2\pi^{-}3\pi^{\circ}$	-	-	.062	4
$\bar{p}p \to \pi^{+}\pi^{-}\pi^{\circ}$	-	-	.014	4
$\bar{p}p \to \pi^{+}\pi^{-}2\pi^{\circ}$	-	-	.040	4
$\bar{p}p \to \pi^{+}\pi^{-}3\pi^{\circ}$	-	-	.073	4
$\bar{p}p \to \pi^{+}\pi^{-}4\pi^{\circ}$	-	-	.122	4
$\bar{p}p \to \pi^{+}\pi^{-}5\pi^{\circ}$	-	-	.134	4
$\bar{p}n \to \pi^{+}2\pi^{-}$	.090	.030	-	4
$\bar{p}n \to \pi^{+}2\pi^{-}\pi^{\circ}$	.151	.059	-	4
$\bar{p}n \to \pi^{+}2\pi^{-}2\pi^{\circ}$	.207	.095	-	4
$\bar{p}n \to \pi^{+}2\pi^{-}3\pi^{\circ}$	.280	.172	-	4
$\bar{p}n \to \pi^{+}2\pi^{-}4\pi^{\circ}$	.340	.165	-	4
$\bar{p}p \to 3\pi^{+}3\pi^{-}$	-	-	.085	6
$\bar{p}p \to 3\pi^{+}3\pi^{-}\pi^{\circ}$	-	-	.086	6
$\bar{p}p \to 2\pi^{+}2\pi^{-}\pi^{\circ}$	-	-	.027	6
$\bar{p}p \to 2\pi^{+}2\pi^{-}2\pi^{\circ}$	-	-	.055	6
$\bar{p}p \to 2\pi^{+}2\pi^{-}3\pi^{\circ}$	-	-	.079	6
$\bar{p}n \to 2\pi^{+}3\pi^{-}$	.239	.075	-	6
$\bar{p}n \to 2\pi^{+}3\pi^{-}\pi^{\circ}$	.306	.125	-	6
$\bar{p}n \to 2\pi^{+}3\pi^{-}2\pi^{\circ}$	.375	.149	-	6

Table 5.5

FSI Model Predictions p = 1.19 GeV/c

Reaction	$\bar{p}n$ FSI	$\bar{p}n$ FSI Leaving $\bar{p}n$ Topology	$\bar{p}p$ FSI Entering $\bar{p}n$ Topology	Topology
$\bar{p}p \rightarrow 2\pi^+2\pi^-$	-	-	.039	4
$\bar{p}p \rightarrow 2\pi^+2\pi^-\pi^\circ$	-	-	.045	4
$\bar{p}p \rightarrow 2\pi^+2\pi^-2\pi^\circ$	-	-	.051	4
$\bar{p}p \rightarrow 2\pi^+2\pi^-3\pi^\circ$	-	-	.061	4
$\bar{p}p \rightarrow \pi^+\pi^-\pi^\circ$	-	-	.014	4
$\bar{p}p \rightarrow \pi^+\pi^-2\pi^\circ$	-	-	.040	4
$\bar{p}p \rightarrow \pi^+\pi^-3\pi^\circ$	-	-	.074	4
$\bar{p}p \rightarrow \pi^+\pi^-4\pi^\circ$	-	-	.123	4
$\bar{p}p \rightarrow \pi^+\pi^-5\pi^\circ$	-	-	.133	4
$\bar{p}n \rightarrow \pi^+2\pi^-$	.089	.031	-	4
$\bar{p}n \rightarrow \pi^+2\pi^-\pi^\circ$	.149	.059	-	4
$\bar{p}n \rightarrow \pi^+2\pi^-2\pi^\circ$	.205	.095	-	4
$\bar{p}n \rightarrow \pi^+2\pi^-3\pi^\circ$	.285	.151	-	4
$\bar{p}n \rightarrow \pi^+2\pi^-4\pi^\circ$	.356	.160	-	4
$\bar{p}p \rightarrow 3\pi^+3\pi^-$	-	-	.083	6
$\bar{p}p \rightarrow 3\pi^+3\pi^-\pi^\circ$	-	-	.086	6
$\bar{p}p \rightarrow 2\pi^+2\pi^-\pi^\circ$	-	-	.026	6
$\bar{p}p \rightarrow 2\pi^+2\pi^-2\pi^\circ$	-	-	.055	6
$\bar{p}p \rightarrow 2\pi^+2\pi^-3\pi^\circ$	-	-	.080	6
$\bar{p}n \rightarrow 2\pi^+3\pi^-$	.240	.076	-	6
$\bar{p}n \rightarrow 2\pi^+3\pi^-\pi^\circ$	.307	.120	-	6
$\bar{p}n \rightarrow 2\pi^+3\pi^-2\pi^\circ$	.372	.146	-	6

Table 5.6

FSI Model Prediction p = 1.31 GeV/c

Reaction	$\bar{p}n$ FSI	$\bar{p}n$ FSI Leaving $\bar{p}n$ Topology	$\bar{p}p$ FSI Entering $\bar{p}n$ Topology	Topology
$\bar{p}p \rightarrow 2\pi^+2\pi^-$	-	-	.039	4
$\bar{p}p \rightarrow 2\pi^+2\pi^-\pi^\circ$	-	-	.044	4
$\bar{p}p \rightarrow 2\pi^+2\pi^-2\pi^\circ$	-	-	.058	4
$\bar{p}p \rightarrow 2\pi^+2\pi^-3\pi^\circ$	-	-	.058	4
$\bar{p}p \rightarrow \pi^+\pi^-\pi^\circ$	-	-	.013	4
$\bar{p}p \rightarrow \pi^+\pi^-2\pi^\circ$	-	-	.037	4
$\bar{p}p \rightarrow \pi^+\pi^-3\pi^\circ$	-	-	.073	4
$\bar{p}p \rightarrow \pi^+\pi^-4\pi^\circ$	-	-	.100	4
$\bar{p}p \rightarrow \pi^+\pi^-5\pi^\circ$	-	-	.140	4
$\bar{p}n \rightarrow \pi^+2\pi^-$	.087	.028	-	4
$\bar{p}n \rightarrow \pi^+2\pi^-\pi^\circ$	.142	.058	-	4
$\bar{p}n \rightarrow \pi^+2\pi^-2\pi^\circ$	.206	.098	-	4
$\bar{p}n \rightarrow \pi^+2\pi^-3\pi^\circ$	.270	.150	-	4
$\bar{p}n \rightarrow \pi^+2\pi^-4\pi^\circ$	.371	.172	-	4
$\bar{p}p \rightarrow 3\pi^-3\pi^-$	-	-	.080	6
$\bar{p}p \rightarrow 3\pi^+3\pi^-\pi^\circ$	-	-	.081	6
$\bar{p}p \rightarrow 2\pi^+2\pi^-\pi^\circ$	-	-	.025	6
$\bar{p}p \rightarrow 2\pi^+2\pi^-2\pi^+$	-	-	.054	6
$\bar{p}p \rightarrow 2\pi^+2\pi^-3\pi^\circ$	-	-	.078	6
$\bar{p}n \rightarrow 2\pi^+3\pi^-$	.237	.074	-	6
$\bar{p}n \rightarrow 2\pi^+3\pi^-\pi^\circ$	.302	.115	-	6
$\bar{p}n \rightarrow 2\pi^+3\pi^-2\pi^\circ$	.380	.145	-	6

Table 5.7

FSI Model Predictions p = 1.43 GeV/c

Reaction	$\bar{p}n$ FSI	$\bar{p}n$ FSI Leaving $\bar{p}n$ Topology	$\bar{p}p$ FSI Entering $\bar{p}n$ Topology	Topology
$\bar{p}p \to 2\pi^+2\pi^-$	-	-	.039	4
$\bar{p}p \to 2\pi^+2\pi^-\pi^\circ$	-	-	.044	4
$\bar{p}p \to 2\pi^+2\pi^-2\pi^\circ$	-	-	.065	4
$\bar{p}p \to 2\pi^+2\pi^-3\pi^\circ$	-	-	.057	4
$\bar{p}p \to \pi^+\pi^-\pi^\circ$	-	-	.011	4
$\bar{p}p \to \pi^+\pi^-2\pi^\circ$	-	-	.034	4
$\bar{p}p \to \pi^+\pi^-3\pi^\circ$	-	-	.071	4
$\bar{p}p \to \pi^+\pi^-4\pi^\circ$	-	-	.096	4
$\bar{p}p \to \pi^+\pi^-5\pi^\circ$	-	-	.143	4
$\bar{p}n \to \pi^+2\pi^-$	.085	.026	-	4
$\bar{p}n \to \pi^+2\pi^-\pi^\circ$	.135	.058	-	4
$\bar{p}n \to \pi^+2\pi^-2\pi^\circ$	.204	.096	-	4
$\bar{p}n \to \pi^+2\pi^-3\pi^\circ$	.266	.128	-	4
$\bar{p}n \to \pi^+2\pi^-4\pi^\circ$	.365	.181	-	4
$\bar{p}p \to 3\pi^+3\pi^-$	-	-	.077	6
$\bar{p}p \to 3\pi^+3\pi^-\pi^\circ$	-	-	.077	6
$\bar{p}p \to 2\pi^+2\pi^-\pi^\circ$	-	-	.026	6
$\bar{p}p \to 2\pi^+2\pi^-2\pi^\circ$	-	-	.052	6
$\bar{p}p \to 2\pi^+2\pi^-3\pi^\circ$	-	-	.075	6
$\bar{p}n \to 2\pi^+3\pi^-$	.231	.069	-	6
$\bar{p}n \to 2\pi^+3\pi^-\pi^\circ$	.295	.109	-	6
$\bar{p}n \to 2\pi^+3\pi^-2\pi^\circ$	.372	.145	-	6

The values of σ_i for the $\bar{p}n$ reactions were obtained in Chapter III. The cross sections for the $\bar{p}p$ annihilations were obtained elsewhere.[3, 13, 35-39] However, the cross sections for the reactions involving two or more π° in the final state were not directly measured. To calculate these cross sections, the Fermi statistical model[40] was used. The model has been shown to be in good agreement with antiproton-nucleon annihilations.[41] Neglecting pion mass difference, the model relates the cross sections for pion production as follows:

$$\sigma_r = \frac{n_0^i! \quad n_-^i! \quad n_+^i!}{n_0^r! \quad n_-^r! \quad n_+^r!} \quad \sigma_i \tag{5.10a}$$

$$n_0^r + n_-^r + n_+^r = n_0^i + n_-^i + n_+^i \ . \tag{5.10b}$$

Here σ_r is the cross section for producing $n_0^r\pi^\circ$, $n_-^r\pi^-$, and $n_+^r\pi^+$. Similarly, σ_i is the cross section for producing $n_0^i\pi^\circ$, $n_-^i\pi^-$, and $n_+^i\pi^+$. The values of σ used in the FSI model are presented in Table 5.8. Multi-π° cross sections found by Equation 5.10 are denoted in the table with an *.

5.4 Initial State Interaction

It is possible for the incident antiproton to elastically scatter from the proton before the $\bar{p}n$ annihilation

Table 5.8

$\bar{p}p$ and $\bar{p}n$ Cross Sections

Reaction	1.09	1.19	1.31	1.43
$\bar{p}n \rightarrow 2\pi^-\pi^+$	2.17 ± .17	1.81 ± .13	1.61 ± .09	1.42 ± .10
$\bar{p}n \rightarrow 2\pi^-\pi^+\pi^0$	11.43 ± .53	10.96 ± .45	9.41 ± .33	8.89 ± .35
$\bar{p}n \rightarrow 2\pi^-\pi^+2\pi^0$	12.3 ± .9*	12.1 ± .7*	11.1 ± .6*	10.1 ± .6*
$\bar{p}n \rightarrow 2\pi^-\pi^+3\pi^0$	6.9 ± .4*	6.5 ± .3*	6.7 ± .3*	6.2 ± .3*
$\bar{p}n \rightarrow 2\pi^-\pi^+4\pi^0$	2.4*	2.5*	2.6*	2.6*
$\bar{p}n \rightarrow 3\pi^-2\pi^+$	4.10 ± .26	4.02 ± .22	3.70 ± .17	3.38 ± .17
$\bar{p}n \rightarrow 3\pi^-2\pi^+\pi^0$	6.85 ± .37	6.46 ± .29	6.74 ± .24	6.24 ± .27
$\bar{p}n \rightarrow 3\pi^+2\pi^-\pi^+$ mm	4.84 ± .28	5.01 ± .24	5.14 ± .21	5.18 ± .24
$\bar{p}p \rightarrow 2\pi^+2\pi^-$	3.6 ± .2°	3.3 ± .2°	3.0 ± .2°	2.8 ± .2°
$\bar{p}p \rightarrow 2\pi^+2\pi^-\pi^0$	13.5 ±1.5°	12.9 ±1.3°	12.0 ±1.2°	11.1 ± 1.0°
$\bar{p}p \rightarrow 2\pi^+2\pi^-2\pi^0$	4.5*	5.0*	5.4*	5.4*
$\bar{p}p \rightarrow 2\pi^+2\pi^-3\pi^0$	3.3*	3.3*	3.3*	3.3*
$\bar{p}p \rightarrow 2\pi^+2\pi^-$ + mm	11.4 ± .5°	11.2 ± .5°	11.0 ± .5°	10.9 ± .5°
$\bar{p}p \rightarrow 3\pi^+3\pi^-$	1.0°	1.1°	1.2°	1.2°
$\bar{p}p \rightarrow 3\pi^+3\pi^-\pi^0$	2.2°	2.2°	2.2°	2.2°
$\bar{p}p \rightarrow 3\pi^+3\pi^-$ + mm	.3 ± .2°	.3 ± .2°	.4 ± .2°	.5 ± .3°
$\bar{p}p \rightarrow \pi^+\pi^-\pi^0$	2.2°	1.8°	1.6°	1.4°
$\bar{p}p \rightarrow \pi^+\pi^-2\pi^0$	7.2*	6.6*	6.0*	5.6*
$\bar{p}p \rightarrow \pi^+\pi^-3\pi^0$	9.0*	8.6*	8.0*	7.4*
$\bar{p}p \rightarrow \pi^+\pi^-4\pi^0$	1.5*	1.7*	1.8*	1.8*
$\bar{p}p \rightarrow \pi^+\pi^-5\pi^0$	.7*	.7*	.7*	.7*
$\bar{p}p \rightarrow \pi^+\pi^-$ + mm	18.8 ± .7°	18.0 ± .1°	16.8 ± .6°	15.8° ± .6°

*Calculated from Eq 5-9.

°Taken from References (see text)

takes place. This process will be referred to as initial state interaction or ISI. ISI will tend to give the proton a momentum in a direction transverse to the beam direction. The momentum transfer between the antiproton and the proton is given by $d\sigma/d\Omega = (d\sigma/d\Omega)_0 e^{At}$. In the momentum range used here, $A = 17.5\ (\mathrm{GeV})^{-2}$ and the total elastic cross section is 42 mb.[38, 39]

Monte carlo events for ISI were generated for $\bar{p}n$ annihilations producing up to seven pions. The Fermi momentum distribution of the deuteron was given by $\phi^2(p)p^2$ and the double scattering probability was assumed to be proportional to $g^2(p)p^2$. This distribution was used to account for the fact that small p-n separations have a greater chance to result in a double scattering. The ISI Monte Carlo events for each reaction were combined into three or four and five or six prong groups. This was done by requiring the number of Monte Carlo events in the group to be proportional to the cross section for that reaction. Then, the events in each group were used to produce distributions of spectator momentum, $M(\pi^+ p_s)$ and cos (θ).

5.5 Fits to the Data

To determine how much of the data can be described by FSI and ISI, fits were made to the data using the spectator distribution, the invariant mass distribution $M(\pi^+ p_s)$, and the cos (θ) distribution. The Monte Carlo events for FSI and ISI were used to produce these distributions. Only the events with spectator momentum greater than or equal to 190 MeV/c were included in the cos (θ) and invariant mass distributions. In this region, the data are dominated by the FSI and ISI processes. This region is used so the $\Delta(1236)$ signal in the $\pi^+ p_s$ invariant mass distribution can be enhanced. Since the $\pi^+ p_s$ scattering is assumed to be elastic, the $\pi^+ p_s$ invariant mass is not modified by the scattering. Only by a sample of events in which the π^+ scatters from the spectator proton, can the $\Delta(1236)$ signal in the invariant mass distribution be observed.

The spectator momentum, cos (θ), and invariant mass distributions were calculated for single scattering events. However, because FSI and ISI are more probable when internal Fermi momentum of the deuteron is high, the shape of the single scattering spectator distribution is modified from the usual $\phi^2(p)p^2$. To determine the shape of the modified single scattering proton distribution, the deuteron wave function, $\phi(p)$, was used. Spectator protons with a momentum distribution given by $\phi^2(p)p^2$ were generated and then randomly selected, using a probability proportional to $g^2(p)p^2$, to be involved in double scattering. The fractional amount of double scattering was required to be consistent with the amount of double scattering in the data.

The modified single scattering spectator proton momentum distribution is given by the momentum distribution of the protons not involved in double scattering. These distributions are shown in Figures 5.7D and 5.8D. These figures show that there is no single scattering above 190 MeV/c. Figures 5.7E-F and 5.8E-F show how the invariant mass and cosine distributions for single scattering events with spectator momentum greater than 190 MeV/c would look if there were no double scattering.

Fits were made to the data using the double scattering distributions. The fits were made by assuming that the data distributions are sums of the Monte Carlo distributions, shown in Figures 5.7G-I and 5.8G-I, for the FSI and ISI contributions. That is, the data distributions were assumed to be given by:

$$F(p) = BF_{FSI}(p) + DF_{ISI}(p), \tag{5.11}$$

$$C(\cos\theta) = BC_{FSI}(\cos\theta) + DC_{ISI}(\cos\theta), \tag{5.12}$$

$$M(\pi^+p_s) = BM_{FSI}(\pi^+p_s) + DM_{ISI}(\pi^+p_s). \tag{5.13}$$

The subscripts FSI and ISI stand for final state interaction and initial state interaction resepectively. To perform the fits, the integrals of the Monte Carlo events in the fitted region were required to be unity. Then, the values of B and

Figure 5.7

Four Prong Double Scattering Fits

(A-C) Data and Fitted Curves

(D-F) Single Scattering Monte Carlo Events

(G-I) FSI Monte Carlo Events

(J-L) ISI Monte Carlo Events

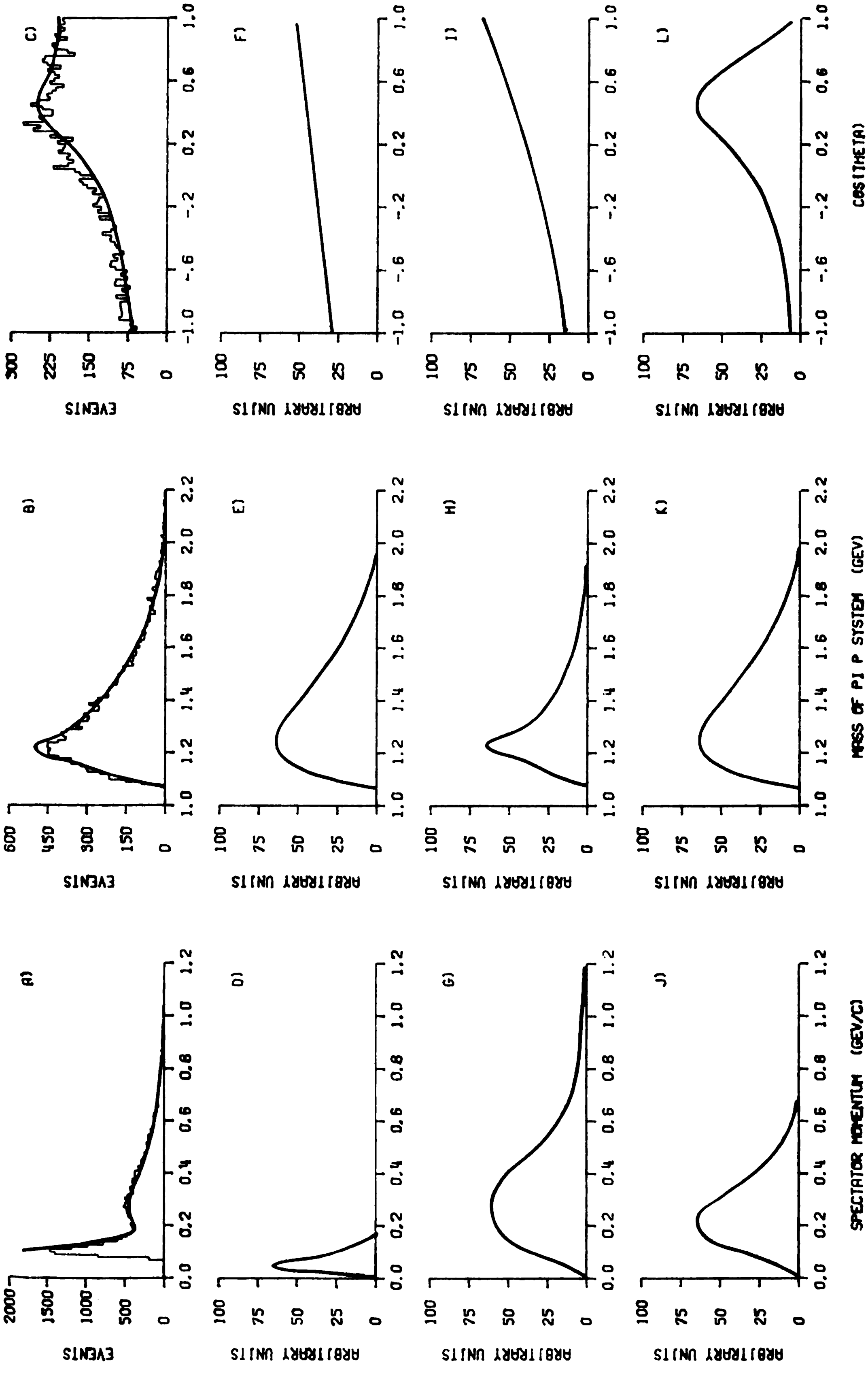
A)
B)
C)
D)
E)
F)
G)
H)
I)
J)
K)
L)
EVENTS
ARBITRARY UNITS
SPECTATOR MOMENTUM (GEV/C)
MASS OF PI P SYSTEM (GEV)
COS(THETA)

Figure 5.8

Six Prong Double Scattering Fits

(A-C) Data and Fitted Curves

(D-F) Single Scattering Monte Carlo Events

(G-I) FSI Monte Carlo Events

(J-L) ISI Monte Carlo Events

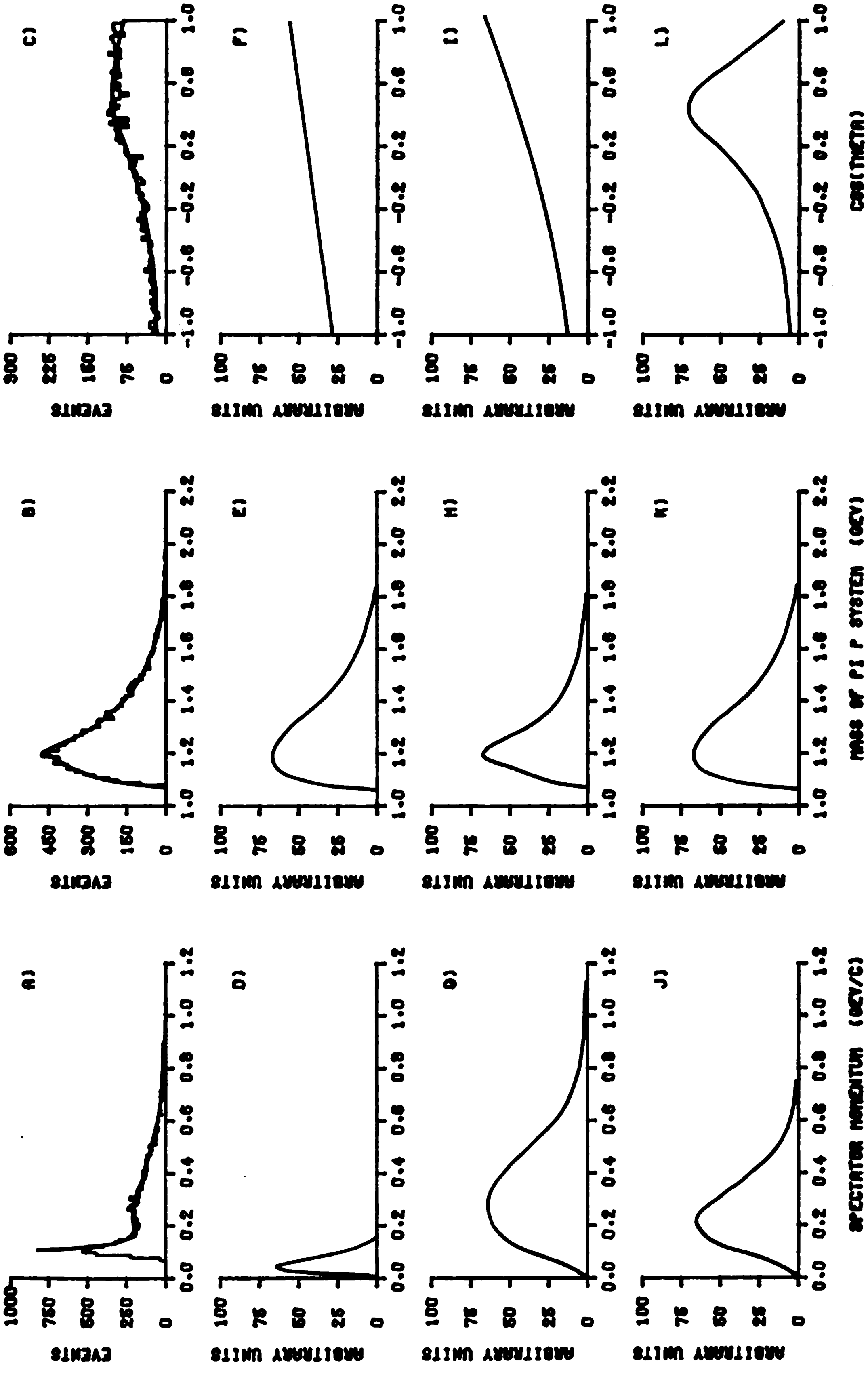
A)
B)
C)
D)
E)
F)
G)
H)
I)
J)
K)
L)
EVENTS
ARBITRARY UNITS
SPECTATOR MOMENTUM (GEV/C)
MASS OF PI P SYSTEM (GEV)
COS(THETA)

D are equal to the numbers of FSI and ISI events in the fitted region. To determine the values of B and D, the χ^2 of the fit was minimized by adjusting the values of B and D. The uncertainty for B and D was determined by varying these parameters one at a time until the χ^2 increases by one unit. This was done to take account of any correlation between B and D. To determine the total amounts of FSI and ISI, the number of events in the fitted region was used to find the number of events below 190 MeV/c. This can be done for FSI and ISI because the fractional amounts of the spectator distributions above 190 MeV/c are determined. The results of the fits are summarized in Table 5.9 and Figures 5.7A-C and 5.8A-C.

Since there are no single scattering events above 190 MeV/c, the amount of single scattering can not be found by using these fits. However, since there are events in the data having visible spectators with momenta values below 190 MeV/c, it is of interest to see how well these events can be described. Therefore, the number of events in the modified single scattering momentum distribution, N_{SS}, plus the total number of FSI and ISI events, $N_{FSI} + N_{ISI}$ was required to be equal to the total number of events in the data, N_d. The resulting normalization gives excellent agreement with the data in the 130-190 MeV/c regions of the spectator momentum distribution (see Figure 5.7A and 5.8A).

Table 5.9

Summary of Fits

	3-4 prong	5-6 prong
Events in fit region	15891	6188
FSI Events in fit	12395 ± 758	4383 ± 307
ISI Events in fit	3072 ± 240	1629 ± 184
Total FSI Events	15474 ± 946	5504 ± 385
Total ISI Events	4376 ± 341	2317 ± 262
Total Events	58167	25398
Fractional Amount of FSI	.266 ± .018	.217± .015
Fractional Amount of ISI	.053 ± .004	.064± .007

Below 130 MeV/c, spectator protons are not always seen in the bubble chamber.

5.6 Considerations of Possible ΔΔ State in the Deuteron

In most cases, the deuteron can be thought of as a bound neutron-proton system. However, it is possible for the deuteron to exist as a virtual ΔΔ state for a fraction of the time. This virtual state must have the same quantum numbers of the deuteron. Two possible states, which have been the subject of both theoretical and experimental work[44-53], are the $\Delta^{++}\Delta^{-}$ and $\Delta^{+}\Delta^{\circ}$ states. This conjecture was used to describe the magnetic moment of the deuteron.[44,45] Previous experimental works attempt to detect the ΔΔ state by observing spectator $\Delta(\Delta_s)$ produced in deuteron break-up reactions.[49-53] To establish the existence of the ΔΔ state in such a direct manner, one must be certain that the observed Δ signal corresponds to spectator Δ_s because these are other mechanisms, such as FSI, which can produce a Δ. This is done by examining kinematic regions which have as little background as possible. Since the existence of ΔΔ states implies the existence of spectator Δ, one expects to observe Δ_s in the backward direction. Previous experimental studies[49-53] make use of this fact since the background from other processes is expected to be smaller in the backward direction. In this section, the double scattering model is used to predict the angular distribution of Δ. An increase over this background would require the existence of $\Delta\Delta$ states.

Since the deuteron is an I=0 state, an equal admixture of the $\Delta^{++}\Delta^{-}$ and $\Delta^{+}\Delta^{\circ}$ states is expected. Both $\pi^{+}p_{s}$ and $\pi^{-}p_{s}$ invariant mass distributions should show the presence of a spectator Δ. Figure 5.3(see section 5.2) compares the $\pi^{+}p_{s}$ and $\pi^{-}p_{s}$ mass distribution for events having protons greater than 190 MeV/c. A comparison shows that $\pi^{+}p_{s}$ distribution has a signal at the Δ mass. However, this signal appears to be well described by double scattering. To detect possible Δ spectators, one must examine for an excess over the background. The distribution which will be examined is the cosine beam direction and the $\pi^{+}p_{s}$ momentum direction.

To observe possible Δ_{s}^{++}, a set of Δ_{s}^{++} candidates is defined. This set is defined so the background from other processes will be small. The Δ_{s}^{++} candidates were selected by requiring the $\pi^{+}p_{s}$ to be in a range 1180-1300 MeV. In addition, since the $\pi^{+}p$ mass distribution for events having visible spectator with a momentum less than 190 MeV/c shows no Δ^{++} signal (see Figure 5.9), these events were not used. The same cut was applied to the double scattering model. Figure 5.10 shows the distribution of the

Figure 5.9

Invariant Mass Distributions of $\pi^+ p_s$ (unshaded) and $\pi^- p_s$ (shaded) Systems

(A) Four prong events

(B) Six prong events

The $\pi^- p_s$ distribution has been normalized to the $\pi^+ p_s$ distribution. The momentum of the spectator proton is less than 190 MeV/c.

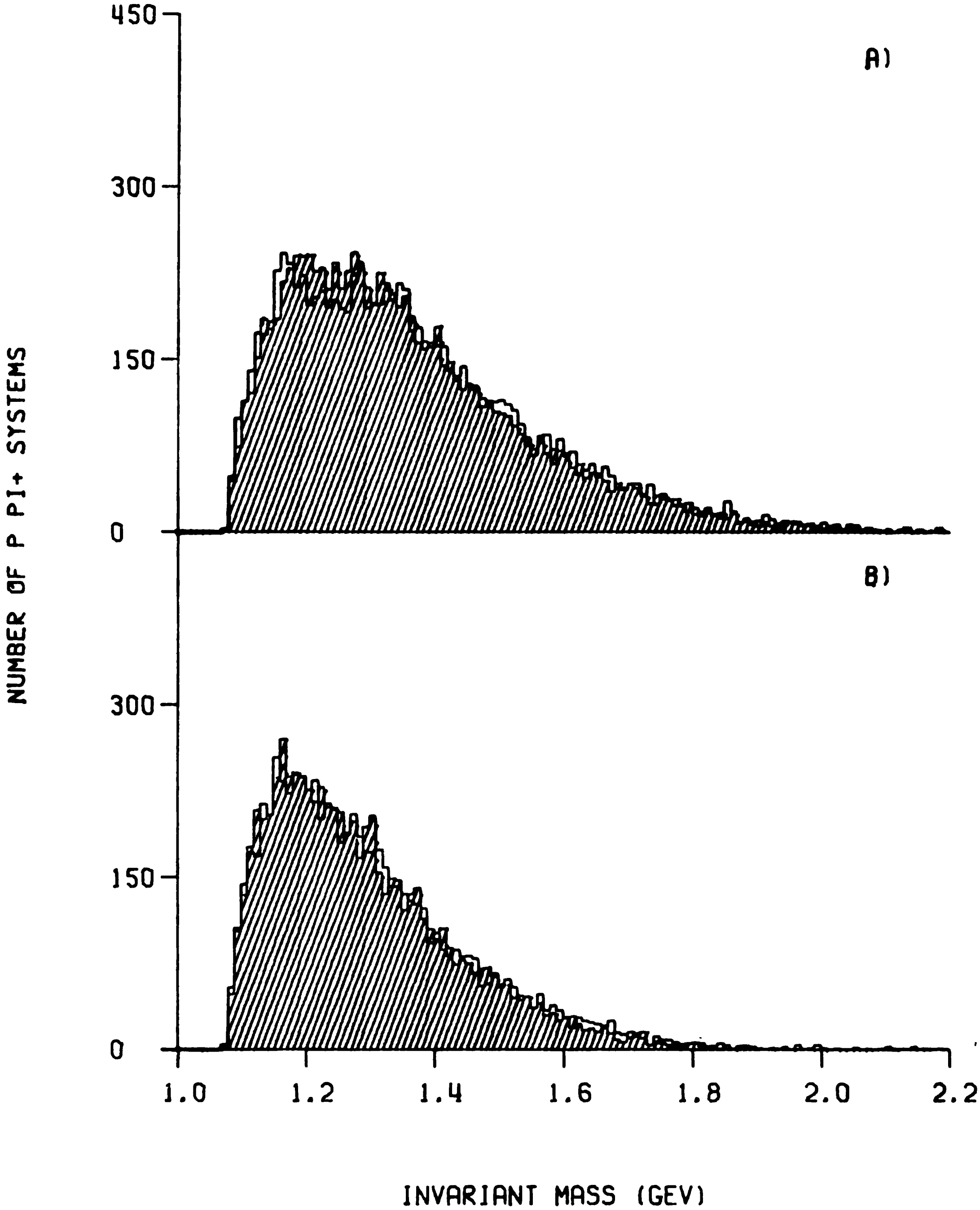

450
300
150
0
300
150
0
A)
B)
NUMBER OF P PI+ SYSTEMS
1.0
1.2
1.4
1.6
1.8
2.0
2.2
INVARIANT MASS (GEV)

Figure 5.10

Cosine between the Beam Direction and the $\pi^+ p_s$ Momentum Direction

(A) Four prong events

(B) Six prong events

The curve is the double scattering prediction.

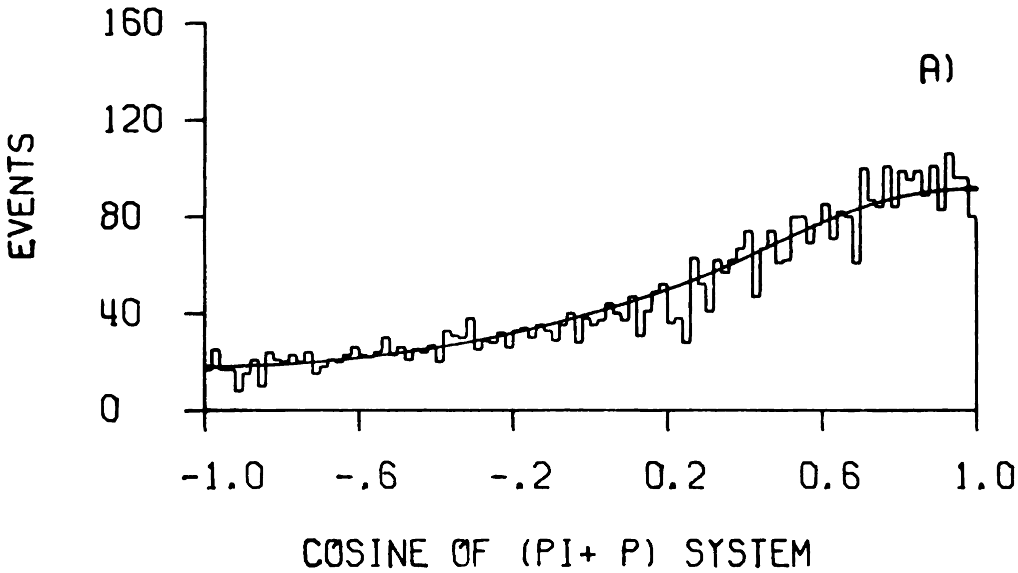
160
120
80
40
0
EVENTS
A)
-1.0
-.6
-.2
0.2
0.6
1.0
COSINE OF (PI+ P) SYSTEM

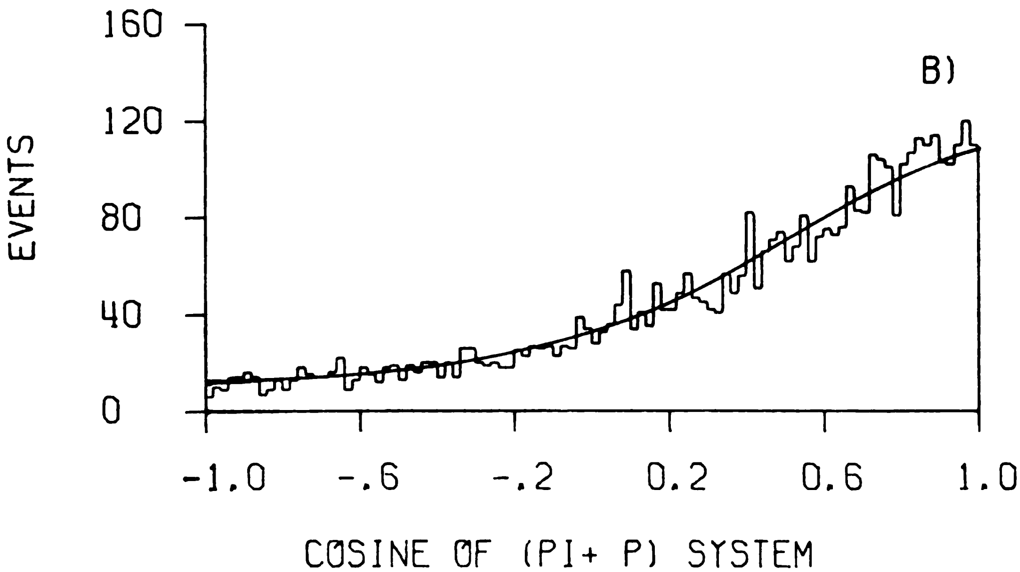
160
120
80
40
0
EVENTS
B)
-1.0
-.6
-.2
0.2
0.6
1.0
COSINE OF (PI+ P) SYSTEM

laboratory cosine between beam and the π^+p system. The data appears to be well described by the double scattering models. In particular, no excess of backward π^+p systems is observed. The $\Delta\Delta$ state is not needed to describe the data here.

5.7 Conclusions

It has been shown that a substantial fraction of the reaction $\bar{p}d \rightarrow p_s$ + pions involves final state interactions or initial state interactions. Final state interaction can sometimes change the topology of the event. The work here shows that only 74% of the FSI events having the topology characteristic of the reaction $\bar{p}d \rightarrow p_s$ + 3 charged pions are due to $\bar{p}n$ annihilations. The remaining fraction, 26%, are $\bar{p}p$ annihilation events which have the "$\bar{p}n$" topology because of charge exchange scattering. The five and six prong events having the $\bar{p}d \rightarrow p_s$ + 5 charged pion topology are 81% pn annihilations and 19% $\bar{p}p$ annihilations. This effect causes an increase in the number of events having the "$\bar{p}n$" topology. This increase is offset by the loss of $\bar{p}n$ events into the $\bar{p}d \rightarrow n_s$ + pions topology. About 33% of the total $\bar{p}n$ annihilations involving FSI which produce three charged pions and zero or more neutral pions leave the "$\bar{p}n$" topology. This number is 27% for $\bar{p}n$ annihilation producing five charged pions and zero or more neutral pions leave the "$\bar{p}n$" topology. This number is 27% for $\bar{p}n$ annihilation producing five charged pions and zero or more neutral pions involved in FSI. The effects of this topological interchange are summarized, for $\bar{p}n$ annihilations, on Table 5.10. In addition to topological interchange, FSI will modify other characteristics of the final state produced by the annihilation. This modification is of interest when examining resonance production.

The effects of ISI are not as striking as those of FSI. First of all, only 5.3-6.4% of the total sample involves ISI. This is to be compared with the percentage of the data, 22-27%, involved in FSI. ISI does not affect the final state as FSI does. Therefore, it does not change the topology of the event. However, ISI does change the center of mass energy of the $\bar{p}N$ system. This change might impair the observation of a narrow s-channel resonance.

The two double scattering models give an excellent description of the distributions involving the spectator proton in the reaction $\bar{p}d \to p_s$ + pions. No evidence which can uniquely establish the existence of a $\Delta\Delta$ state in the deuteron was found in this work.

Table 5.10

Effects of FSI

	3-4 prong	5-6 prong
Fractional amount of FSI with $\bar{p}n$ topology in the data (fitted)	.266 ± .018	.217 ± .015
Fractional amount of fake $\bar{p}n$ events in all the data	.069	.041
Fraction of $\bar{p}n$ annihilation events lost	.095	.062

CHAPTER VI

CONCLUSIONS

The reaction and topological cross sections for $\bar{p}n$ interactions producing three or five charged particles and zero or more neutral particles have been determined by using a deuterium target. The effects of unseen elastic scattering were considered. Also, a screening correction factor was used in obtaining the $\bar{p}n$ reaction cross sections. The resulting cross section values are in good agreement with the result at the higher momenta values found by Eastman *et al.*[13]

A study of the s-channel dependence of the $\rho^\circ\rho^\circ\pi^-$ intermediate state produced in the reaction $\bar{p}n \rightarrow 3\pi^-2\pi^+$ was made. This was done using individual beam momentum setting as well as 40 MeV wide bands in the center of mass energy. In particular, the bump in the $\rho^\circ\rho^\circ\pi^\circ$ state at 2190 MeV observed by Kalbfleisch *et al.*[2] in the reaction $\bar{p}p \rightarrow 2\pi^-2\pi^+\pi^\circ$ was sought for. Kalbfleisch suggests that this bump might be a possible source of the I=1 enhancement observed by Abrams *et al.*[1] in the total $\bar{p}N$ cross sections. No enhancement in the $\rho^\circ\rho^\circ\pi^-$ state was found at 2190 MeV even though the $\bar{p}n$ system is a pure I=1 state. However, the similarities in the distributions produced by the $\rho^\circ\rho^\circ\pi^-$ and $\rho^\circ\pi^-\pi^-\pi^+$ intermediate states limit how well the fractional amount of $\rho^\circ\rho^\circ\pi^-$ production can be determined. If there were to be any s-channel structure in the $\rho^\circ\rho^\circ\pi^-$ state, then the $\rho^\circ\rho^\circ\pi^-$ and $\rho^\circ\pi^-\pi^-\pi^+$ states must change simultaneously in such a manner that the fractional amount of ρ signal is constant. Using the cross section values for the reaction $\bar{p}n \rightarrow 3\pi^-2\pi^+$ and the fractional amounts of $\pi^+\pi^-$ pairs in the ρ signal, it was concluded that there is no enhancement, having an assumed width of ±50 MeV, greater than 0.7 mb at 2190 MeV with a 90% confidence level.

Finally, a model which describes the double scattering processes in the reaction $\bar{p}d \rightarrow p_s$ + pions was developed. Two types of double scattering were considered. The first type involves an interaction between a final state particle and the spectator nucleon. The other type involves an interaction between the incoming antiproton and the spectator nucleon. Evidence for both these models is shown in distributions involving the spectator proton. The model developed for the two types of double scattering give an excellent description of the data.

The double scattering model was used to study the characteristics of Δ production in the deuteron. The angular distribution of π^+p systems in the Δ mass are well described by the double scattering model. Therefore, the existence of the $\Delta\Delta$ state is not warranted here.

APPENDICES

APPENDIX A

SUMMARY OF FIT SELECTION PROCEDURES

Using the fit selection procedure discussed in Chapter II and a cut on the vertex position with the reaction colume defined in Chapter III, the numbers of events corresponding to each type of fit may be estimated. These are summarized in Tables A.1 and A.2.

The events contained in measuring categories A and B are summarized in Table A.1. At this stage, there are three groups of events that have not been assigned fits. They are "Bad Mark 30", "No Missing Mass Fit", and "Ambiguous". The events in the "Bad Mark 30" group had Mark 30 type fits, $\bar{p}d \rightarrow p_s k^+ k^- \pi^-$ or $\bar{p}d \rightarrow p_s k^+ k^- 2\pi^- \pi^+$, but were not Mark 30 events. This was determined by the ionization scan made on events with Mark 30 type fits. These events in the "Bad Mark 30" group were then assigned a fit that agrees with the ionization scan. The results are listed in Table A.3. The "No Missing Mass Fit" group contains events which lost a constraint due to improper measuring or missing information. A possible cause of this type of event could be due to very short or obscured tracks. Such events were assigned fits with the same ratio of the already assigned

Table A.1

Events in Measuring Categories A and B

P = 1.09 GeV/c

Prong	Mark 3	Mark 8	Mark 9	Mark 30	Multi-neutral	Mark 16-17	Bad Mark 30	No Missing Mass Fit	Ambiguous
3	37	232	1026	22	2431	0	25	84	4
4	13	73	406	4	819	16	11	32	62
5	0	436	678	14	572	0	18	59	3
6	0	134	234	2	144	6	3	24	5

P = 1.19 GeV/c

Prong	Mark 3	Mark 8	Mark 9	Mark 30	Multi-neutral	Mark 16-17	Bad Mark 30	No missing Mass Fit	Ambiguous
3	135	315	1566	46	3583	0	24	153	14
4	32	87	480	11	1197	16	5	72	117
5	0	651	1022	15	811	0	28	108	3
6	0	177	326	4	205	5	2	28	14

Table A.1 (Con't.)

P = 1.31 GeV/c

Prong	Mark 3	Mark 8	Mark 9	Mark 30	Multi-neutral	Mark 16-17	Bad Mark 30	No Missing Mass Fit	Ambiguous
3	550	518	2474	65	6738	0	57	220	20
4	175	161	862	14	2213	29	22	108	184
5	0	1194	1966	42	1580	0	35	168	4
6	0	299	625	8	422	10	11	45	19

P = 1.43 GeV/c

Prong	Mark 3	Mark 8	Mark 9	Mark 30	Multi-neutral	Mark 16-17	Bad Mark 30	No Missing Mass Fit	Ambiguous
3	716	292	1518	52	4409	0	52	162	11
4	175	97	542	8	1368	23	13	83	128
5	0	729	1262	22	1094	0	50	124	1
6	0	207	389	5	266	8	7	31	22

Table A.2

Events in Measuring Category C

P = 1.09 GeV/c

Prong	Mark 3	Mark 8	Mark 9	Mark 10	Mark 30-31	Mark 16-17	$n_s+K^+K^-$	No Missing Mass Fit	Ambiguous	Missing
4	0	93	612	1115	37	1826	156	122	67	96
6	0	153	268	131	1	240	49	52	19	29

P = 1.19 GeV/c

Prong	Mark 3	Mark 8	Mark 9	Mark 10	Mark 30-31	Mark 16-17	$n_s+K^+K^-$	No Missing Mass Fit	Ambiguous	Missing
4	25	106	922	1601	53	2448	213	172	93	59
6	0	238	341	295	21	357	91	63	27	16

P = 1.31 GeV/c

Prong	Mark 3	Mark 8	Mark 9	Mark 10	Mark 30-31	Mark 16-17	$n_s+K^+K^-$	No Missing Mass Fit	Ambiguous	Missing
4	48	192	1570	3132	111	4311	411	281	218	90
6	0	399	808	601	34	753	132	112	66	20

P = 1.43 GeV/c

Prong	Mark 3	Mark 8	Mark 9	Mark 10	Mark 30-31	Mark 16-17	$n_s+K^+K^-$	No Missing Mass Fit	Ambiguous	Missing
4	79	133	935	2392	99	3116	351	148	173	89
6	0	231	464	391	27	498	84	79	38	40

fits and are listed in Table A.3. Finally, the events in the "Ambiguous" group could not be assigned fits using the missing mass or confidence level. These events had multiple one constraint fits or multiple zero constraint hypotheses involving $\bar{p}d \rightarrow p_s + \ldots$ and/or $\bar{p}d \rightarrow n_s + \ldots$ type of reactions. The odd prong ambiguous events were either Mark 9 or Mark 10 type events. The even prong events were shown, by an ionization scan, to be half $\bar{p}p$ type events and half $\bar{p}n$ type events. Therefore, half of this even prong sample was assumed to be $\bar{p}p$ type events. The remaining half of the ambiguous even prong events and all of the ambiguous odd prong events were assumed to be either Mark 9 or Mark 10 type events. They were assigned to either the Mark 10 or Mark 9 group using the ratio of the previously assigned events. The resulting numbers of $\bar{p}d \rightarrow p_s + \ldots$ type events in measuring categories A and B are summarized in Table A.3.

Table A.2 summarizes the events contained in measuring category C. There are three groups of events in Table A.2 which must be assigned fits. The events in the group called "No Missing Mass Fit", which is defined in the same way as the events in measuring category A and B, include only those that were determined to be the $\bar{p}d \rightarrow p_s + ..$ reaction by the ionization scan. Therefore, all of these were assigned either Mark 9 or Mark 10 fits using the ratio of the already assigned events. The ionization scan did

Table A.3

$\bar{p}d \rightarrow p_s + \ldots$ Events in Measuring Categories A and B

P = 1.09 GeV/c

Prong	Mark 3	Mark 8	Mark 9	Mark 30	Multi-neutral	Total
3	38	237	1057	22	2507	3861
4	13	75	429	4	867	1388
5	0	450	713	14	603	1780
6	0	140	250	2	155	547

P = 1.19 GeV/c

Prong	Mark 3	Mark 8	Mark 9	Mark 30	Multi-neutral	Total
3	139	323	1620	47	3707	5836
4	33	90	517	11	1289	1940
5	0	679	1083	16	860	2658
6	0	183	345	4	216	748

P = 1.31 GeV/c

Prong	Mark 3	Mark 8	Mark 9	Mark 30	Multi-neutral	Total
3	561	529	2603	66	6937	10696
4	180	166	920	14	2363	3643
5	0	1236	2057	43	1653	4989
6	0	308	659	8	444	1419

P = 1.43 GeV/c

Prong	Mark 3	Mark 8	Mark 9	Mark 30	Multi-neutral	Total
3	732	299	1680	36	4556	7303
4	181	100	642	8	1471	2402
5	0	758	1340	22	1162	3282
6	0	214	415	5	283	917

not provide any information about the events in the "Ambiguous" or "Missing" groups. The "Ambiguous" group of events had positive tracks pointing almost directly toward or away from the camera.

Therefore, the projected ionization density was too high to provide information on the proper mass interpretation of the track. The events in the "Missing" group simply could not be found in the ionization scan. This could have been caused by a mislabeled frame or tracks observing the event. Therefore, the events in the "Ambiguous" or "Missing" group were assigned to other groups in the ratios of the already assigned events. Table A.4 summarizes the measuring category C $\bar{p}d \to p_s + \ldots$ type events.

Table A.4

$\bar{p}d \quad p_s + \ldots$ Events in Measuring Category C

P = 1.09 GeV/c

Prong	Mark 3	Mark 8	Mark 9	Mark 10	Mark 30	Mark 31	Total
4	0	106	674	1237	19	30	2066
6	0	176	309	151	1	0	637

P = 1.19 GeV/c

Prong	Mark 3	Mark 8	Mark 9	Mark 10	Mark 30	Mark 31	Total
4	28	117	995	1758	12	47	2957
6	0	262	376	325	23	0	986

P = 1.31 GeV/c

Prong	Mark 3	Mark 8	Mark 9	Mark 10	Mark 30	Mark 31	Total
4	53	211	1665	3431	40	82	5464
6	0	436	885	658	37	0	2016

P = 1.43 GeV/c

Prong	Mark 3	Mark 8	Mark 9	Mark 10	Mark 30	Mark 31	Total
4	86	145	997	2586	30	68	3922
6	0	258	519	437	30	0	1244

APPENDIX B

SCANNING EFFICIENCY

There is a finite probability that a scanner will miss an event at random. Therefore, the number of events must be corrected for this loss. To determine the correction factor, three rolls of film at each momentum were independently rescanned. Then, a conflict scan was performed on the rescanned rolls of film. This was done by examining and comparing the sample of events obtained in the original scan, scan 1, to the sample of events obtained in the second scan. This comparison involved examining the event on the scan table to decide if it was correctly located and identified in scan 1 and/or scan 2. One of the following codes was assigned to each event:

Code	
1	good event in scan 1; major error in scan 2
2	good event in scan 2; major error in scan 1
4	junk event
5	good event in scan 1; minor error in scan 2
6	good event in scan 2; minor error in scan 1
7	good event in both scans
8	duplicate event

(1) A major error is defined as follows:

(a) The event was not found.

(b) The event had the wrong prong assignment which was not caused by missing a short spectator proton track.

(2) A minor error is defined as follows:

(a) The event had a wrong prong assignment because a spectator proton track was not seen.

(b) The wrong frame number was recorded.

The conflict scan results are presented in the Tables B1-B5. The true number of events, N, can be found from the number of events found in scan 1 or scan 2, N_1 or N_2, if the scanning efficiencies for scan 1 or scan 2, S_1 or S_2, are known. The true number of events is given by:

$$N = N_1/S_1 \tag{B.1}$$

or

$$N = N_2/S_2 \tag{B.2}$$

The number of events common to both scans is given by:

$$N_1 \cap N_2 = S_1 \ S_2 \ N \tag{B.3}$$

Equations B.1, B.2, and B.3 give the following scanning efficiencies:

$$S_1 = \frac{N_1 \cap N_2}{N_2} \tag{B.4}$$

Table B.1

Events in Categories A and B

P(GeV/c)	Roll/Scan		CODE 1	2	4	5	6	7
1.09	Roll 61	S1	43	0	30	5	25	627
		S2	0	75	77	5	25	627
1.09	Roll 65	S1	65	0	11	3	2	683
		S2	0	74	70	3	2	683
1.09	Roll 69	S1	44	0	19	3	5	541
		S2	0	59	44	3	5	541
1.19	Roll 44	S1	67	0	43	6	13	748
		S2	0	53	52	6	13	748
1.19	Roll 49	S1	120	0	53	1	10	920
		S2	0	169	103	1	10	920
1.19	Roll 53	S1	70	0	48	0	0	967
		S2	0	173	97	0	0	967
1.31	Roll 24	S1	85	0	29	11	2	786
		S2	0	120	73	11	2	786
1.31	Roll 28	S1	68	0	44	4	3	981
		S2	0	119	63	4	3	981
1.31	Roll 34	S1	128	0	47	3	20	1008
		S2	0	173	59	3	20	1008
1.43	Roll 5	S1	106	0	47	6	13	1118
		S2	0	124	81	6	13	1118
1.43	Roll 10	S1	201	0	74	4	11	1466
		S2	0	233	94	4	11	1466
1.43	Roll 14	S1	209	0	78	6	3	1377
		S2	0	175	116	6	3	1377

Table B.2

Events in Category C (4 prong)

P(GeV/c)	Roll/Scan		CODE 1	2	4	5	6	7	8
1.09	Roll 61	S1	62	0	19	2	0	355	4
		S2	0	61	84	2	0	355	0
1.09	Roll 65	S1	68	0	76	1	2	369	4
		S2	0	67	97	1	2	369	0
1.09	Roll 69	S1	64	0	32	0	3	334	7
		S2	0	66	42	0	3	334	0
1.19	Roll 44	S1	81	0	38	1	0	450	9
		S2	0	46	95	1	0	450	0
1.19	Roll 49	S1	79	0	40	0	1	499	8
		S2	0	133	64	0	1	499	0
1.19	Roll 53	S1	143	0	48	3	2	509	7
		S2	0	81	84	3	2	509	0
1.31	Roll 24	S1	74	0	36	1	2	413	5
		S2	0	89	86	1	2	413	0
1.31	Roll 28	S1	91	0	20	0	1	467	2
		S2	0	112	96	0	1	467	0
1.31	Roll 34	S1	182	0	49	2	5	614	9
		S2	0	113	66	2	5	614	0
1.43	Roll 5	S1	186	0	46	3	4	679	9
		S2	0	95	127	3	4	679	0
1.43	Roll 10	S1	158	0	48	2	2	867	19
		S2	0	193	125	2	2	867	0
1.43	Roll 14	S1	216	0	51	1	6	718	16
		S2	0	180	65	1	6	718	0

Table B.3

Events in Category C (6 prong)

P(GeV/c)	Roll/Scan		CODE 1	2	4	5	6	7	8
1.09	Roll 61	S1	12	0	6	2	1	120	2
		S2	0	23	15	2	1	120	0
1.09	Roll 65	S1	6	0	9	0	0	127	4
		S2	0	18	14	0	0	127	0
1.09	Roll 69	S1	16	0	5	2	2	132	3
		S2	0	21	20	2	2	132	0
1.19	Roll 44	S1	18	0	9	2	1	144	0
		S2	0	22	26	2	1	144	0
1.19	Roll 49	S1	30	0	15	1	1	209	1
		S2	0	49	40	1	1	209	0
1.19	Roll 53	S1	36	0	10	0	3	197	2
		S2	0	25	34	0	3	197	0
1.31	Roll 24	S1	28	0	5	0	0	153	1
		S2	0	24	27	0	0	153	0
1.31	Roll 28	S1	23	0	10	0	1	189	2
		S2	0	36	45	0	1	189	0
1.31	Roll 34	S1	34	0	6	3	2	256	3
		S2	0	42	53	3	2	256	0
1.43	Roll 5	S1	23	0	14	1	0	272	3
		S2	0	39	28	1	0	272	0
1.43	Roll 10	S1	58	0	16	1	3	307	5
		S2	0	75	37	1	3	307	0
1.43	Roll 14	S1	55	0	14	3	3	274	1
		S2	0	27	33	3	3	274	0

Table B.4

Classification of the Code 4 Events
in Measuring Categories A and B

P(GeV/c)	Scan	a	b	c	d	e	f
1.09	1	24	10	1	17	7	1
1.09	2	77	18	24	49	14	9
1.19	1	70	26	10	28	9	1
1.19	2	104	16	34	76	12	10
1.31	1	71	21	5	10	7	2
1.31	2	91	16	22	58	6	2
1.43	1	114	18	14	45	6	2
1.43	2	111	27	48	88	8	9

a) Event does not belong in measuring category A or B.

b) Event is out of measurement region.

c) Event is a result of a secondary interaction.

d) Event assigned wrong event type.

e) Event is unmeasurable because of obscured vertex or tracks.

f) Event cannot be located.

Table B.5

Classification of the Code 4 Events
in Measuring Category C

P(GeV/c)	Scan	Prong	a	b	c	d	e	f	g
1.09	1	4	85	2	5	2	3	6	5
1.09	2	4	139	8	20	25	3	4	24
1.09	1	6	9	0	3	7	0	0	1
1.09	2	6	19	3	5	14	0	0	8
1.19	1	4	79	6	9	20	5	1	6
1.19	2	4	141	13	24	33	8	1	23
1.19	1	6	8	5	6	11	2	0	2
1.19	2	6	36	8	12	12	5	0	27
1.31	1	4	55	7	13	16	7	7	0
1.31	2	4	145	15	28	19	9	2	30
1.31	1	6	7	2	3	5	2	1	1
1.31	2	6	53	3	18	18	5	1	27
1.43	1	4	93	9	15	14	3	6	11
1.43	2	4	180	13	37	44	7	8	28
1.43	1	6	18	4	9	6	0	2	5
1.43	2	6	38	6	12	18	3	2	19

a) Event does not belong in measuring category C.

b) Event out of measurement region.

c) Event is a result of a secondary interaction.

d) Event was assigned wrong event type.

e) Event is unmeasurable because of obscured vertex or tracks.

f) Event can not be located in conflict scan.

g) Event type misidentified because of short spectator.

$$S_2 = \frac{N_1 \cap N_2}{N_1} \tag{B.5}$$

The number $N_1 \cap N_2$ is equal to the total number of events with codes 5, 6, or 7. N_1 is the number of events with codes 1, 5, 6, 7. Similarly, N_2 is the number of events with codes 2, 5, 6, or 7. S_1 is the scanning efficiency of the original scan. The scanning efficiencies were calculated for the events contained in measuring categories A and B. Also scanning efficiencies were found for both the 4 prong and 6 prong events in measuring category C. The resultant scanning efficiencies are shown in Table B.6.

Table B.6

Scanning Efficiencies

Events in Categories A and B

P	S_1
1.09	.901 ± .007
1.19	.871 ± .006
1.31	.872 ± .006
1.43	.883 ± .005

Events in Category C

P	4 Prong	6 Prong
1.09	.846 ± .010	.862 ± .016
1.19	.849 ± .009	.853 ± .014
1.31	.830 ± .009	.856 ± .013
1.43	.831 ± .007	.860 ± .011
Weighted average	.836 ± .004	.857 ± .007

APPENDIX C

MEASURING EFFICIENCY

Only the events which successfully pass through the PANAL-TVGP-SQUAW chain of programs appear on the final data tape. However, the events that failed include some $\bar{p}n$ type events. To take account of the events which failed, the measuring efficiency must be determined. The measuring efficiency is defined as:

$$\varepsilon_m' = N_p/N_m \tag{C.1}$$

where N_p is the number of events on the final tape and N_m is the number of measured events. Table C.1a presents the measuring efficiencies found by using equation C.1 and the numbers on Tables 2.1 and 2.2 in Chapter II. However, in Appendix B, it was shown that there is a class of events in the data which should not have been measured. These events were assigned a code 4 in Appendix B. Certain types of these code 4 events have a particularly high fail rate. In particular, there are 285 events listed in subcategories d, e, and f on Tables B.5 and B.6. This group of events has a measuring efficiency of $\varepsilon_m'' = .59$.

Table C.1

Measuring Efficiencies

C.1a Uncorrected Measuring Efficiencies

Momentum (GeV/c)	3 prong	4 prong	5 prong	6 prong
1.09	.934 ± .0034	.926 ± .0030	.907 ± .0058	.880 ± .0067
1.19	.953 ± .0024	.926 ± .0026	.912 ± .0047	.867 ± .0058
1.31	.943 ± .0019	.934 ± .0018	.904 ± .0035	.880 ± .0040
1.43	.952 ± .0021	.937 ± .0021	.912 ± .0042	.877 ± .0049

C.1b Corrected Measuring Efficiencies

Momentum (GeV/c)	3 prong	4 prong	5 prong	6 prong
1.09	.938 ± .0034	.930 ± .0030	.911 ± .0050	.884 ± .0067
1.19	.957 ± .0024	.930 ± .0026	.916 ± .0047	.871 ± .0058
1.31	.947 ± .0019	.938 ± .0018	.908 ± .0035	.884 ± .0040
1.43	.956 ± .0021	.941 ± .0021	.916 ± .0042	.881 ± .0049

The measuring efficiency of the sample excluding these events, ε_m, is given by:

$$\varepsilon_m = \frac{N_t \varepsilon_m' - N_f \varepsilon_m''}{N_t - N_f} , \tag{C.2}$$

where the total number of events in scan 1 is N_t and the number of high fail rate events in scan 1 is N_f. The values of N_t = 22224 and N_f = 285 are obtained from Tables B.2-B.6 in Appendix B. Table C.1b presents the values of ε_m. These values, which are .004 higher than the values in Table C.1a, are the measuring efficiencies used for the cross section calculations.

APPENDIX D

BEAM COUNT

To calculate the cross sections, the number of beam particles entering a defined reaction volume must be determined. A track was counted as a beam particle if it crossed the first fiducial cut-off line (see Figure 2.1 in Chapter II) without any obvious interaction before that point. The counting was done using every 50th frame on each of the 72 rolls. The total number of beam tracks was calculated by:

$$N_b = N_{bc} \frac{N_{ft}}{N_{fs}} \tag{D.1}$$

Here, N_b is the total number of beam tracks; N_{bc} is the number of beam tracks counted; N_{ft} is the total number of frames; and N_{fs} is the number of frames used in the counting. The results are summarized in Tables D.1-D.4. The reaction volume, which was defined in Chapter III, is downstream of the fiducial cut-off lines used for beam count purpose. The number of beams entering this volume may be obtained from the beam count. The geometrical properties of the bubble chamber require the beam particle to travel an average of 7.2 cm from the first fiducial cut-off line to reach the defined reaction volume. Therefore, number

Table D.1

Beam Count P = 1.09 GeV/c

Roll	Number of beams	Number of frames scanned	Total frames
57	186	41	2092
58	169	41	2098
59	239	41	2093
60	210	41	2094
61	235	41	2092
62	210	41	2096
63	171	41	2088
64	238	41	2093
65	250	42	2112
66	196	42	2107
67	230	42	2131
68	232	41	2091
69	236	41	2087
70	199	41	2088
71	194	41	2082
72	203	41	2079
TOTAL	3499	659	33514

Total number of beams = 178,000 ± 3000

Table D.2

Beam Count P = 1.19 GeV/c

Roll	Number of beams	Number of frames scanned	Total frames
41	251	41	2089
42	270	41	2090
43	272	41	2098
44	275	41	2095
45	210	41	2089
46	183	41	2088
47	307	42	2102
48	334	41	2095
49	422	41	2094
50	432	41	2090
51	413	42	2109
52	462	39	1999
53	443	41	2087
54	386	41	2098
55	382	41	2090
56	309	42	2110
TOTAL	5351	657	33423

Total number of beams = 272,200 ± 3700

Table D.3

Beam Count P = 1.31 GeV/c

Roll	Number of beams	Number of frames scanned	Total frames
17	592	41	2093
18	549	42	2102
19	431	41	2092
20	382	41	2090
21	386	41	2095
22	417	41	2098
23	365	42	2100
24	291	41	2198
25	575	42	2107
26	392	41	2081
27	393	42	2112
28	378	42	2106
29	364	41	2097
30	549	41	2096
31	593	42	2104
32	500	42	2101
33	512	42	2106
34	400	41	2096
35	462	41	2066
36	321	42	2099
37	400	42	2099
38	366	41	2091
39	300	41	2089
40	411	41	2088
TOTAL	10333	994	50406

Total number of beams = 524,000 ± 5200

Table D.4

Beam Count P = 1.43 GeV/c

Roll	Number of beams	Number of frames scanned	Total frames
1	187	24	1224
2	452	42	2087
3	447	42	2099
4	514	41	2092
5	417	41	2096
6	250	41	2086
7	301	41	2073
8	392	41	2055
9	298	41	2085
10	567	41	2093
11	649	42	2099
12	578	41	2076
13	396	42	2108
14	635	42	2102
15	518	42	2102
16	284	41	2092
TOTAL	6885	645	32569

Total number of beams = 347,700 ± 4200

of beams entering the reaction volume is given by:

$$N_{br} = N_b \, e^{-eA_o \ell \sigma_{obs}/2} \tag{D.2}$$

Here e = .14 gm/cc is the density of liquid deuterium; ℓ = 7.2 cm is the path length before entering the reaction volume; and σ_{obs}, see Appendix F, is the total $\bar{p}d$ cross section less the unobservable part of the elastic scattering. The numbers of beam tracks entering the reaction volume for each momentum value are summarized in Table D.5.

Table D.5

Summary of Beam Count

P(GeV/c)	Beams N_b	Beams Entering Reaction Volume[(1)]	Beams Entering Reaction Volume[(2)]
1.09	178000 ± 3000	167400	168700
1.19	272200 ± 3700	256500	258400
1.31	524000 ± 5200	494400	498000
1.43	347700 ± 4200	328700	331100

(1) No elastic correction

(2) 28.9 mb elastic correction

APPENDIX E

SCANNING BIAS FOR SPECTATOR PROTONS

E.1 Slow Protons

The spectator distribution about an axis defined by the direction of the beam, the y axis, should be symmetric. Therefore, if the distribution for $\phi \equiv \arctan(z/x)$ is not isotropic, it would be indicative of a scanning bias. Figure E.1a shows such a distribution. It is apparent that there are dips in the ϕ distribution at ϕ near 0° and 180°. These values of ϕ correspond to spectator protons moving toward or away from the scanner and the projection of the track on the film becomes short. Since a low momentum track has a shorter track length in a bubble chamber, it is expected that some low momentum tracks will be missed. This loss can be determined by fitting the following expression to the data:

$$N_{obs}(\phi) = A + B|\sin \phi| \tag{E.1}$$

$$N_{corr}(\phi) = A + B \tag{E.2}$$

Figure E.1

Spectator Proton ϕ Distribution

(A) Slow protons ($p < 100$ MeV/c)

(B) Fast protons ($p > 400$ MeV/c)

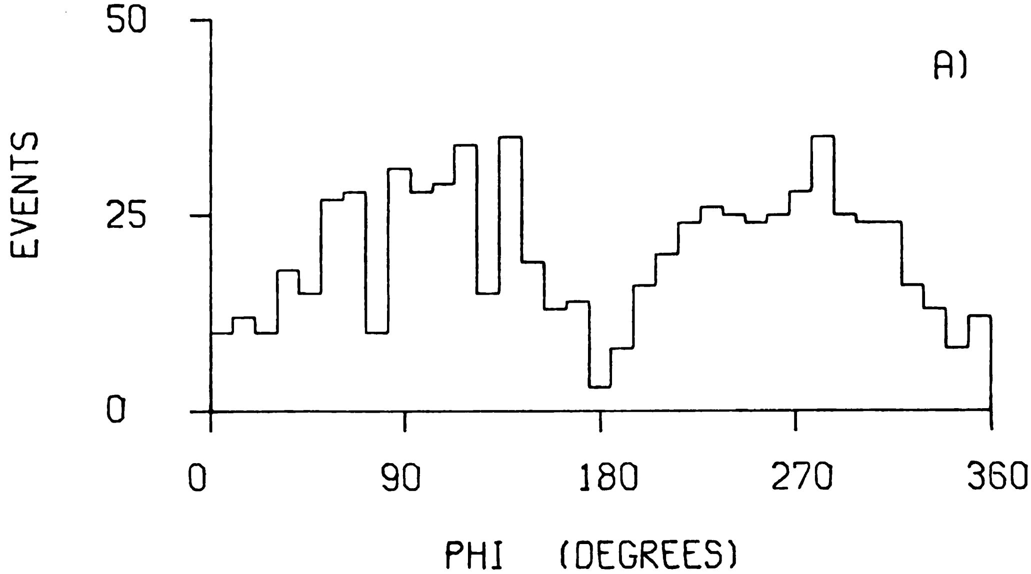
A)
EVENTS
50
25
0
0
90
180
270
360
PHI (DEGREES)

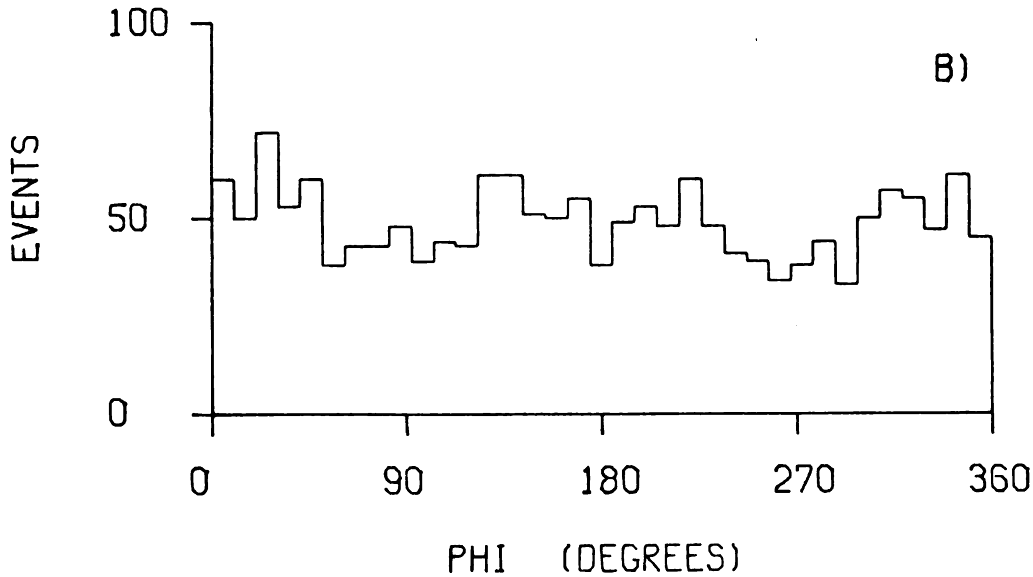
B)
EVENTS
100
50
0
0
90
180
270
360
PHI (DEGREES)

Here A and B are the fit parameters; N_{obs} (ϕ) is the fitted ϕ distribution; and N_{corr} (ϕ) is the expected ϕ distribution. The values of A and B are found by fitting expression E.1 to the data. Then the number of events in the data is given by:

$$M_{obs} = \int_0^{2\pi} (A + B|\mathrm{Sin}\ \phi|)d\phi \tag{E.3}$$

$$= 2\pi A + 4B \tag{E.4}$$

The actual number of events is given by:

$$M_{corr} = \int_0^{2\pi} (A + B)d\phi \tag{E.5}$$

$$= 2\pi(A + B) \tag{E.6}$$

The correction factor is then given by:

$$C = M_{corr}/M_{obs} \tag{E.7}$$

$$C = (A + B)/(A + 2B/\pi) \tag{E.8}$$

The values of C are presented in Table E.1.

Table E.1

Scanning Loss Corrections for Slow Spectator Protons

Spectator Momentum MeV/c	C(4 Prong)	C(6 Prong)
50-90	1.57	1.57
70-110	1.39 ± .02	1.50 ± .03
90-130	1.14 ± .02	1.22 ± .04
> 130	1.00	1.00

This loss causes events to change topology. Even prong events with a low momentum spectator proton will be measured as odd prong events. Since in the conflict scan, this type of mislabeling was considered a minor error, this loss will not change the total cross sections. However, this loss must be considered when studying the spectator distribution of the data.

E.2 Fast Protons

The ϕ angle distribution of fast spectator protons also shows a scanning bias. This bias appears as a loss of events with fast spectator protons moving perpendicular to the line of sight. This corresponds to ϕ equal to 90° or 270°. The reason for this loss is the way an event was selected to be measured. When a track is perpendicular to the line of sight, it appears lighter than a similar track in any other orientations. Therefore, an event with a fast proton with ϕ equal to 90° or 270° might not be measured because it looks like a $\bar{p}p$ type event. Figure E.1b shows such a distribution.

To determine how many events are not measured, expression E.1 was fitted to the ϕ angle distribution of events whose proton has a momentum greater than 250 MeV/c. In this case, the values of B were negative. The corrected number of events is given by:

$$M_{corr} = \int_{o}^{2\pi} A \, d\phi \tag{E.9}$$

$$M_{corr} = 2\pi A \tag{E.10}$$

Table E.2 presents the numbers of events that were lost for different reactions.

Table E.2

Scanning Losses for Events with Fast Spectator Protons

Reaction Type	1.09 GeV/c	1.19 GeV/c	1.31 GeV/c	1.43 GeV/c
4 Prong Mark 8	0	0	0	0
4 Prong Mark 9	28	55	69	64
4 Prong Mark 10	42	27	74	100
6 Prong Mark 8	0	0	9	8
6 Prong Mark 9	5	0	20	8
6 Prong Mark 10	0	0	12	8

APPENDIX F

UNSEEN ELASTIC SCATTERING

The cross section measurements involve the use of the total $\bar{p}d$ cross sections. However, in this experiment some of the $\bar{p}d$ interactions are not observed. These unseen interactions are low t elastic scattering. There are three types of elastic scattering in deuterium: (a) $\bar{p}d$ elastic scattering; (b) quasi-elastic $\bar{p}p$ scattering; and (c) quasi-elastic $\bar{p}n$ scattering.

To determine the amount of unseen elastic events, one must estimate the minimum momentum transfer that can be detected. In a bubble chamber, an elastic scattering event is detected in two ways. First, if the recoil particle is charged and has a large enough momentum, it will produce a visible track. If the recoil particle is a neutron the only way to detect the interaction is to observe the deflection of the incident particle. In the case of charged recoil particles, either a proton or a deuteron, one can estimate the smallest detectable t if the lower limit of momentum for detecting protons is known. The sample of 4 and 6 prong events shows that there are very few protons with momentum less than 80 MeV/c. From a study of the azimuthal angle distribution (see Appendix E), it was known that the detection efficiency of proton with momentum between 80 MeV/c and 100 MeV/c is low. Therefore, the momentum values of 100 MeV/c for protons will be used for the lower limits of $\sqrt{-t}$. The corresponding value for a deuteron with the same range is 80 MeV/c. If the neutron is the recoil particle, the event can only be seen by observing the deflection of the incident particle. If the deflection angle is less than 6°, the event is difficult to observe. At a beam momentum of 1.3 GeV/c, a 6° deflection angle corresponds to a t transfer of -.0185 $(\text{GeV/c})^2$. This will be considered the minimum t transfer for $\bar{p}n$ elastic scattering.

The differential elastic cross section can be written as:

$$\frac{d\sigma}{dt} = Ae^{bt} \tag{F.1}$$

Then the missing cross section is given by:

$$\sigma_{missing} = \sigma_{el}\, b \int_0^{t_{min}} e^{bt}\, dt \tag{F.2}$$

$$= \sigma_{el}\,(1 - e^{bt_{min}}) \tag{F.3}$$

In equations F.2 and F.3, σ_{el} is the total elastic cross sections. The values of σ_{el} and b were determined elsewhere.[22, 42, 43] Table F.1 shows the results of the

Table F.1

Estimate of Unseen Elastic Scattering

Elastic Scattering	$t_{min}(GeV/c)^2$	σ_{EL}(mb)	$b(GeV/c)^{-2}$	$\sigma_{missing}$(mb)
$\bar{p}d$	.0064	38	44	9.1
$\bar{p}p$	.0100	43	18	7.8
$\bar{p}n$	.0185	43	18	12.0

Total missing cross section is 28.9 mb.

Table F.2

Total and Observable $\bar{p}d$ Cross Section

P(GeV/c)	σ_{total} (mb)	σ_{obs} (mb)
1.09	200.3	171.4
1.19	195.6	166.7
1.31	191.5	162.6
1.43	184.6	155.7

estimation. Table F.2 shows the observable part of the total $\bar{p}d$ cross section. The quantity σ_{obs} is the total $\bar{p}d$ cross section less the missing elastic cross section. The values of the total $\bar{p}d$ cross section were taken from Abrams *et al*.[1]

LIST OF REFERENCES

LIST OF REFERENCES

1. R. J. Abrams *et al*., Phys. Rev. Lett. 18 (1967) 1209; R. J. Abrams *et al*., Phys. Rev. D1 (1970) 1917.

2. G. Kalbfleisch *et al*., Phys. Lett. 29B (1969) 259; G. Kalbfleisch, R. C. Strand and V. VanderBurg, Report submitted to Experimental Meson Spectroscopy Conference, Northeastern Univ. - April 1974, "Status of $\bar{p}p \to \pi(2190) \to \rho^\circ\rho^\circ\pi^\circ$".

3. R. A. Donald *et al*., Phys. Lett. 40B (1972) 586. R. A. Donald *et al*., Nuc. Phys. B61 (1973) 333.

4. T. Handler, P. Jacques, M. Jones, R. J. Plano, H. Preissner, A. P. Sheng, T. L. Watts, P. Yamin, E. B. Brucker, E. L. Koller, and C. R. Sun, Report submitted to Experimental Meson Spectroscopy Conference, Northeastern Univ. - April 1974, "$\bar{p}p$ Annihilation into Four and Five Pion Final States in the T(2190) Region".

5. J. Alspector *et al*., Phys. Rev. Lett. 30 (1973) 511; K. J. Cohen, "Direct Channel T and U Meson Formation in $\bar{p}p$ Interactions", *Experimental Meson Spectroscopy - 1972*, ed. A. H. Rosenfeld and K-W. Lai (New York: American Institute of Physics, 1972) 242.

6. D. B. Cline, "Comments on Meson States with $M > 2M_N$", *Experimental Meson Spectroscopy - 1972*, ed. A. H. Rosenfeld and K-W. Lai (New York: American Institute of Physics, 1972) 205.

7. G. A. Smith, "A Search for $\rho^\circ\rho^\circ\pi^-$ Enhancement in Antiproton-Neutron Annihilation in the T-Meson Region", *Proceedings of the Symposium on Antiproton-Nucleon Interactions*, (Liblice-Prague, 1974) 105.

8. J. Chapman, B. Green, A. Honma and B. P. Roe, "$\rho^\circ\rho^\circ\pi^\circ$ in the T Region", *Proceedings of the Symposium on Antiproton-Nucleon Interactions*, (Liblice-Prague, 1974) 108.

9. R. J. Sprafka, Michigan State Univ.; Note Number p-004.

10. F. T. Solmitz, A. P. Johnson and T. B. Day, Univ. of California, Berkeley; Note Number p-117.

11. O. I. Dahl, T. B. Day and F. T. Solmitz, Univ. of California, Berkeley; Note Number p-126.

12. J. M. Mountz, Ph.D. Thesis, Michigan State Univ. (1974).

13. P. S. Eastman et al., Nuc. Phys. B51 (1973) 29.

14. W. A. Cooper et al., Phys. Rev. Lett. 20 (1968) 1059.

15. G. R. Kalbfleisch, "The T Region", Experimental Meson Spectroscopy, ed. C. Baltay and A. H. Rosenfeld (New York: Columbia Univ. Press, 1970) 409.

16. J. Friedman, SAGE, A Las Vegas Event Generator, Univ. of California, Berkeley; Note Number p-189, 1969.

17. B. S. Aladashvili et al., JINR, E1-8092, Dubna, 1974.

18. R. Poster et al., Phys. Rev. Lett. 27 (1974) 1625.

19. N. W. Dean, Phys. Rev. Lett. 27 (1971) 276.

20. R. J. Glauber, Phys. Rev. 100 (1955) 242.

21. V. Franco and R. J. Glauber, Phys. Rev. 142 (1966) 1195.

22. Z. Ming Ma and G. A. Smith, Phys. Rev. Lett. 27 (1971) 344.

23. R. Reid, Annals of Physics 50 (1968) 411.

24. T. Hamada and I. D. Johnson, Nuc. Phys. 34 (1962) 382.

25. S. Gartenhaus, Phys. Rev. 100 (1955) 900.

26. L. Hulthen and M. Sugawara, Handbuch der Physick 39 (1957) 141.

27. M. Moravcsik, Nuc. Phys. 7 (1958) 113.

28. I. J. McGee, Phys. Rev. 151 (1966) 772.

29. A. Jurewicz and L. Satta, Lettere Al Nuovo Cimento 10 (1974) 217.

30. B. Y. Oh and G. A. Smith, Nuc. Phys. B40 (1972) 151.

31. A. A. Carter et al., Nuc. Phys. B26 (1971) 445.

32. E. Bracci, J. Droulez, E. Flaminio, J. Hansen, and D. Morrison, "Compilation of Cross Sections, I-π^- and π^+ Induced Reactions", CERN/HERA 72-1 (May 1972).

33. G. Giacomelli, P. Pini, and S. Stagni, "A Compilation of Pion Nucleon Scattering Data", CERN/HERA 69-1 (nov. 1969).

34. A. Donnachie, R. G. Kirsopp, and C. Lovelace, CERN Report Th-838 (1967) unpublished.

35. W. A. Cooper et al., "Inelastic $\bar{p}p$ Interactions Between 1.2 and 1.6 GeV/c", Argonne National Laboratory, unpublished.

36. R. A. Donald et al., Nuc. Phys. B11 (1969) 551.

37. N. Xuong and G. R. Lynch, Phys. Rev. 128 (1962) 1849.

38. R. Burns et al., Nuc. Phys. B27 (1971) 109.

39. Liverpool - LPNHE (Paris) Collaboration, "Antiproton-Proton Cross Sections in the T and U Regions", Report submitted to XVI International Conference on High Energy Physics, Batavia, Ill., 1972.

40. E. Fermi, Phys. Rev. 81 (1951) 683.

41. Z. Ming Ma, B. Y. Oh, D. L. Parker and G. A.Smith, Phys. Lett. 47B (1973) 177.

42. D. L. Parker, B. Y. Oh, G. A. Smith and R. J. Sprafka, Nuc. Phys. B32 (1971) 29.

43. W. A. Cooper et al., Nuc. Phys. B16 (1970) 155.

44. H. Arenhövel, M. Danos and H. T. Williams, Phys. Lett. 31B (1970) 109.

45. H. Arenhövel, M. Danos and H. T. Williams, Nuc. Phys. A162 (1971) 12.

46. H. T. Williams, H. Arenhövel and H. G. Miller, Phys. Lett. 36B (1971) 278.

47. N. R. Nath, H. J. Weber and P. K. Kabir, Phys. Rev. Lett. 26 (1971) 1404.

48. L. S. Kisslinger, Phys. Lett. 48B (1974) 410.

49. M. Goldhaber, "Trends in Nuclear Physics: What Can We Learn From High-Energy Interactions?", Proceedings of the International Conference on Nuclear Physics, ed. J. De Boer and Mang, (Munich, 1973) Vol. 2, 14.

50. C. P. Horne et al., Phys. Rev. Lett. 33 (1974) 380.

51. P. Benz and P. Söding, "Possible Nucleon Resonance Admixture in the Deuteron", DESY 74/28 (June 1974).

52. B. S. Aladashvili et al., JINR, E1-8334, Dubna, 1974.

53. A. Fridman, "Features Connected with the Use of Deuteron Targets in $\bar{p}d$ Interactions at 5.55 GeV/c", Proceedings of the Symposium on Antiproton-Nucleon Interactions, (Liblice-Prague, 1974).

54. Z. Ming Ma et al., Nuc. Phys. B51 (1973) 77.